UNIVERSITÀ
DI PARMA

Department of Chemical Life Sciences and Environmental Sustainability

PhD program in Biotechnologies and Biosciences

XXX cycle

Novel mechanisms and small-molecule inhibitors of tumorigenesis: Xanthohumol-mediated repression of angiogenesis via AMPK and DEC1-dependent enhancement of tumor aggressiveness by interplay with NOTCH1

Coordinator:
Prof. Simone Ottonello

Supervisors:
Prof. Simone Ottonello
Dr. Alessia Ciarrocchi

PhD student: Dr. Cristina Gallo

2014/2017

“To strive, to seek, to find and not to yield”

Ulysses, Tennyson

ABSTRACT

I: The increasing interest in the field of chemo and angio-prevention field resulted in the opportunity to obtain a considerable number of new synthetic molecules derived from natural compounds with properties able to prevent or to delay tumors development. Among them, Xanthohumol (XN) displays multiple beneficial activities and represents a promising candidate to be employed in supporting cancer therapies. Since the incomplete knowledge about XN antiangiogenic mechanism of action, we hypothesized the involvement of AMPK signaling activation in the XN mediated antiangiogenic properties. Here we confirmed the role of XN as powerful anti-angiogenic molecules and we showed that it has greater activity on endothelial cells of another recognized angio-preventive flavonoid, the epigallocatechin-3-gallate (EGCG). Moreover we unveiled for the first time that XN activates AMPK via CaMMKβ in a LKB1 independent manner. Further we elucidated the XN downstream mechanism and suggested the existence of two independent pathways by which XN exerts its antiangiogenic effect: the AMPK/eNOS axis and the AKT signaling. Finally, we identified new powerful anti-angiogenic molecules within a series of novel synthetic analogues of XN.

II: In the last years a role for the basic helix-loop-helix transcription factors DEC1 and DEC2 in cancer began to emerge. In tumor cells these transcription factors seems to play multiple functions affecting apoptosis, proliferation and angiogenesis by orchestrating response to chemokines and hypoxia. However, a complete picture of the role of these factors in cancer (and in particular in thyroid cancer) is missing as well as the knowledge of the molecular mechanisms through which DEC factors influence cancer cells is still limited. Since we found DEC1 and DEC2 significantly up-regulated in a cellular model of highly aggressive papillary thyroid carcinoma (PTC), we hypothesized that these factors might be part of the intricate mechanisms driving PTC progression. Here we demonstrated that DEC1 more than DEC2 regulates the aggressive features of PTC. DEC1 promotes cell proliferation and invasiveness by interplay with NOTCH1. Moreover we unveiled that DEC1 represses DEC2 expression and activates genes involved in the regulation of the cell cycle G1/S transition and the chromosomal segregation. Finally we evaluated the expression of DEC1 in a cohort

of patients with different thyroid tumor histotypes and we showed for the first time that DEC1 expression is specific of tumor cells ant its expression characterizes all thyroid histotypes, including the most aggressive anaplastic thyroid carcinomas (ATC).

Contents

SESSION I

XANTHOHUMOL EXERTS

ANTI-ANGIOGENIC ACTIVITY VIA AMPK

INTRODUCTION

Angiogenesis

Angiogenesis is the physiologic process of new vessels formation from the pre-existing vasculature. It is a fundamental step in several processes such as tissue growth, embryonic development and wound healing.

Pathological angiogenesis is a hallmark of several diseases including diabetes, cardiovascular and chronic inflammation related diseases. Angiogenesis also represents a crucial step in tumor growth and metastatic dissemination [1, 2].

In the first stage of tumorigenesis, cellular growth and apoptosis are in balance and the tumor takes nutrient and oxygen from surrounding vessels (avascular phase). When the tumor overtake 1-2 mm in diameter, it reaches a fatal step: cellular hyper-proliferation stops because the lack of nutrients and oxygen and the formation of new blood vessels is a necessary condition for the tumor to feed on and to restart proliferation. New vessels formation is also a crucial step for dissemination to distant sites. The transition from the avascular phase to the angiogenic phase is referred as to the "angiogenic switch" [3] (Figure 1).

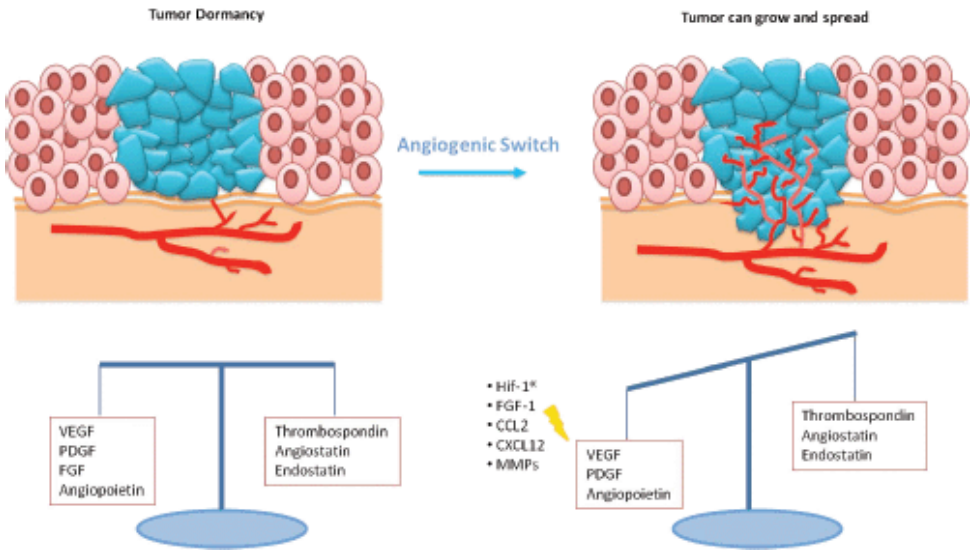

Figure 1. The Angiogenic Switch. From "*Tumor dormancy and clinical implications in breast cancer". L. Gelao et al.,Ecancer Medical Science*.

This mechanism occurs when the tumor starts to secrete pro-angiogenic factors and/or to suppress anti-angiogenic effectors, resulting in the induction of endothelial cell proliferation and migration, vessel sprouting and tube formation. These processes overall are the first features that confer aggressiveness to the tumor, enhancing invasiveness and its ability to metastasize new sites.

Strategies aimed at blocking or delaying tumor angiogenesis represent promising therapeutic approaches for cancer prevention and therapy [4, 5]. This concept represents an indirect anti-tumor strategy, aimed at targeting host components rather than tumor cells.

Chemo/angio-prevention

In 1976, Sporn defined chemoprevention "the use of pharmacologic or natural agents that inhibits the development of invasive breast cancer either by blocking the DNA damage that initiates carcinogenesis, or by arresting or reversing the progression of premalignant cells in which such damage has already occurred". Chemopreventive drugs are molecules that, when used regularly, prevent or retard the development of cancer [4]. Dietary phytochemicals, plant derived molecules and other natural synthetic compounds for their anti-proliferative, pro-apoptotic or anti-oxidant activities in tumor cells are potential chemopreventive agents [6, 7]. Among these, Aspirin which derives originally from salicylic acid of the willow tree and Metformin, a widely used antidiabetic drug, which derives from the natural product galegine extracted from *Galega officinalis* [8, 9]. Other phytochemicals with potential chemopreventive properties include resveratrol, curcumin, Epigallocatechin-3 gallate (EGCG), hyperforin, curcumin, synthetic triterpenoids, and the synthetic retinoid fenretinide (4-HPR). Several natural compounds with chemo-preventive activity, especially flavonoids (such as epigallocatechin-3-gallate, quercetin and resveratrol), exert their antiangiogenic effects through the activation of AMPK [10-12]. (Table 1).

Besides counteracting tumor cells proliferation, these phytochemical-derived agents can also act as anti-angiogenic and anti-inflammatory drugs. As a parallelism with the concept of chemoprevention Albini and Sporn as proposed to call this effect "angioprevention" [4].

Flavonoids	Source	AMPK activation	Related pathways
Epigallocatechin-3-gallate (EGCG)	Green tea, apples, plums, onions, hazelnuts, pecans, cacao	yes	AKT, FOXO1
Quercetin	Apples, citrus fruits, leafy vegetables, red onions, Dill weed, Capers	yes	IL-1β
Resveratrol (RSV)	Red wine, grapes, cranberries, blueberries, peanuts	yes	SIRT1
Xanthohumol (XN)	Beer, hops	?	AKT

Table1. AMPK-activating flavonoids with antiangiogenic activity. *From "Hop derived flavonoid xanthohumol inhibits endothelial cell functions via AMPK activation" Gallo et al., Oncotarget. 2016; 7:59917-59931.*

Xanthohumol

Substantial attention has been addressed to flavonoids and their synthetic precursors, chalcones, a class of polyphenolic compounds that, within their wide range of activities, also exhibit anti-angiogenic properties [13]. During the last decades, the prenylated chalcone Xanthohumol (XN, figure 4A) has emerged as a cancer chemopreventive agent [14]. It is the major prenylated chalcone present in the female inflorescences of the hop plant (Humulus lupulus L.), used to preserve and flavor beer (4B).

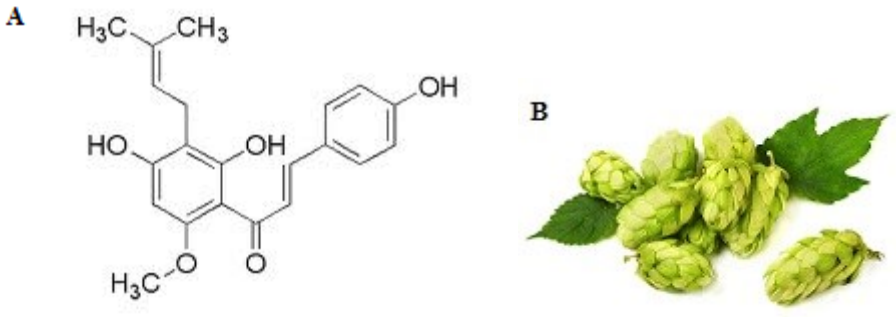

Figure 4. Xhantohumol chemical structure (A) and the inflorescence of hop plant (B).

The beneficial properties of hops are well known from ancient times and have been used in traditional medicines since the IX century. Xanthohumol was first isolated by Power in 1913 and its structure

was elucidated in 1957 by Verzele [15]. However, only in the last decades, we assisted to an increasing interest to this molecule, since it is endowed with multiple biological activities including antidiabetic, anti-inflammatory, anti-oxidant, anti-cancer, anti-invasive, and anti-angiogenic activities [16-18]. Given the promising results from *in vitro* and *in vivo* preclinical studies that have pointed out the numerous benefits exerted by XN, clinical trials are currently being developed evaluating the feasibility of XN treatment in the context of metabolic syndrome and prevention of DNA damage (https://clinicaltrials.gov/) [19, 20].

AMP-activated protein kinase:

AMPK is a highly evolutionarily conserved heterotrimeric serine/threonine kinase. This complex consists of one catalytic subunit (which may be either α1 or α2 isoforms) and two regulatory subunits (β1 or β2 and γ1, γ2 or γ3) (Figure 2).

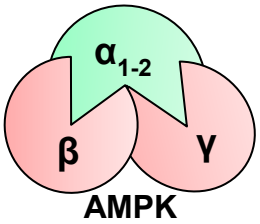

Figure 2. AMPK protein structure.

AMPK is a molecular hub, involved in many cellular processes, including metabolism, homeostasis regulation, growth, proliferation, apoptosis and autophagy [21-22]. AMPK activation in response to different stimuli occurs by the phosphorylation of Thr-172 [23] (Figure 3). Under energy-stress conditions, LKB1 (Liver Kinase B1) is the major AMPK activator, leading to an increase in the intra-cellular AMP: ATP ratio [24-27]. In addition, AMPK can be also activated by other protein kinases, including CaMKKβ (Calcium/calmodulin dependent protein kinase kinase β), which is able to induce AMPK activation following stimuli leading to increased intracellular Ca^{2+} levels [28,29]. The kinase

TAK1 (transforming growth factor β-activated kinase) activates AMPK in response to VEGF (vascular endothelial growth factor) and cytokines [30, 31]. AMPK plays a crucial role in angiogenesis and homeostasis of vascular tissues. In endothelial cells, AMPK mediates the response to hormones, vascular mediators, the anti-inflammatory molecule aspirin and the antidiabetic drug metformin [32-34]. It is able to activate several signaling pathways in order to protect from hypoxia, shear and oxidative stress [35]. The activity of AMPK on the endothelium is exerted through an activating phosphorylation of endothelial nitric oxide synthase (eNOS) at Ser1177 with the subsequent formation of NO (nitric oxide), a central signaling molecule in the regulation of vascular homeostasis [36]. Endothelium-derived NO stimulates blood flow, vascular remodeling and angiogenesis [37].

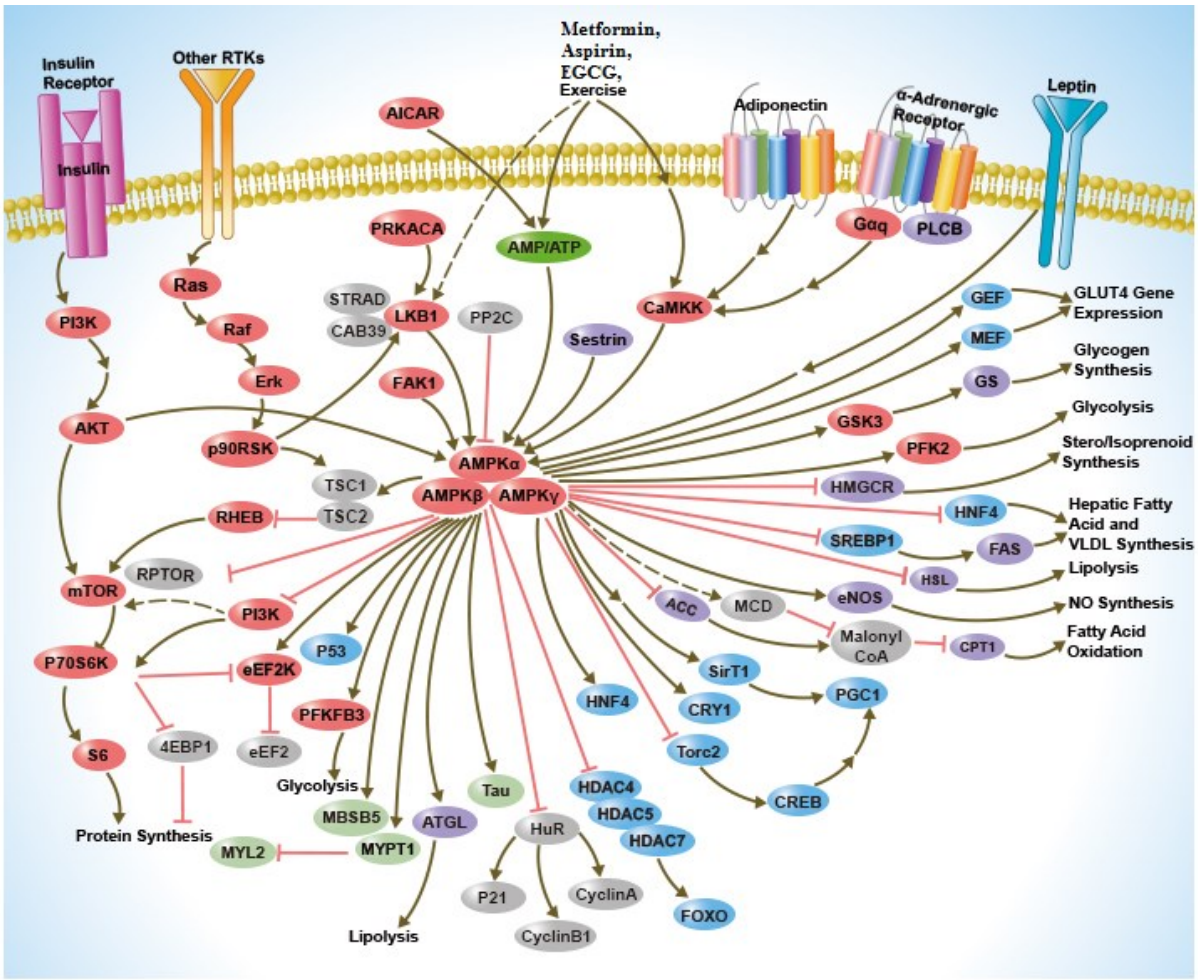

Figure 3. The AMPK signaling. Modified from Sino Biological Biological Solution Specialist.

AIM OF THE PROJECT

The arising interest in the field of chemo and angio-prevention resulted in the opportunity to obtain a plethora of new molecules derived from natural compounds less toxic than drugs and able to prevent or to delay tumors development. Among them, XN displays a multiple beneficial activities and represents a promising candidate to be employed in supporting cancer therapies. Since the incomplete knowledge about XN anti-angiogenic mechanism of action, and the key role of AMPK in flavonoids antiangiogenic effects, we hypothesized that the AMPK activation signaling might mediate XN anti-angiogenic activities.

The aims of this project were:

1) Confirm the strong anti-angiogenic activity of XN;
2) Deciphering the potential involvement of AMPK as mediator of XN anti-angiogenic activity;
3) Dissect the molecular AMPK pathway in response to XN;
4) Identify new powerful anti-angiogenic molecules within a series of novel synthetic analogues of XN.

Human endothelial cells derived from umbilical cord (HUVEC) were employed as gold model for angiogenic studies. The synthetic analogues of XN were synthesized by the team of Professor Armando Rossello, at the Department of Pharmacy (University of Pisa). This project was conducted under the supervision of Dr. Adriana Albini, director of the *Fondazione MultiMedica Onlus* (IRCCS Multimedica, Milan).

MATERIALS AND METHODS

Reagents

Xanthohumol ((2E)-1-[2,4-dihydroxy-6-methoxy-3-(3-methyl-2-buten-1-yl)phenyl]-3-(4-hydroxyphenyl)-2-propen-1-one) was purchased as powder from Alexis Biochemicals (San Diego, CA, USA) and was solubilized in DMSO. Epigallocatechin-3-gallate (EGCG) was purchased as powder by Sigma Aldrich (Sigma-Aldrich, St Louis, MO, USA) and was solubilized in water. The ON-TARGET plus SMART pool siRNAS targeting AMPK α1 (PRKAA1 L-0502700) and ON-TARGET plus Nontargeting Pool negative control siRNA (D-001810) were purchased from Dharmacon (Lafayette, CO). Lipofectamine RNAiMAX (catalog number 13778-075) was purchased from Invitrogen (Eugene, OR).

Cell lines and cell culture medium

Human umbilical vein endothelial cells (HUVEC) were obtained from PromoCell (Heidelberg, Germany) and cultured from passage 4 to 6 at 37 °C in 5 % CO_2 in M199 medium (Sigma Aldrich) supplemented with 10% heat-inactivated fetal bovine serum, 1% glutamine, fibroblast growth factors (1µg acidic-fibroblast growth factor plus 1µg basic-fibroblast growth factor/100 ml, PeproTech London UK), epidermal growth factor (1µg/100 ml, PeproTech), heparin (10 mg/100 ml, Sigma Aldrich) and hydrocortisone (0.1 mg/100 ml, Sigma Aldrich). HUVEC were seeded on 0.1% gelatin coated flasks.

MTT assay

In vitro cell proliferation/viability was measured by the MTT test. We seeded 1000 cells/well into 96-multiwell plates in complete medium. Following adhesion, medium was replaced with fresh medium containing the different treatments or vehicle (DMSO) and the medium was refresched every 48 hours. XN and EGCG were used in a concentration range from 2.5 to 40 µM, up to 96 hours, whereas XN or XN derivatives were used in a range from 1-20 µM. 3 hours before each time point, MTT reagent (3-(4,5-dimethylthiazol-2-yl)-2,5-diphenyltetrazolium bromide; Sigma Aldrich, Milano) was

added to the wells and plates were incubated at 37ºC. MTT reagent was prepared solubilizing the powder in PBS 1X plus Ca and Mg at the final concentration of 0.005g/ml. During the incubation time the metabolic enzymes reduced the tetrazolium dye into its insoluble formazan, which precipitate on the bottom has a colored crystalls. Then we added 200µl of DMSO to dissolve formazan into a purple solution. Absorbance at 540 nm was then measured by a FLUOstar spectrophotometer (FLUOstar Omega BMG LABTECH).

Apoptosis assay

Apoptosis was evaluated by 7-AAD staining, followed by flow cytometry analysis. HUVE cells were plated at a density of 2.5 x 10^5 cells/well on 6-well plates and grown overnight. The subsequent day, the cells were treated either with XN or EGCG in a concentration range from 5 to 20 µM, up to 96 hours. DMSO or medium alone were used as vehicle. At each time point, cells were harvested, counted, transferred into flow tubes, pelleted, resuspended in 50 µl and stained with the 7-aminoactinomycin-D (7-AAD) dye. Samples were analyzed by flow cytometry within 1 hour using a FACSCantoII (BD). The proportion of viable (7-AAD-negative) cells was analyzed using the BD FACSDiva Software 6.0 and expressed as a percentage of the total cell number excluding debris.

Cell cycle assay

Assessment of cell cycle was evaluated with Propidium Iodide (PI) followed by flow cytometry. 2 x 10^5 HUVE cells were plated on 6-well plates. The following day cells were treated either with Xanthohumol or EGCG in a concentration range from 5 to 20 µM, for 24 or 48 hours. DMSO or medium alone were used as vehicle. Cells were fixed and permeabilized with 70% cold ethanol for 1 hour at -20°C, then washed twice with cold Phosphate Buffer Solution 1X and stained for 40 minutes at 37°C with PI solution (50 µg/ml PI in H_2O, 0.1% Triton-X100, 0.1% trisodium citrate dehydrate, 6.25 µg/ml RNase A). Cells were analyzed by flow cytometry within 1 hour using a FACSCanto machine (BD) and analyzed with BD FACSDiva Software 6.0.

Migration and invasion assays

Chemoinvasion and chemotaxis assay was performed as previously described [38, 39]. Briefly, polycarbonate membrane filters with 8 μm pore-diameter (Whatman, GE Healthcare Europe GmbH, Milano) were pre-coated with collagen IV (50 μg/mL, Sigma Aldrich Milano) for chemotaxis assay or matrigel (1 mg/mL, BD Biosciences, Milano) for chemoinvasion assay and placed in modified Boyden chambers (Neuro Probe, Gaithersburg, MD, USA). HUVEC (5×10^4), previously treated with XN or EGCG (range 5 to 20 □M) for 24h, were washed with PBS 1X, resuspended in serum-free medium and placed in the upper compartment. Serum (10% in M199) was used as chemoattractant and added to the lower compartment of the chambers. Cells were incubated for 6h (chemotaxis) or 24h (chemoinvasion) at 37°C, filters were then recovered, cells on the upper surface were mechanically removed with a cotton swab. Migrating or invading cells were fixed with absolute ethanol and stained with DAPI (Vectashield, Vector Laboratories, Orton Southgate, Peterborough, United Kingdom). Cells were counted in a double-blinded manner in five consecutive fields with a fluorescent microscope (Nikon Eclipse Ni). All experiments were performed three times in duplicate.

Matrigel morphogenesis assay

When cultured on a tree-dimensional membrane-basement matrix, HUVEC are able to form capillary like structures, mimicking the events occurring during vessel lumen formation in vivo. A 24-microwell plate, pre-chilled at -20°C, was carefully filled with 300 μl/well of liquid matrigel (10 mg/ml, BD Biosciences, Milano) at 4°C with a pre-chilled pipette. The matrigel was then polymerized for 1 h at 37°C. 5×10^4 HUVEC, previously treated with XN or EGCG (range 5 to 20 □M) for 24h, were suspended in 1 ml of complete medium layered on the top of the polymerized matrigel. After 6 h of incubation at 37°C, the formation of capillary-like networks was examined under an inverted microscope (Nikon Eclipse TS100), equipped with charge-coupled device optics and a digital analysis system. The number of segments and their length were quantified by the ImageJ software, using the "Angiogenesis Analyzer" tool [40].

Transfection by siRNA

Transient transfection of AMPKα1 siRNA was performed using Lipofectamine RNAiMAX, according to the manufacturer's protocol. Briefly, on day 1, HUVEC were seeded at a density of 2 x 10^5 per well in a gelatin pre-coated six-well plate, without antibiotics. The following day, cells were transfected with 10 nM siRNA for 6 h. Transfection efficiency was verified 24 and 48 h later by western blotting.

Western Blotting

HUVEC were grown in complete medium and treated with increasing concentrations of XN (1–20 μM). Cells were then washed with PBS 1X at and snap-frozen at -80°C. After thawing, cells were placed in lysing buffer (Cell Signaling Technology, Beverly, MA) and total lysate was obtained. Protein concentration was evaluated by the Bradford Protein Assay (Bio-Rad, Hercules, CA). Equal amounts of proteins for each sample were resolved on 4-20% sodium dodecyl sulfate–polyacrylamide gel electrophoresis and blotted onto polyvinylidene fluoride membranes (Amersham Biosciences, Otelfingen, CH). Following blocking with 5% non-fat milk powder (wt/vol) in Tris-buffered saline (10mM Tris–HCl, pH 7.5, 100mM NaCl, 0.1% Tween-20) for 1h at room temperature, membranes were incubated with primary antibodies directed against the following human antigens: β-actin (Sigma Aldrich), AMPKα1, phospho-AMPKα (Thr172), total and phospho-ACC, total and phospho-eNOS, total and phospho-LKB1, total and phosphor-mTOR(Ser2448), total and phospho-AKT (Thr308 and Ser473), total and phosphor-p70S6k, total and phospho-4EBP1 (all purchased from Cell Signaling Technology, Danvers, MA). The antibodies were diluted in 2% bovine serum albumin–Tris-buffered saline–0.1% Tween according to the manufacturer's instructions. The bound antibodies were visualized by horseradish-peroxidase-conjugated secondary antibodies and an enhanced chemiluminescence detection system from Amersham Biosciences (Pittsburg, PA).

Griess assay

Nitric oxide (NO) release was indirectly analyzed by measuring nitrite (NO_2^-), a stable and non-

volatile breakdown product of NO. HUVE cells were grown in complete medium and treated with 10 μM XN in a time range from 1h up to 12h. At the indicated time points, the medium was collected. The assay was performed according to the manufacturer's protocol for Griess Reagent System (Promega, Milan, Italy). Briefly, 50 μl of each sample was transferred to a 96 multi-well plate. Each sample was then incubated with 50 μl of Sulfanilamide Solution for 10 minutes, followed by a second incubation with 50 μl of N-1-napthylethylenediamine dihydrochloride (NED) Solution for 10 minutes. Absorbance was measured at 540 nm by using a FLUOstar spectrofotometer (FLUOstar Omega BMG LABTECH) and then compared using a Nitrite Standard reference curve.

ATP assay

The CellTiter-Glo® Luminescent Cell Viability Assay (Promega, Milan, Italy) was used to measure the amount of ATP produced by endothelial cells. HUVEC (6000/well) were plated into 96-multiwell plates in complete medium. Cells were then serum-starved for 18 hours. Then, XN was added to each well to a final concentration of 10 μM. Control cells (NT) were treated with vehicle alone (DMSO). 1 h after treatment, 100 μL of CellTiter-Glo® Reagent, previously prepared by mixing the CellTiter-Glo® Buffer and the lyophilized CellTiter-Glo® Substrate, was added to each well. Luminescence was read by using NanoLuc Luciferase Ready (GloMax Discover, Promega, Milan, Italy).

Statistical analysis

Data are expressed as means ± SEM. The statistical significance between multiple data sets was determined by one-way ANOVA using Graph-Pad PRISM FACS data were analyzed by the FACSDiva6 software. ImageJ software was used for western blotting quantification.

RESULTS

Xanthohumol (XN) exerts a more pronounced anti-angiogenic activity as compared to epicallocatechin-3 gallate (EGCG).

XN has been shown to exert anti-angiogenic, anti-oxidant and anti-inflammatory activities both *in vitro* and *in viv*o [13-20]. There is evidence that XN could be a promising angio-preventive compound.

To confirm this hypothesis we first assessed the anti-angiogenic activity of XN in human endothelial cells. As control, we also used epicallocatechin-3 gallate (EGCG) which is a widely recognized anti-angiogenic flavonoid abundant in green tea leaves [41]. We compared the effects of these two anti-angiogenic flavonoids by analyzing proliferation, viability and cell functions in HUVEC.

Noticeably, we observed that XN has a powerful effect in endothelial cells greater than the one observed with EGCG, as determined by the analysis of cell proliferation/viability by MTT assay and by the calculation of the IC50 value at 96h: 28 μM for XN and 56 μM for EGCG (Fig. 1A-C). Furthermore, cell cycle analysis revealed that 24h and 48h treatment with XN resulted in a decreased percentage of cells undergoing S-phase corresponding to an increased accumulation in the G0/G1 phase, while cells treated with ECGC display no effects. (Figure 1D-E).

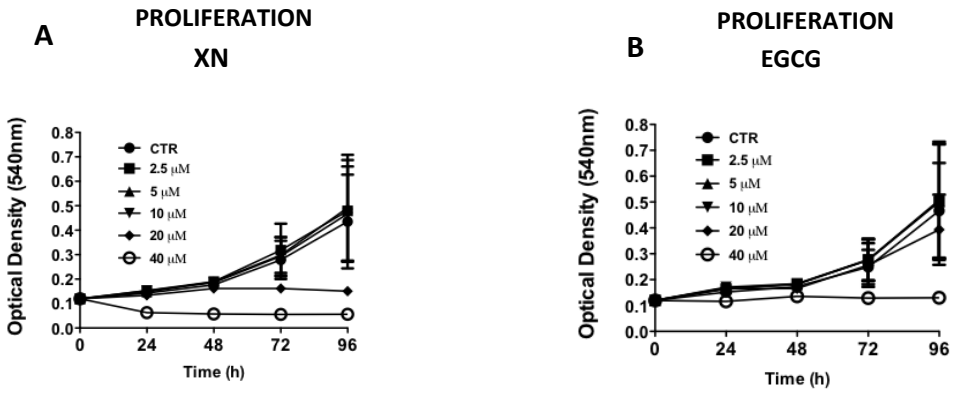

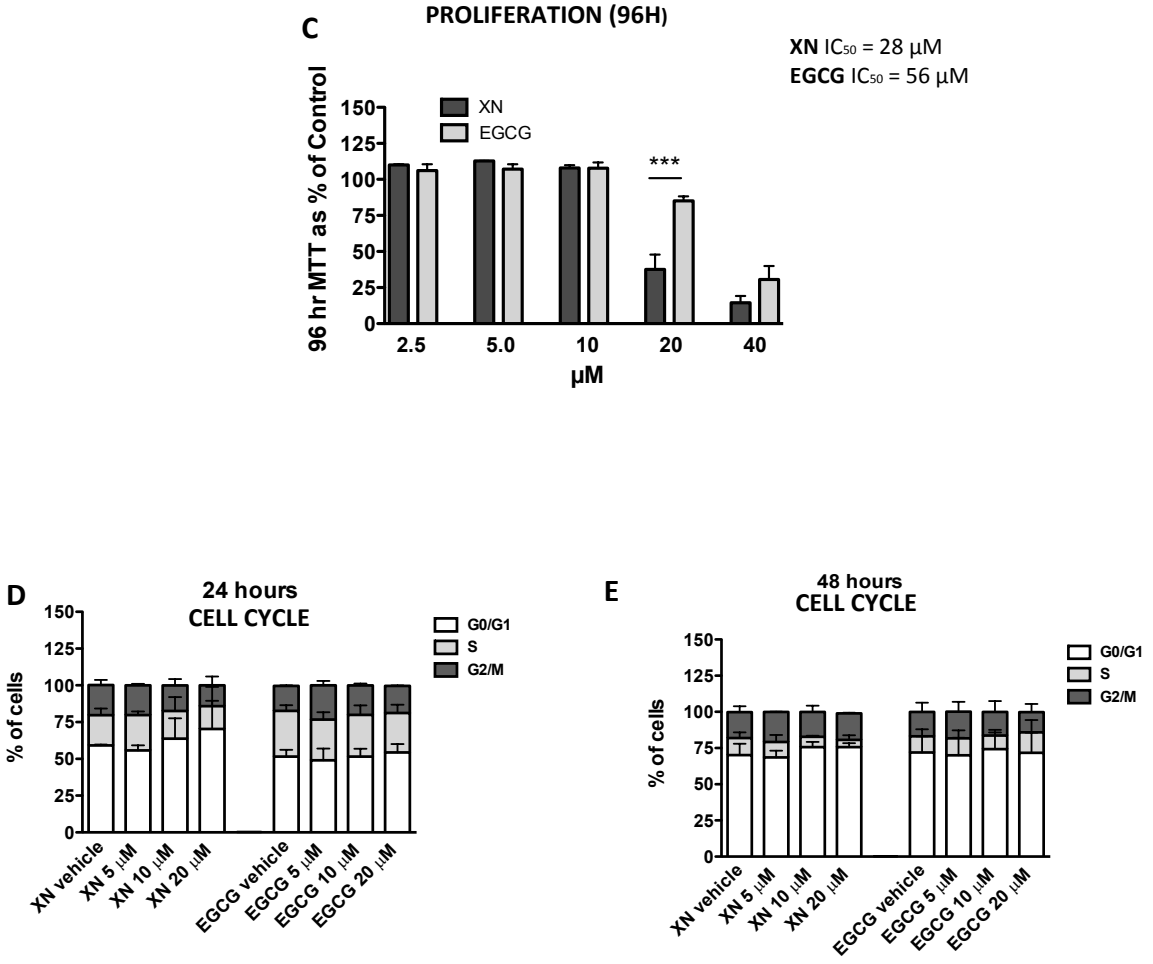

Figure 1: Comparison of anti-angiogenic effects of XN and EGCG. A–C. HUVEC were treated with various concentrations of XN (A) or EGCG (B) (0, 2. 5, 5, 10, 20 and 40 µM) (C) up to 96h and cell proliferation was determined using the MTT assay. Data are expressed in terms of optical density at 540 nm. HUVEC were treated with XN and EGCG at different doses (5-10-20 µM) or vehicle. Cell cycle was evaluated 24h (D) and 48h (E) following treatments by flow cytometry analysis after propidium iodide staining. Histograms show the distribution of cell populations in each phase of the cell cycle.

We also observed that administration of XN induced apoptosis after a prolonged time of treatment (10 µM at 96h, fig. 2A) or at high doses (20 µM at 24h, fig. 2B), whereas EGCG did not show a similar effect at any concentration or time of treatment (Fig. 2A, B, C, D).

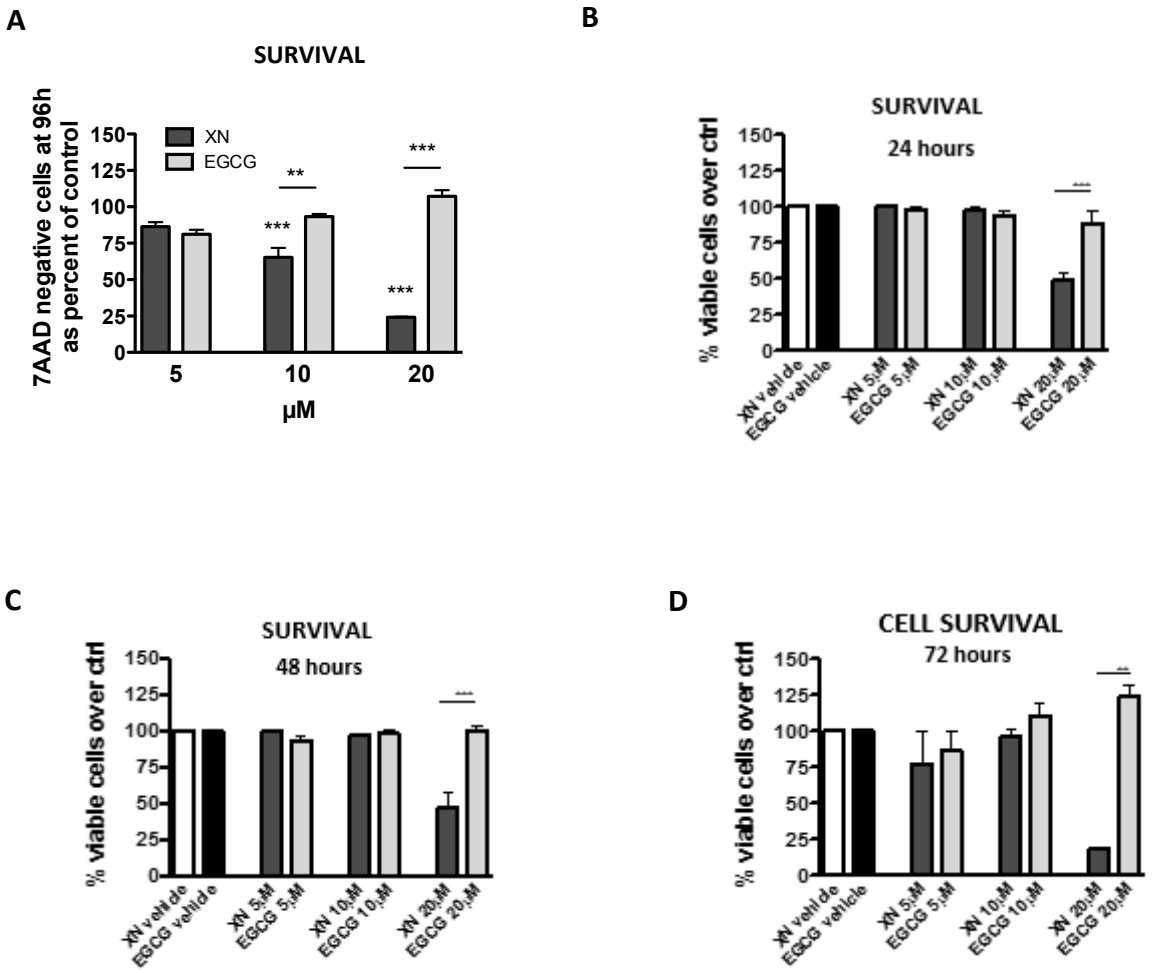

Figure 2. Apoptosis was measured on cells treated with 5, 10, 20 μM XN or 5, 10, 20 μM EGCG at 96 hours (A), 24h (γ), 48h (δ), 72h (ε) by 7AAD staining. 7ADD-negative (viable) cells were determined by FACS analyses and data reported as percent of untreated control.

We then evaluated the ability of XN and ECGC to interfere with key angiogenic functions, such as migration, invasion and the ability to form capillary-like networks on matrigel. Cells were pre-treated for 24h with XN or EGCG at doses ranging from 5 to 20 μM and migration, invasion and morphogenesis assays were performed as described in M&M. XN significantly reduced endothelial cell migration (Figure 3A) and invasion (Figure 3B).

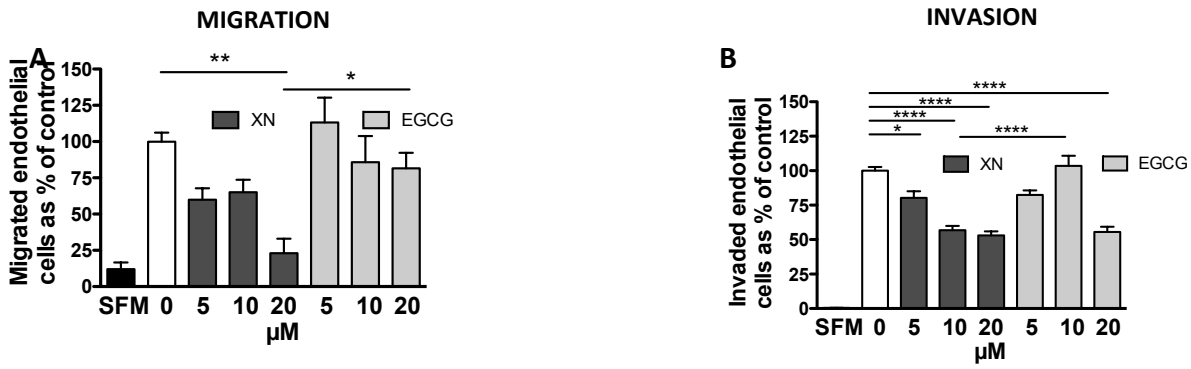

Figure 3. HUVEC cells were pre-treated for 24 hours with increasing concentrations (5, 10 and 20 μM) of XN or EGCG, then seeded in serum free medium in the upper compartment of Boyden chamber. (A) Cell migration (N=5) was measured at 6h and (B) invasion (N=10) at 24h.

The formation of the endothelial cell networks induced by 10% FBS was inhibited to a greater extent by XN as compared with EGCG (Figure 4A-B), confirming the more potent anti-angiogenic activities of XN.

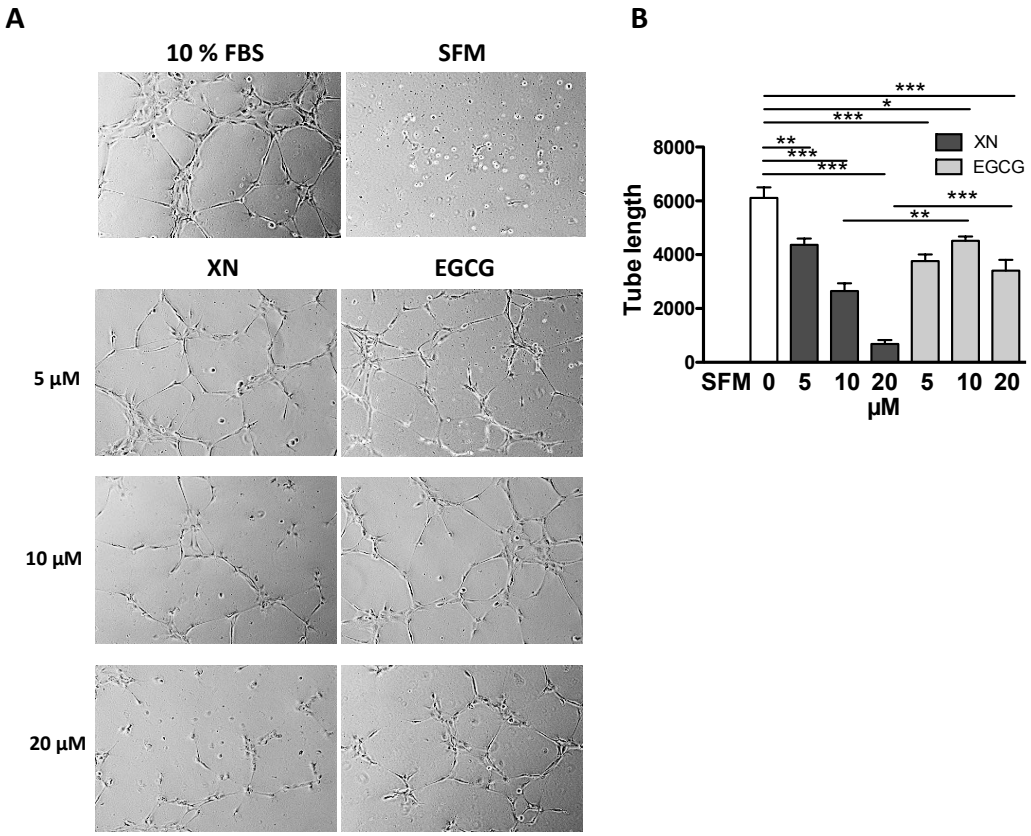

Figure 4: HUVEC were seeded on matrigel pre-coated plates and incubated for 6 hours in complete growth medium to monitor

morphogenesis. Microphotographs (A) were taken at 10X magnification (N ranging from 3 to 7) and capillary-like tube length was quantified (B) by the Angiogenesis analyzer ImageJ tool kit. All experiments were performed three times in duplicate. Data in H are expressed as the mean±SEM of the percentage of control values from independent experiments, with respect to control or as indicated by the bars (****p<0.0001; ***p<0.001; **p<0.01; *p<0.05; One-Way ANOVA).

Xanthohumol activates AMPK in endothelial cells

The anti-angiogenic activity of XN is exerted, at least in part, through the activation of NF-kB and AKT pathways [42, 43]. The involvement of AMPK in XN-induced inhibition of angiogenesis has never being investigated in endothelial cells. Thus, we explored how AMPK activation status changes in a time and dose dependent manner in response to XN. To this end, HUVEC were treated with increasing concentrations of XN for 1h (Figure 5A) or with 10 μM XN in a time ranging from 5 minutes to 1 hours (Figure 5B). We focused on XN at 10 μM or lower concentrations as it reduced endothelial cell functions without affecting cell viability or proliferation. AMPK activation was measured by analyzing the level of phospho-AMPK (Thr172) by western blot analysis. XN induced phosphorylation of AMPK in a dose-dependent manner, from 2.5 μM up to 10 μM (Figure 5A).

AMPK activation upon treatment with 10 μM XN was observed already at 5 minutes and increased up to 1h (Figure 5B). To elucidate whether XN-induced AMPK activation is of functional relevance, we also analyzed ACC (Acetyl-CoA Carboxylase) phosphorylation at Ser79, a downstream marker of AMPK activity. In line with our hypothesis, XN rapidly induced ACC phosphorylation in a dose-dependent manner, consistently with AMPK activation kinetic (Figure 5 A-B).

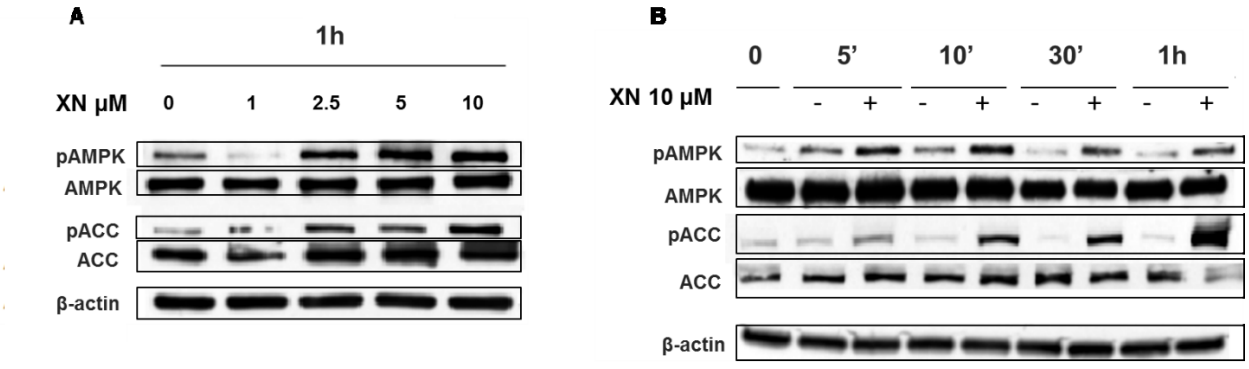

Figure 5. AMPK activation by XN in human endothelial cells. A–B. HUVEC were treated with increasing doses of XN (2.5-10μM) for 1 hour (A) or treated with 10μM XN at the indicated time points and lysed (B). AMPK activation was evaluated by determination of phospho-AMPK and phospho-ACC levels. AMPK, phospho-AMPK (Thr-172), ACC and phospho-ACC (Ser79) in all lysates were analyzed by western blot. Anti-β-actin antibody was used as loading control.

Xanthohumol anti-angiogenic effects are mediated by AMPK

Next we tested whether AMPK activation mediates the anti-angiogenic effects exerted by XN on endothelial cells. AMPK-α1 is the most abundant AMPK isoform expressed by endothelial cells [33]. We therefore down-regulated AMPK-α1 levels by short interfering RNA (siAMPKα1) in HUVEC. Silencing efficiency was over 70% and was verified by western blot analysis (Figure 6).

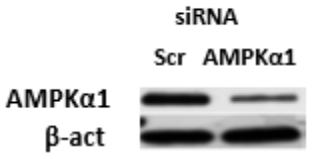

Figure 6. AMPK silencing efficiency. Silencing was evaluated by western blot analysis at 48 hours. Following 24h of transfection with siAMPKα1 or scramble siRNAs, HUVEC were treated with increasing concentrations of XN for 24h.

Cell migration, invasion and the ability to form capillary-like networks were then assessed (Figure 7A-D). As expected based on its already established role in angiogenesis, silencing of AMPKα1 reduced endothelial cell migration and invasion (Figure 7A-B). Further, following silencing of AMPK, XN administration only partially impaired migration (Figure 7A). After AMPK silencing, XN treatment failed to block and even promoted invasion (Figure 7B) and the ability to form capillary-like structures in HUVE cells (Figure 7C-D). In line with our hypothesis, these data indicate that XN-induced inhibition of angiogenesis requires the activation of AMPK.

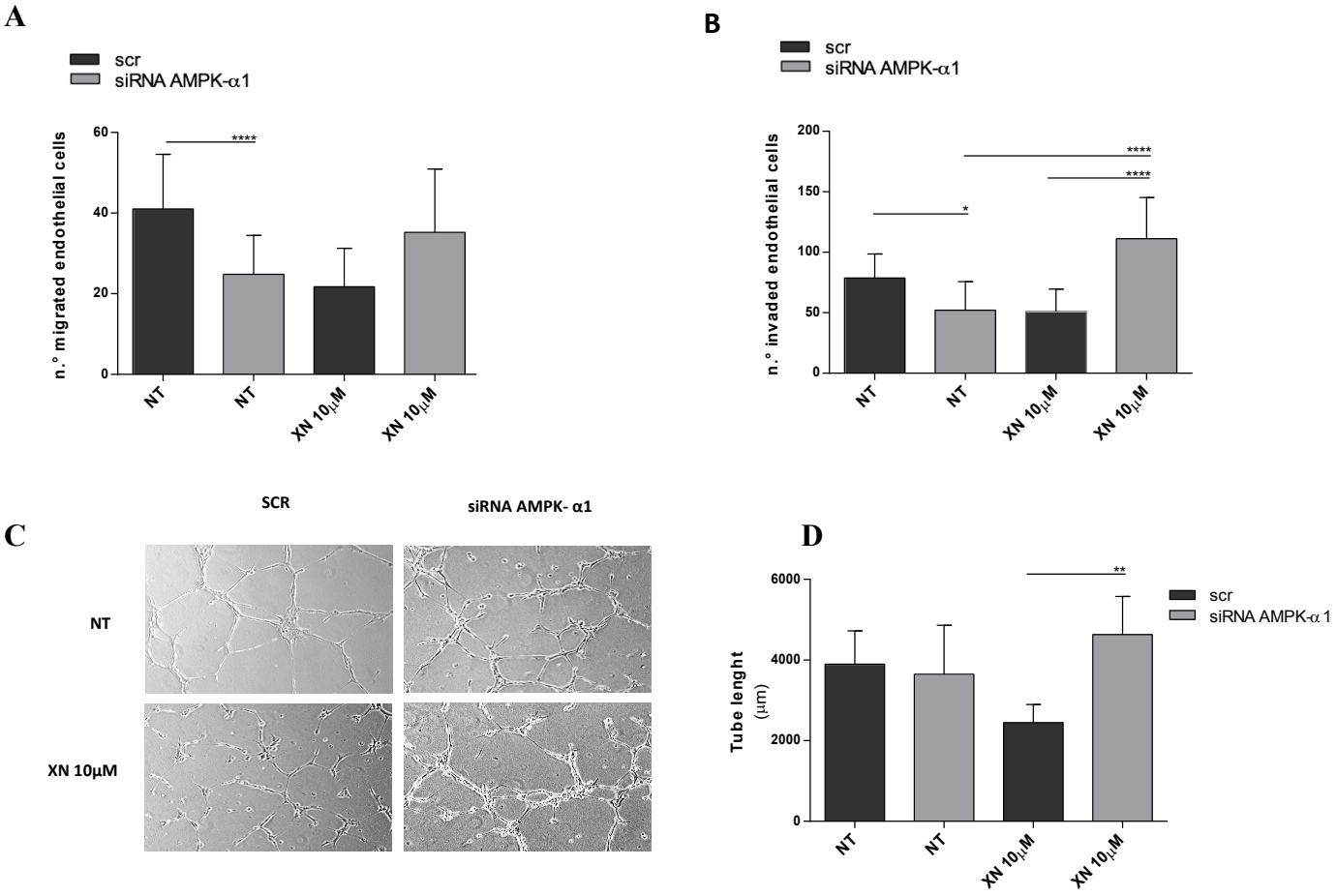

Figure 7. AMPK requirement for XN-induced anti-angiogenic effects. AMPKα1-specific siRNA (siRNA-α AMPK) was used to down-regulate AMPK in HUVEC. Scramble siRNA (scr) treated cells were used as controls. 24 hours after scr or siRNA AMPKα1 transfection, cells were treated with 10μM XN for 24h. Viable cells were used to perform migration and invasion assays. AMPKα1 downregulation restored XN-reduced HUVEC ability to migrate (A), invade (B) and organize in capillary-like structures (C). Microphotographs were taken at 10X magnification and representative endothelial tubes are shown. Capillary-like tube length was quantified by the Angiogenesis analyzer ImageJ tool (D). Data are expressed as mean±SEM of the percentage of control values from independent experiments. Statistical significance (****p<0.0001; ***p<0.001; **p<0.01; *p<0.05; One-Way ANOVA) are with respect to control or as indicated by the bars.

Xanthohumol activates AMPK in a LKB1 independent manner

Generally, AMPK is directly activated by the decreased ATP/AMP ratio, leading to activation of LKB1 [44]. To elucidate XN-induced molecular mechanisms upstream AMPK activation, we first assessed the contribution of the major molecular upstream regulator of AMPK in response to XN in in endothelial cells. Treatment of HUVEC with XN reduced the levels of LKB1-Ser428

phosphorylation, without affecting LKB1 expression levels (Fig. 8B) even though XN significantly reduced intra-cellular ATP levels in HUVEC (Figure 8A). This observation suggests that LKB1 is dispensable for XN-mediated AMPK activation in endothelial cells.

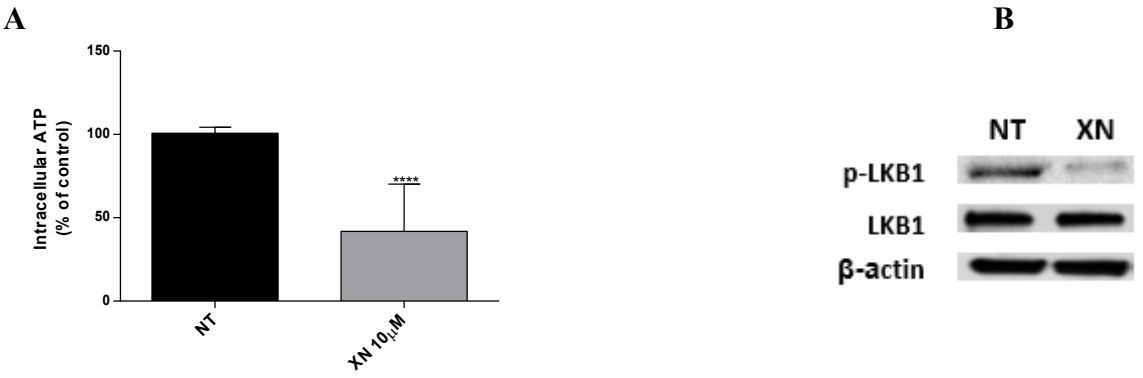

Figure 8. (A) ATP levels were measured in HUVEC treated with 10 µM XN for 1h. Data are expressed as the mean ± standard deviation from two independent experiments in triplicate (***p<0.001; **p<0.01; *p<0,05 Student's t-test; ns: not significant). (B) HUVEC were treated with 10 µM XN for 1 hour and LKB1 and phospho-LKB1 (Ser428) levels were analyzed by Western blotting.

CaMKKβ is the upstream activator of XN-mediated AMPK signaling

Since LKB1 did not activate AMPK in our context, we therefore investigated the involvement of CaMKKβ as alternative pathway in the XN-induced AMPK activation [45]. To this purpose, we treated HUVEC with STO-609, a selective CaMKKβ inhibitor, in presence or absence of XN or vehicle and we analyzed AMPK phosphorylation. Noticeably, treatment with STO-609 (20 µM) for 30 minutes prevented AMPK phosphorylation at Thr172 induced by XN (Fig. 9). These data suggest that XN activates AMPK through CaMKKβ.

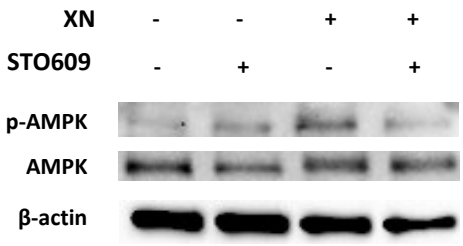

Figure 9. The role of CaMKKβ in XN-induced AMPK activation. A) Cells were pre-treated with the CaMKKβ inhibitor, STO-609 (20μM; 30 min), followed by treatment with 10 μM XN. Phospho-AMPK and total AMPK protein levels were analyzed by western blotting. Anti- β-actin antibody was used as loading control.

In line with these data, CaMKKβ inhibition by STO-609 prevented the reduction of tube formation following XN treatment (Figure 10A) and reverted XN inhibition of HUVEC migration (Fig. 10B). These data indicate that XN activates AMPK through CaMKKβ, which mediates XN-induced anti-angiogenic activities.

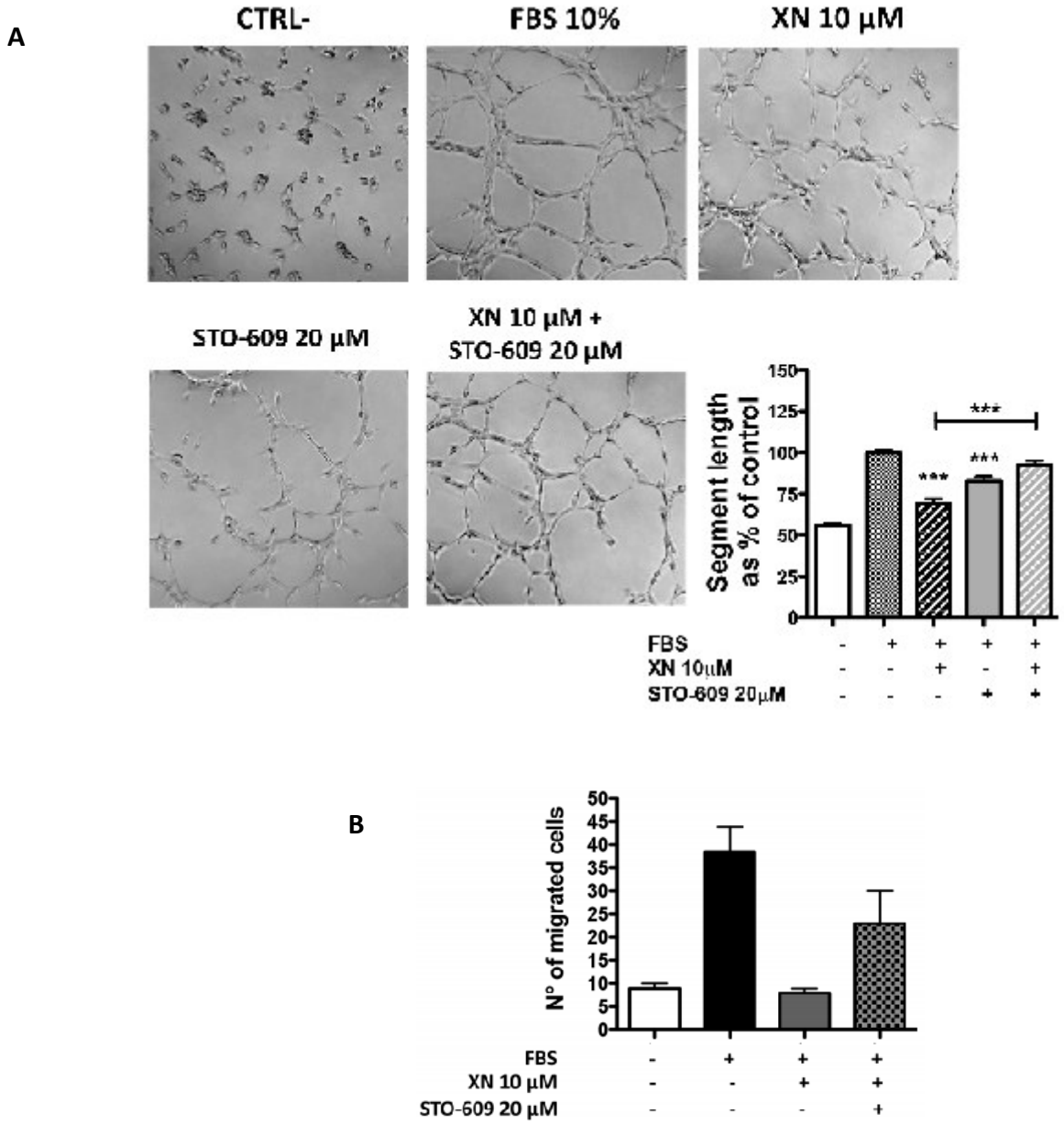

Figure 10. HUVE cells were pretreated with STO-609 (20 μM) for 30 and then treated with 10 μM XN, and then seeded for (A) matrigel morphogenesis assay or for (B) migration assay. Microphotographs were taken at 10X magnification, representative images are shown. Capillary-like tube length was quantified by Angiogenesis analyzer ImageJ tool kit. Data are expressed as mean±SEM of the percentage of control values from independent experiments. Statistical significance (****p<0.0001; ***p<0.001; **p<0.01; *p<0.05; One-Way ANOVA) are with respect to control or as indicated by the bars. HUVEC were seeded in serum free medium in the upper compartment of Boyden chamber. Cell migration was measured at 6h.

XN inhibits eNOS activation in an AMPK dependent manner

Activation of AMPK may result in phosphorylation and induction of eNOS [44]. Since eNOS is both a target of AMPK and a modulator of angiogenic functions, we evaluated the putative involvement of eNOS downstream to AMPK activation by XN, by analyzing eNOS phosphorylation on HUVEC. Surprisingly, administration of XN for 1h led to a reduction of eNOS phosphorylation at Ser1177 (Figure 11).

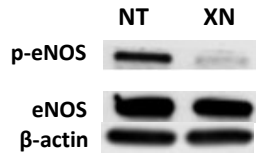

Figure 11. HUVEC were treated with 10 μM XN for 1 hour. Total and phospho-eNOS (Ser1177) were analysed by western blotting.

Since nitrite and nitrate anions are the final products of Nitric-oxide (NO) oxidation and their presence in the media reflects the endogenous eNOS activity, we quantified the concentration of nitrite by the Griess assay following XN administration. Treatment of HUVEC with XN strongly decreased NO levels at 12h as compared to untreated control, while NO levels were quite stable in controls in 12h time frame (Figure 12).

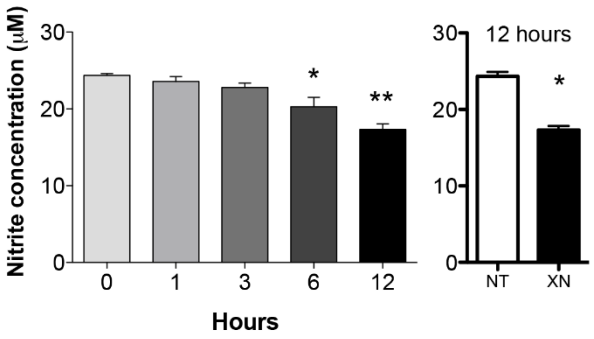

Figure 12. Nitrite concentration following XN treatment was measured in HUVEC treated with 10 μM XN at different times up to 12 hours. Data are expressed as the mean± standard deviation of values from two independent experiments (*p<0,01; Student's t-test).

To verify whether AMPK is involved in XN-induced reduction of eNOS activity, we analyzed eNOS phosphorylation by western blotting in HUVEC in presence of XN by using Compound C, an inhibitor of AMPK (Figure 13A), and by down-regulating AMPK-α1 expression with an AMPK-α1-specific siRNA (Figure 13B). Treatment with 20 μM Compound C inhibited basal eNOS phosphorylation and partially reverted XN-induced phospho-eNOS reduction (Fig. 13A). Likewise, siRNA transfection abolished XN-induced phospho-eNOS decrease (Fig. 13B). Overall these data indicate that XN induces a strong repression of eNOS activity and that AMPK mediates this mechanism.

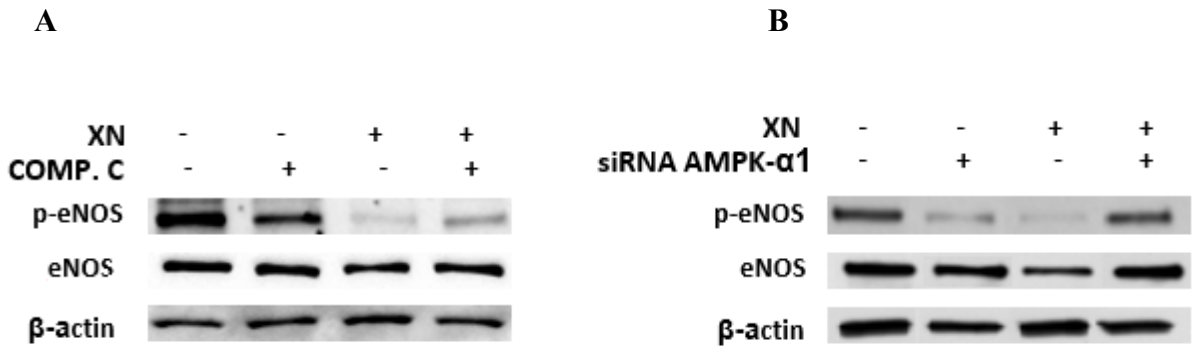

Figure 13. HUVEC were pre-treated with 20 μM AMPK-inhibitor Compound C for 30 min (A) or transfected with AMPKα1-specific siRNA for 48hours (B) then treated with 10 μM XN for 1 hour. Total and phospho-eNOS (Ser1177) were analyzed by western blotting. Anti- β-actin antibody was used as loading control.

XN independently modulates AMPK and AKT pathways

We have previously demonstrated that XN inhibits TNF-α-induced AKT phosphorylation in human endothelial cells [43]. AKT is a serine/threonine kinase supporting endothelial cell migration, with the ability to directly activate eNOS in an AMPK-dependent manner. AMPK and AKT are also responsible for the activation of the mTORC1 complex. AKT is activated by the phosphorylation on Thr308, following by the phosphorylation on Ser473. We therefore investigated the involvement of AKT pathway in the anti-angiogenic activity exerted by XN and we investigated the potential crosstalk with AMPK.

Treatment of HUVEC with 10μM XN for 1h induced a substantial decrease in Thr308-AKT phosphorylation, but failed to alter phospho-Ser473 levels (Fig. 14).

To confirm the effects of XN on AKT pathway, we evaluated the phosphorylation of mTOR at Ser2448 and activation of its down-stream target, p70S6K and 4EBP1. As shown in Figure 14, XN treatment decreased the phosphorylation of mTOR, p70S6K and 4EBP1, in accordance with the observed decrease in AKT phosphorylation at the same time points.

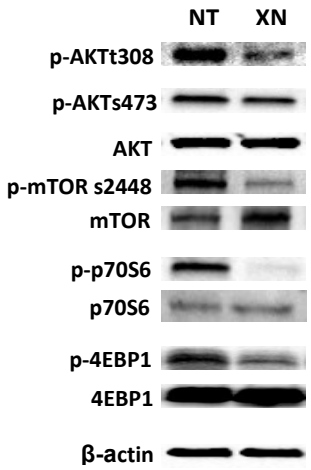

Figure 14. HUVEC were treated with 10 μM XN for 1 h and the phosphorylation of AKT and its downstream targets mTOR (Ser2448), p70S6k (Thr389), 4EBP1 (Thr37/46) was assessed by Western Blotting;

To evaluate the potential role of AMPK in XN-induced decrease of phospho-AKT levels, we inhibited AMPK activity using Compound C or AMPK-α1 siRNA in HUVEC in presence or absence of XN. Direct inhibition of AMPK by compound C or siRNA did not significantly influence AKT phosphorylation after XN treatment (Fig. 15 A-B).

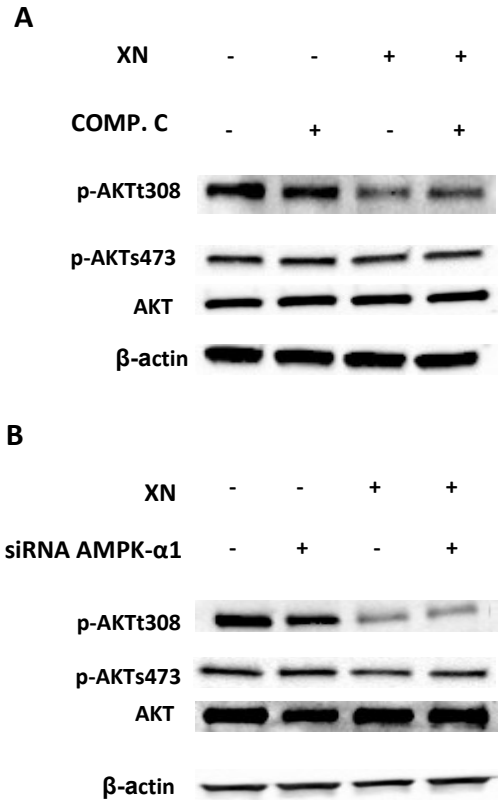

Figure 15. XN independently modulates AMPK and AKT activities. HUVEC were either pre-treated with 20 μM AMPK-inhibitor Compound C for 30 min (A) or transfected with AMPKα1- specific siRNA for 48h (B) then treated with 10 μM XN. AKT phosphorylation at Ser308 and Ser473 was analyzed by western blotting. Anti- β-actin antibody was used as loading control.

These data suggest that XN inhibits the AKT/mTOR pathway in addition to AMPK (Figure 16).

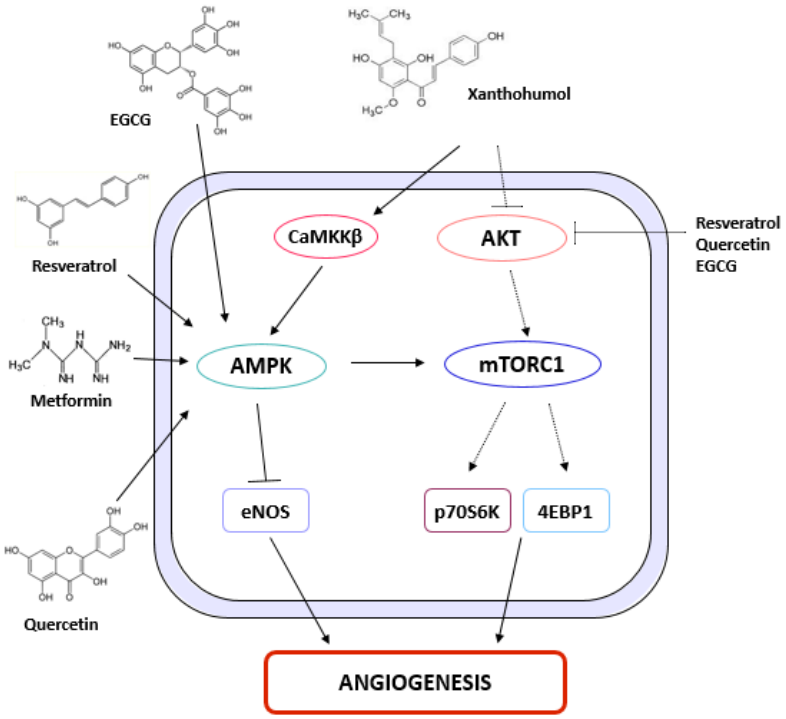

Figure 16. Representative illustration of XN activated pathways.

Synthesis of XN derivatives and their effects on HUVEC proliferation

Since the anti-angiogenic power of XN and the arising interest in the synthesis of new derived flavonoids for long-term and low toxic treatments, we decided to determine whether chemical modification of the XN-scaffold resulted in more effective inhibition of angiogenesis. Therefore, we developed a series of novel synthetic analogues of XN, compounds 2-14 (Table 2).

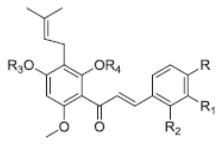

2-14

Compd	R	R_1	R_2	R_3	R_4
2	Cl	Cl	H	MOM	H
3	Cl	Cl	H	H	H
4	F	H	H	MOM	H
5	F	H	H	H	H
6	H	H	F	MOM	H
7	H	H	F	H	H
8	OCH_3	F	H	MOM	MOM
9	OCH_3	F	H	MOM	H
10	OCH_3	F	H	H	H
11	OCH_3	H	F	MOM	MOM
12	OCH_3	H	F	MOM	H
13	OCH_3	H	F	H	H
14	NO_2	H	H	MOM	H

Table 2. Synthetic derivatives of Xantohohumol. MOM, Partial methoxymethyl. From *"Synthesis and antiangiogenic activity study of new hop chalcone Xanthohumol analogues."* Nuti et al., European Journal of Medicinal Chemistry, 2107.

Among the newly synthesized compounds, listed in Table 1, only compounds 2 and 3 were considered unfit for testing due to some solubility issues. Thus, we tested compounds from 4 to 14 for cytotoxicity on HUVEC. We treated HUVEC with increasing doses of XN (the positive control for anti-angiogenesis effects) and its derivatives ranging from 1 μM to 20 μM in a time lapse from 24 to 96 hours. Cell viability was then assessed by the MTT assay.

As shown in figure 17, we observed that most of the XN derivatives inhibited HUVEC proliferation in a dose and time dependent manner.

At the 10 μM concentration and at the 96 h time point, several derivatives statistically inhibited HUVEC viability as compared to XN alone: in particular compounds 8 and 11. Noteworthy, derivative 14 was the only compound to show toxicity at 10 μM dose, as also indicated by increased apoptosis on HUVEC (data not shown). Finally, compound 12 was not able to inhibit endothelial cell growth, as well as compound 10.

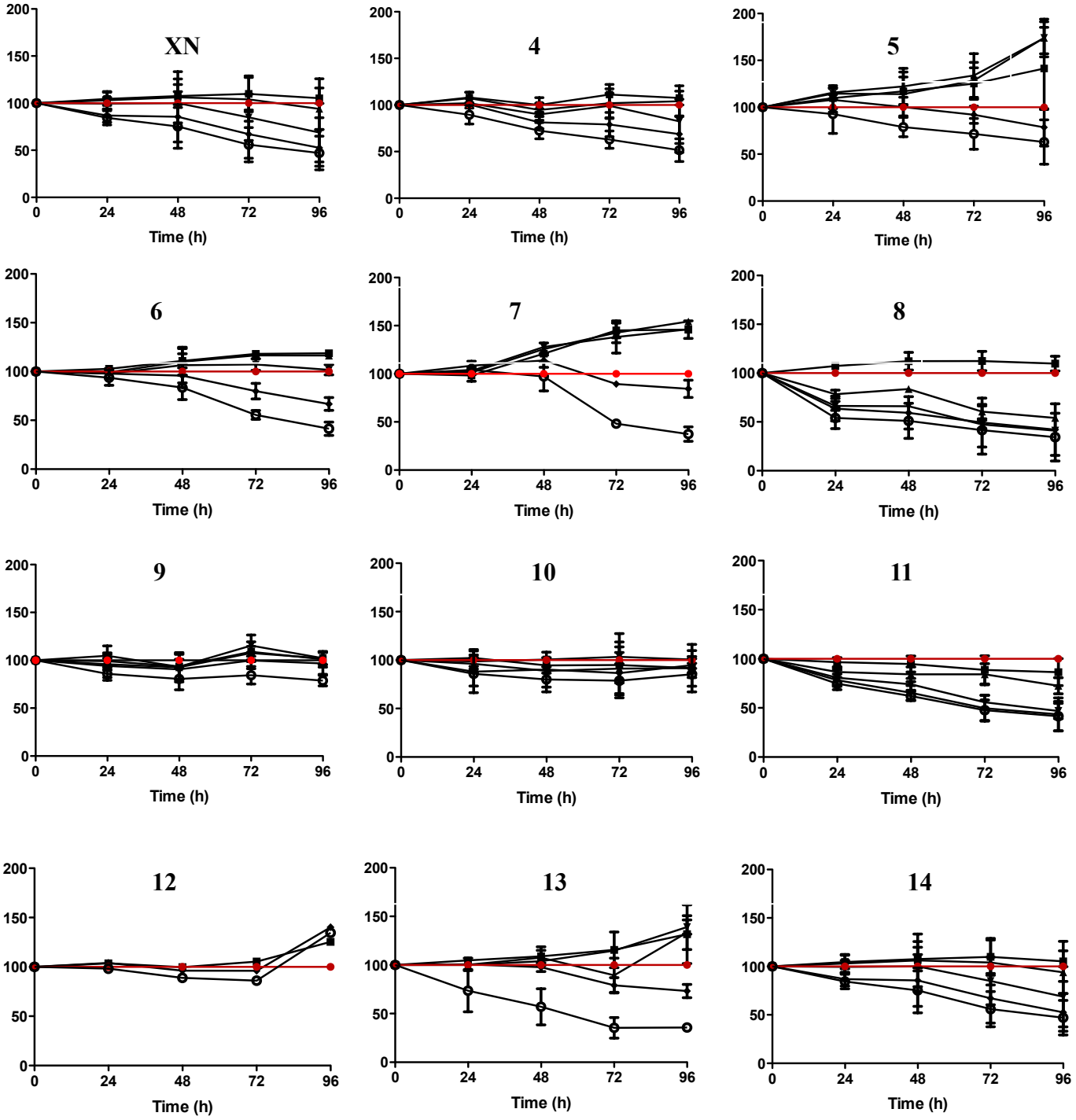
XN
4
5
6
7
8
9
10
11
12
13
14
Time (h)
0
24
48
72
96
50
100
150
200
Vehicle
1μM
2.5 μM
5μM
10μM
20μM

Figure 17. Effects of XN derivatives on HUVEC proliferation. XN and XN derivatives interfere with endothelial cell (HUVEC) proliferation, as assessed by MTT assay. "Vehicle" indicates cells treated with vehicle (DMSO in the medium). From *"Synthesis and antiangiogenic activity study of new hop chalcone Xanthohumol analogues."* Nuti et al., European Journal of Medicinal Chemistry, 2107.

We also calculated the concentration that inhibits cell proliferation by 50%, the IC50 value after 96 hours of treatment with each compounds. In order to obtain not confounding results depending on the strong toxicity, we exclude from the analysis data at 20μM. IC50 values were calculated by the software GraphPadPrism7. As expected, the most effective compounds were 8, 11 and 13 (figure 18).

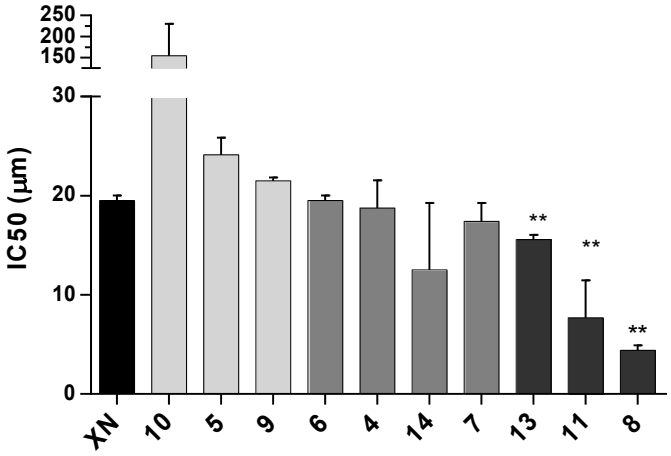

Figure 18. IC50 values at 96h. Data were compared to XN as control (**p<0,001; Student's t-test).

Finally we evaluated the ability of our compounds to induce cell apoptosis or affect the angiogenic features (invasion, migration and ability to form capillary-like structures). Data were collected in the paper *"Synthesis and antiangiogenic activity study of new hop chalcone Xanthohumol analogues",* Nuti et al., European Journal of Medicinal Chemistry, 2107.

DISCUSSION

In the last few years, great efforts have been addressed to the anti-tumor and anti angiogenic activities of natural products extracted from vegetables, plants, spices, herbs and fruits such as carotenoids, polyphenols and terpenoids, and their synthetic counterparts [63]. These compounds may be of particular interest in clinical applications as they are easily available, often included in every day-diets and display low toxicity. Many of these compounds show anti-oxidant [12], anti-proliferative, and pro-apoptotic effects on a variety of cancer cells, including leukemia, prostate, breast, colon, brain, melanoma, and pancreatic tumors [18, 46, 47, 48].

Flavonoids are the most abundant polyphenols in dietary components and can be found in a variety of foods and vegetables. Many works reported the anti-tumor activity of flavonoids, whose anti-tumor effects affect both tumor cells and surrounding microenvironment. In particular, there are several reports demonstrating the anti-angiogenic activities of many flavonoids. Xanthohumol is among the chemo-preventive natural compounds with the ability to target the tumor vasculature. *In vitro*, we and others have shown that XN negatively interferes with endothelial cell growth, migration, invasion and the ability to form a network of tubular-like structures [16, 42]. *In vivo*, XN reduces the number of vessels in matrigel plugs and wound healing assays [13, 14] and inhibits tumor-associated angiogenesis in different contexts [16, 43]. In this work we confirmed the ability of XN to inhibit human endothelial cells functions and we showed that XN anti-angiogenic related activities are stronger than those exerted by Epigallocatechin-3-gallate (EGCG), a well-characterized anti-angiogenic natural compound found in green tea. We demonstrated that AMPK is a target of XN and a crucial mediator of its anti-angiogenic effects in human endothelial cells, providing relevant details on the molecular mechanism and identifying both intermediate and downstream players.

First, we confirmed the ability of XN to decrease endothelial cell functions *in vitro*. We used different XN dosages and time points and focused on 10 μM, a dose sufficient to decrease endothelial cell migration, invasion and tube formation without significantly reducing cell proliferation or viability.

This is consistent with other *in vitro* studies showing a strong reduction of cell viability with 20μM XN [16]. At the same doses, XN is more effective than EGCG, which is a known potent preventive agent for tumor invasion and angiogenesis [49].

It has been shown that XN exerts its anti-angiogenic effects by inhibiting NF-κB activation and IκBα phosphorylation, and subsequently blocking NF-κB translocation to the nucleus [42]. In addition, XN inhibits phosphorylation of endothelial AKT [43]. In the last few years, AMPK pathway has emerged as another molecular pathway playing a key role in angiogenesis. AMPK activation is associated with the inhibition of angiogenesis induced by natural product-derived compounds used in clinical settings, such as metformin [34, 47, 48], salicylate (the active form of aspirin) [50], EGCG [32], quercetin [11] and resveratrol [12]. Our data showed that XN activates AMPK and that AMPK activation is necessary for the anti-angiogenic effects induced by XN, as well as the downregulation of AMPK reverts endothelial cell ability to migrate and invade upon treatment with XN. To the best of our knowledge, this is the first report demonstrating that AMPK is a functional target of XN in human endothelial cells. This is in line with recent observations showing that XN activates AMPK in mouse liver cells and mouse embryonic fibroblasts [51, 52]. We also investigated the mechanisms through which XN leads to AMPK activation. Genetic and biochemical evidence supports the idea that LKB1 is the major AMPK-kinase regulator in several mammalian cell types in response to changes in the AMP/ATP ratio [25, 26, 27]. Pharmacological drugs decreasing ATP levels lead to a reduction in the ATP:AMP ratio, which finally activates AMPK [23, 53]. Since XN interferes with ATP production [17] and ATP is required for tubulogenesis processes at early time points [54], it has the potential to activate AMPK through LKB1 in our system as well. However, we found that XN decreases LKB1 phosphorylation instead of inducing it, excluding a role for LKB1 in AMPK activation by XN. The imbalance of AMP:ATP and ADP:ATP ratio can also activate other kinases, such as CaMKKβ [55], a well-known regulator of AMPK. We therefore analyzed CaMKKβ activation and our data support its involvement as the main kinase responsible for AMPK activation in endothelial cells following treatment with XN. This is in line with the ability of XN to increase intra-cellular calcium observed

in other systems [18, 56]. Moreover, CaMKKβ inhibition by STO-609 partially impaired XN mediated anti-angiogenic activity on HUVEC *in vitro*. It is reported that AMPK activation in endothelial cells leads to the phosphorylation of endothelial nitric oxide synthase (eNOS) [37, 44]. Interestingly, we observed a reduction of activated eNOS in XN treated cells, accompanied by a decrease in the release of NO. Other reports show XN ability to inhibit NO production by decreasing iNOS (inducible-NOS) activity or expression [57]. Moreover, Negrao and colleagues demonstrated that in rats XN ingestion decreased NO release (77.06%) [58]. Our data are consistent with these findings.

Extensive data suggest the existence of a cross-talk between AMPK and AKT signaling in angiogenesis [35]. A mutual suppression of AKT and AMPK pathways by chemo-preventive agents, such as quercetin, has been reported [59]. Resveratrol suppresses PI3K signaling by binding to the ATP-binding site of PI3K [60]. In a previous work, we have shown that XN inhibits AKT activation in endothelial cells, possibly through the inhibition of the PI3K pathway [42]. AKT is activated by phosphorylation of Ser473 and Thr308, by mTORC2 and PI3K, respectively. Here we observed that XN decreases AKT phosphorylation at Thr308. In contrast, following treatment with XN, we did not observe any modulation of Ser473 phosphorylation on AKT [61]. Consistent with XN-induced inhibition of PI3K/AKT/mTORC1 axis, we found inhibition of mTOR pathway in endothelial cells treated with XN. Our data suggest that XN mechanism of action in endothelial cells involves two distinct molecular cascades. On one hand, XN activates CaMMK/AMPK/eNOS axis. On the other hand, XN inhibits AKT/mTORC1 axis. These two mechanisms of action seem to proceed simultaneously, leading to inhibition of angiogenesis (Figure 16).

Overall, our study elucidates the molecular mechanisms of the anti-angiogenic activity of XN. Given the ability of tumors to resist anti-angiogenic therapies by activating alternative pathways, there is an increasing need to therapeutically block tumor angiogenesis by targeting multiple anti-angiogenic pathways [62]. Polyphenols, such as EGCG, affect the activity of multiple pathways and mediators involved in the carcinogenesis process and were previously suggested as valuable inhibitors of cancer

cell growth and angiogenesis [64]. Our results provide evidences that XN might be a more potent and suitable compound for the inhibition of angiogenesis, both in therapeutic and prevention settings, acting on the AMPK and the AKT signaling.

In order to develop more effective compounds offering the possibility of long-term low toxic treatments substantial attention has been addressed to the synthesis of new derived flavonoids. Among them, chalcones is a class of polyphenolic compounds that exhibit anti-angiogenic properties and a series of XN analogues has been recently synthesized by Zhang et al. These compounds shown to have toxicity toward HeLa cells by inhibiting the selenoprotein thioredoxin reductases (TrxRs) [65]. Here, we compared the antiangiogenic effects of XN against a new class of XN analogues *in vitro*, where HUVEC were used as a model for cell proliferation, apoptosis, cell adhesion, migration, invasion and formation of capillary-like structures. Our results suggest that modification of the chemical structure of XN, changes the ability of derivatives to affect angiogenic features. Thus the importance of understanding the effects of each substitution. Among all synthesized compounds the best activity results were exhibited by compound 13, which was the strongest inhibitor of cell adhesion, migration and ability to organize in network, even compared to XN. Overall, these preliminary data highlight that the newly synthesized XN derivatives may represent relevant compounds able to affect crucial steps of angiogenesis. Further studies must be conducted to assess the pharmacokinetic properties of the most promising compounds in comparison with XN**.**

In conclusion, we confirmed the role of XN as powerful anti-angiogenic molecule and its activity is stronger than EGCG. Moreover we unveiled for the first time that XN activated AMPK via CaMMKβ in a LKB1 independent manner. Further we elucidated the XN downstream mechanism and suggested the existence of two independent pathways by which XN exerts its antiangiogenic effect: the AMPK/eNOS axis and the AKT signaling. Finally, we identified new powerful anti-angiogenic molecules within a series of novel synthetic analogues of XN.

REFERENCES

1. Hanahan D and Weinberg RA. Hallmarks of cancer: the next generation. Cell. 2011; 144:646-674.

2. Folkman J. Angiogenesis. Annu Rev Med. 2006; 57:1-18.

3. Kerbel RS. Tumor angiogenesis. N Engl J Med. 2008; 358:2039-2049.

4. Albini A and Sporn MB. The tumour microenvironment as a target for chemoprevention. Nat Rev Cancer. 2007; 7:139-147.

5. Albini A, Tosetti F, Benelli R and Noonan DM. Tumor inflammatory angiogenesis and its chemoprevention. Cancer Res. 2005; 65:10637-10641.

6. Rossi T, Gallo C, Bassani B, Canali S, Albini A and Bruno A. Drink your prevention: beverages with cancer preventive phytochemicals. Pol Arch Med Wewn. 2014; 124:713-722.

7. Ferrari N, Tosetti F, De Flora S, Donatelli F, Sogno I, Noonan DM and Albini A. Diet-derived phytochemicals: from cancer chemoprevention to cardio-oncological prevention. Curr Drug Targets. 2011; 12:1909-1924.

8. Vigneri R, Goldfine ID. Role of metformin in treatment of diabetes mellitus. Diabetes Care. 1987;10:118-22.

9. Antonio Nicolucci. Recommending Aspirin for Primary Prevention in Diabetic Patients: What May We Conclude from the Data? Ther Adv Chronic Dis. 2011; 2: 157–160.

10. Hardie DG. AMPK: a target for drugs and natural products with effects on both diabetes and cancer. Diabetes. 2013; 62:2164-2172.

11. Wu J, Xu X, Li Y, Kou J, Huang F, Liu B and Liu K. Quercetin, luteolin and epigallocatechin gallate alleviate TXNIP and NLRP3-mediated inflammation and apoptosis with regulation of AMPK in endothelial cells. Eur J Pharmacol. 2014; 745:59-68.

12. Guo H, Chen Y, Liao L and Wu W. Resveratrol protects HUVECs from oxidized-LDL induced

oxidative damage by autophagy upregulation via the AMPK/SIRT1 pathway. Cardiovasc Drugs Ther. 2013; 27:189-198.

13. Monteiro R, Calhau C, Silva AO, Pinheiro-Silva S, Guerreiro S, Gärtner F, Azevedo I and Soares R. Xanthohumol inhibits inflammatory factor production and angiogenesis in breast cancer xenografts. J Cell Biochem. 2008; 104:1699-1707

14. Gerhauser C, Alt A, Heiss E, Gamal-Eldeen A, Klimo K, Knauft J, Neumann I, Scherf HR, Frank N, Bartsch H and Becker H. Cancer chemopreventive activity of Xanthohumol, a natural product derived from hop. Mol Cancer Ther. 2002; 1:959-969.

15. Verzele M, de Keukeleire D. Chemistry and Analysis of Hop and Beer Bitter Acids. Elsevier. 1991.

16. Negrão R, Costa R, Duarte D, Gomes TT, Coelho P, Guimarães JT, Guardão L, Azevedo I and Soares R. Xanthohumol-supplemented beer modulates angiogenesis and inflammation in a skin wound healing model. Involvement of local adipocytes. J Cell Biochem. 2012; 113:100-109.

17. Strathmann J, Klimo K, Sauer SW, Okun JG, Prehn JH and Gerhauser C. Xanthohumol-induced transient superoxide anion radical formation triggers cancer cells into apoptosis via a mitochondria-mediated mechanism. FASEB J. 2010; 24:2938-2950.

18. Koo JH, Kim HT, Yoon HY, Kwon KB, Choi IW, Jung SH, Kim HU, Park BH and Park JW. Effect of xanthohumol on melanogenesis in B16 melanoma cells. Exp Mol Med. 2008; 40:313-319.

19. Legette L, Karnpracha C, Reed RL, Choi J, Bobe G, Christensen JM. Human pharmacokinetics of xanthohumol, an antihyperglycemic flavonoid from hops. Mol Nutr Food Res. 2014; 58:248-55.

20. Legette LC, Reed R, Miranda C, Karnpracha C, Christensen JM, Stevens JF. Human pharmacokinetics of xanthohumol, a flavonoid from hops with anti-diabetic activity. The FASEB Journal. 2013; 27:1103.

21. Mihaylova MM and Shaw RJ. The AMPK signalling pathway coordinates cell growth, autophagy and metabolism. Nat Cell Biol. 2011; 13:1016-1023.

22. Hardie DG. AMP-activated protein kinase: an energy sensor that regulates all aspects of cell function. Genes Dev. 2011; 25:1895-1908.

23. Hardie DG, Schaffer BE and Brunet A. AMPK: An Energy- Sensing Pathway with Multiple Inputs and Outputs. Trends Cell Biol. 2016; 26:190-201.

24. Alexander A and Walker CL. The role of LKB1 and AMPK in cellular responses to stress and damage. FEBS Lett. 2011; 585:952-957.

25. Shaw RJ, Kosmatka M, Bardeesy N, Hurley RL, Witters LA, DePinho RA and Cantley LC. The tumor suppressor LKB1 kinase directly activates AMP-activated kinase and regulates apoptosis in response to energy stress. Proc Natl Acad Sci U S A. 2004; 101:3329-3335.

26. Woods A, Johnstone SR, Dickerson K, Leiper FC, Fryer LG, Neumann D, Schlattner U, Wallimann T, Carlson M and Carling D. LKB1 is the upstream kinase in the AMP-activated protein kinase cascade. Curr Biol. 2003; 13:2004-2008.

27. Hawley SA, Boudeau J, Reid JL, Mustard KJ, Udd L, Mäkelä TP, Alessi DR and Hardie DG. Complexes between the LKB1 tumor suppressor, STRAD alpha/beta and MO25 alpha/beta are upstream kinases in the AMP-activated protein kinase cascade. J Biol. 2003; 2:28.

28. Gormand A, Henriksson E, Strom K, Jensen TE, Sakamoto K and Goransson O. Regulation of AMP-activated protein kinase by LKB1 and CaMKK in adipocytes. J Cell Biochem. 2011; 112:1364-1375.

29. Hawley SA, Selbert MA, Goldstein EG, Edelman AM, Carling D and Hardie DG. 5'-AMP activates the AMP-activated protein kinase cascade, and Ca2+/calmodulin activates the calmodulin-dependent protein kinase I cascade, via three independent mechanisms. J Biol Chem. 1995; 270:27186-27191.

30. Herrero-Martín G, Høyer-Hansen M, García-García C, Fumarola C, Farkas T, López-Rivas A et al. TAK1 activates AMPK-dependent cytoprotective autophagy in TRAIL-treated epithelial cells. EMBO J. 2009; 28:677-85.

31. Zippel N, Malik RA, Frömel T, Popp R, Bess E et al. Transforming growth factor-β-activated kinase 1 regulates angiogenesis via AMP-activated protein kinase-α1 and redox balance in endothelial cells. Arterioscler Thromb Vasc Biol. 2013; 33:2792-9.

32. Reiter CE, Kim JA and Quon MJ. Green tea polyphenol epigallocatechin gallate reduces endothelin-1 expression and secretion in vascular endothelial cells: roles for AMP-activated protein kinase, Akt, and FOXO1. Endocrinology. 2010; 151:103-114.

33. Fisslthaler B and Fleming I. Activation and signaling by the AMP-activated protein kinase in endothelial cells. Circ Res. 2009; 105:114-127.

34. Dallaglio K, Bruno A, Cantelmo AR, Esposito AI, Ruggiero L, Orecchioni S, Calleri A, Bertolini F, Pfeffer U, Noonan DM and Albini A. Paradoxic effects of metformin on endothelial cells and angiogenesis. Carcinogenesis. 2014; 35:1055-1066.

35. Nagata D, Mogi M and Walsh K. AMP-activated protein kinase (AMPK) signaling in endothelial cells is essential for angiogenesis in response to hypoxic stress. J Biol Chem. 2003; 278:31000-31006.

36. Morrow VA, Foufelle F, Connell JM, Petrie JR, Gould GW and Salt IP. Direct activation of AMP-activated protein kinase stimulates nitric-oxide synthesis in human aortic endothelial cells. J Biol Chem. 2003; 278:31629-31639.

37. Dimmeler S and Zeiher AM. Nitric oxide-an endothelial cell survival factor. Cell Death Differ. 1999; 6:964-968.

38. Albini A and Benelli R. The chemoinvasion assay: a method to assess tumor and endothelial cell invasion and its modulation. Nat Protoc. 2007; 2:504-511.

39. Albini A, Iwamoto Y, Kleinman HK, Martin GR, Aaronson SA, Kozlowski JM and McEwan RN. A rapid in vitro assay for quantitating the invasive potential of tumor cells. Cancer Res. 1987; 47:3239-3245.

40. Carpentier G. Contribution: Angiogenesis Analyzer. ImageJ News. 2012.

41. Benelli R, Venè R, Bisacchi D, Garbisa S and Albini A. Anti-invasive effects of green tea polyphenol epigallocatechin-3- gallate (EGCG), a natural inhibitor of metallo and serine proteases. Biol Chem. 2002; 383:101-105.

42. Dell'Eva R, Ambrosini C, Vannini N, Piaggio G, Albini A and Ferrari N. AKT/NF-kappaB inhibitor xanthohumol targets cell growth and angiogenesis in hematologic malignancies. Cancer. 2007; 110:2007-2011.

43. Albini A, Dell'Eva R, Vené R, Ferrari N, Buhler DR, Noonan DM and Fassina G. Mechanisms of the antiangiogenic activity by the hop flavonoid xanthohumol: NF-kappaB and Akt as targets. FASEB J. 2006; 20:527-529.

44. Thors B, Halldórsson H and Thorgeirsson G. eNOS activation mediated by AMPK after stimulation of endothelial cells with histamine or thrombin is dependent on LKB1. Biochim Biophys Acta. 2011; 1813:322-331.

45. Carling D, Sanders MJ and Woods A. The regulation of AMP-activated protein kinase by upstream kinases. Int J Obes (Lond). 2008; 32:S55-59.

46. Quader ST, Bello-DeOcampo D, Williams DE, Kleinman HK and Webber MM. Evaluation of the chemopreventive potential of retinoids using a novel in vitro human prostate carcinogenesis model. Mutat Res. 2001; 496:153-161.

47. Orecchioni S, Reggiani F, Talarico G, Mancuso P, Calleri A, Gregato G, Labanca V, Noonan DM, Dallaglio K, Albini A and Bertolini F. The biguanides metformin and phenformin inhibit angiogenesis, local and metastatic growth of breast cancer by targeting both neoplastic and

microenvironment cells. Int J Cancer. 2015; 136:E534-544.

48. Talarico G, Orecchioni S, Dallaglio K, Reggiani F, Mancuso P, Calleri A, Gregato G, Labanca V, Rossi T, Noonan DM, Albini A and Bertolini F. Aspirin and atenolol enhance metformin activity against breast cancer by targeting both neoplastic and microenvironment cells. Sci Rep. 2016; 6:18673.

49. Ouchi N, Shibata R and Walsh K. AMP-activated protein kinase signaling stimulates VEGF expression and angiogenesis in skeletal muscle. Circ Res. 2005; 96:838-846.

50. Hawley SA, Fullerton MD, Ross FA, Schertzer JD, Chevtzoff C, Walker KJ, Peggie MW, Zibrova D, Green KA, Mustard KJ, Kemp BE, Sakamoto K, Steinberg GR and Hardie DG. The ancient drug salicylate directly activates AMP-activated protein kinase. Science. 2012; 336:918-922.

51. Doddapattar P, Radović B, Patankar JV, Obrowsky S, Jandl K, Nusshold C, Kolb D, Vujić N, Doshi L, Chandak PG, Goeritzer M, Ahammer H, Hoefler G, Sattler W and Kratky D. Xanthohumol ameliorates atherosclerotic plaque formation, hypercholesterolemia, and hepatic steatosis in ApoE-deficient mice. Mol Nutr Food Res. 2013; 57:1718-1728.

52. Zimmermann K, Baldinger J, Mayerhofer B, Atanasov AG, Dirsch VM and Heiss EH. Activated AMPK boosts the Nrf2/HO-1 signaling axis-A role for the unfolded protein response. Free Radic Biol Med. 2015; 88:417-426.

53. Kemp BE, Stapleton D, Campbell DJ, Chen ZP, Murthy S, Walter M, Gupta A, Adams JJ, Katsis F, van Denderen B, Jennings IG, Iseli T, Michell BJ and Witters LA. AMP-activated protein kinase, super metabolic regulator. Biochem Soc Trans. 2003; 31:162-168.

54. Tahanian E, Peiro S and Annabi B. Low intracellular ATP levels exacerbate carcinogen-induced inflammatory stress response and inhibit in vitro tubulogenesis in human brain endothelial cells. J Inflamm Res. 2011; 4:1-10.

55. Chung JH, Manganiello V and Dyck JR. Resveratrol as a calorie restriction mimetic:

therapeutic implications. Trends Cell Biol. 2012; 22:546-554.

56. Lee YM, Hsieh KH, Lu WJ, Chou HC, Chou DS, Lien LM, Sheu JR and Lin KH. Xanthohumol, a Prenylated Flavonoid from Hops (Humulus lupulus), Prevents Platelet Activation in Human Platelets. Evid Based Complement Alternat Med. 2012; 2012:852362.

57. Zhao F, Nozawa H, Daikonnya A, Kondo K and Kitanaka S. Inhibitors of nitric oxide production from hops (Humulus lupulus L.). Biol Pharm Bull. 2003; 26:61-65.

58. Negrão R, Incio J, Lopes R, Azevedo I and Soares R. Evidence for the Effects of Xanthohumol in Disrupting Angiogenic, but not Stable Vessels. Int J Biomed Sci. 2007; 3:279-286.

59. Lee YK and Park OJ. Regulation of mutual inhibitory activities between AMPK and Akt with quercetin in MCF-7 breast cancer cells. Oncol Rep. 2010; 24:1493-1497.

60. Frojdo S, Cozzone D, Vidal H and Pirola L. Resveratrol is a class IA phosphoinositide 3-kinase inhibitor. Biochem J. 2007; 406:511-518.

61. Liu M, Wilk SA, Wang A, Zhou L, Wang RH, Ogawa W, Deng C, Dong LQ and Liu F. Resveratrol inhibits mTOR signaling by promoting the interaction between mTOR and DEPTOR. J Biol Chem. 2010; 285:36387-36394.

62. Scott EN, Gescher AJ, Steward WP and Brown K. Development of dietary phytochemical chemopreventive agents: biomarkers and choice of dose for early clinical trials. Cancer Prev Res. 2009; 2:525-530.

63. Sogno I, Vannini N, Lorusso G, Cammarota R, Noonan DM, Generoso L, Sporn MB and Albini A. Anti-angiogenic activity of a novel class of chemopreventive compounds: oleanic acid terpenoids. Recent Results Cancer Res. 2009; 181:209-212

64. Masuelli L, Di Stefano E, Fantini M, Mattera R, Benvenuto M, Marzocchella L, Sacchetti P, Focaccetti C, Bernardini R, Tresoldi I, Izzi V, Mattei M, Frajese GV, Lista F, Modesti A and Bei R. Resveratrol potentiates the in vitro and in vivo anti-tumoral effects of curcumin in head and neck

carcinomas. Oncotarget. 2014; 5:10745-10762

65. Zhang B, Duan D, Ge C, Yao J, Liu Y, Li X, Fang J. Synthesis of xanthohumol analogues and discovery of potent thioredoxin reductase inhibitor as potential anticancer agent. J Med Chem. 2015;

SESSION II

DEC1 PROMOTES PAPILLARY THYROID CARCINOMAS AGGRESSIVENESS BY INTERPLAY WITH NOTCH1

INTRODUCTION

Thyroid Carcinomas

Thyroid cancers are the most common malignancies of the endocrine system and their incidence has increased significantly over recent years worldwide. It occurs at all age, mainly over 40 years, and women are more susceptible than men [1].

The thyroid gland is composed of two major cell types: the thyrocytes and the C cells (figure1). Thyrocytes are epithelial cells responsible for production of thyroid hormone. C cells, also called parafollicular cells, are neuroendocrine cells responsible for the secretion of calcitonin, a hormone involved in the calcium homeostasis. C cells appear as group of cells intermingled between the thyroid follicles.

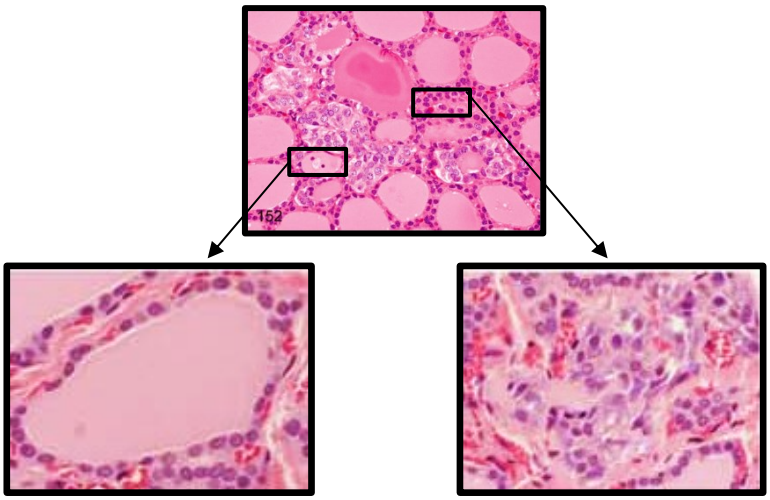

Figure 1. Thyroid tissue. On the left a picture of thyrocytes, on the ride C cells.

The majority of thyroid neoplasms originate from thyrocytes cells type. The degree of cell differentiation distinguishes the thyrocytes-derived malignant lesions into well-differentiated thyroid carcinomas (WDTC), poorly differentiated thyroid carcinomas (PTDC) and anaplastic thyroid carcinomas (ATC). WDTC comprise two major histotypes: papillary thyroid carcinomas (PTC) and follicular thyroid carcinomas (FTC) where the tumor aggressiveness and lethality are inversely

correlated to the degree of their differentiation. [2, 3] Instead, malignant transformation of C cells gives rise to medullary thyroid carcinomas (MTC) [4].

Papillary Thyroid Carcinomas (PTC)

The most common type of thyroid cancer is the well-differentiated PTC that accounts for about 80% of all thyroid malignancies. Usually, these tumors behave as indolent lesions with slow rate of growth, low metastatic potential and a favorable outcome (up to 95% of survival after 10 years). Nevertheless, the occurrence of an aggressive behavior of PTC is not a rare event and most often these tumors show resistance to canonical therapies. The presence of distant metastases, occurring in a small percentage (~10%) of the entire PTC population, represents the major clinical feature reliably associated with a negative outcome of PTC patients [5]. There are more than 10 different histological variants of papillary thyroid cancer described [6].

Genetic features of PTC

In accordance with the low aggressiveness and rate of lethality, PTC are in general characterized by genetic stability with an overall low degree of mutational burden, chromosomic alterations and rare microsatellite instability.

In thyroid cancer, the most frequently altered mutations are in the MAPK pathway which are affecting genes, such as activating mutations *BRAF* and *RAS*, *RET*, in some cases, *ALK* mutations [7]. In particular, between 50 to 80% of PTC are characterized by the presence of mutations in the *BRAF* kinase [8]. Among all *BRAF* mutations, the point mutation T1799A, which led to the BRAFV600E amino acidic substitution and to the constitutive activation of the *BRAF* kinase activity, is the most frequent. Conflicting results are showing high prevalence of *BRAF* mutations in papillary carcinomas with classical histology profile and as well associated to PTC with aggressive phenotype [9-13]. On the contrary, *BRAF* mutations are rare in the follicular variant and in tumors arising from

preexisting follicular carcinoma. Other and rare events in *BRAF* include the less reported K601E point mutation (~7%) and AKAP9-BRAF rearrangement, detected in the follicular variant and in carcinomas associated with radiation exposure, respectively [14].

Another common alteration in PTC is the translocation *RET/PTC*. This chromosomal rearrangement, found in about 10-20% of PTC, involves the translocation of the genomic locus containing the receptor RET and lead to the expression of aberrant *RET/PTC* fusion oncoproteins. Many forms have been identified, but the most common are *RET/PTC1* and *RET/PTC3* [15]. In patients exposed to ionizing radiation, the incidence of *RET/PTC* recombination events is higher and account both in the pediatric populations (~40%) and in adults (15–20%) [16]. *RET* point mutations are also crucial for the development of medullary thyroid carcinomas [17].

RAS mutations (together with *PAX8-PPARγ* rearrangement) are the most frequent alterations in follicular carcinomas (25–100%) and relatively infrequent in PTC. They occur in ~10% of PTC generally belonging to the follicular variant [18, 19].

Other mutations associated to PTC with aggressive features are on *TERT* promoter and high numbers of mutations are on *MET*, *KIT*, *PI3KCA*, and *PTEN* genes [20, 21]. These genes are essential for tumor maintenance and progression not only in PTC but also in other human cancers.

Moreover, the Cancer Genome Atlas project identified novel mutations including *EIF1AX* (eukaryotic translation initiation factor 1A, X-linked), an entirely novel mutation in PTC. *EIF1AX* encodes a protein that mediates transfer of Met-tRNAf to 40S ribosomal subunits to form the 40S preinitiation complex for protein translation. Moreover they found novel alterations of known drivers (*RET*, *BRAF* and *ALK* fusions) and mutations in individual genes (*CHEK2*, *ATM*, and *TERT*) [22].

The basic helix-loop-helix (bHLH) family: DEC1 and DEC2

Transcription factors containing basic domains can be classified based on their specific motif(s) [23]. The HLH (helix-loop-helix) region is a highly conserved motif, which mediates protein–protein

interactions, as well as a basic DNA binding domain [24]. The basic helix-loop-helix (bHLH) transcription factors form homodimers or heterodimers that bind a consensus conserved DNA sequence called E box sequence (5'-CANNTG-3') in the promoter region of responsive genes and generally work as transcriptional activators (figure 2) [25].

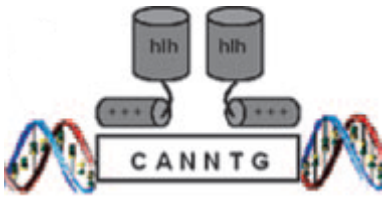

Figure 2. Activation of transcription by homo or hetero-dimerization of bHLH factors by binding target gene promoter on E-box sequence. Modified from "Id Family of Transcription Factors and Vascular Lesion Formation", Arteriosclerosis Thrombosis and Vascular Biology, 2004.

The inhibitors of DNA binding/differentiation (Id) family proteins interfere with the activity of these bHLH transcription factors acting as dominant negative. Indeed, the four Id proteins (Id1-4) lack the basic region adjacent to the HLH domain required for binding to DNA. Thus, these factors interact with various members of the bHLH transcription factor, restraining their binding capability to the E box sequence and their transcriptional activities (figure 3) [26].

Figure 3. Inhibition of the binding to E-box sequence and consequently of the transcription by hetero-dimerization of bHLH factors with Id proteins. Id is represented by the red block. Modified from "Id Family of Transcription Factors and Vascular Lesion Formation", Arteriosclerosis Thrombosis and Vascular Biology, 2004.

The bHLH factors can be classified based on phylogenic evolution or on their protein sequences [27, 28]. According this last classification bHLH can be divided into six class (A-F).

DEC1 and DEC2 (DECs) belong to the bHLH proteins class E. This class of proteins is further classified into three groups:

1) HES1, HES2, HES4, and HES6;
2) HEY1, HEY2, HEYL, HESL, HES5, and HES7;
3) HES3, DEC1, and DEC2 [29];

In addition to the well characterizing bHLH motif, all proteins belonging to these groups are characterized by the presence of a highly conserved unique orange domain. The orange domain is a motif of ~35 amino acids presents in eukaryotic transcriptional repressors, which regulates several biological processes. Further, they share a WRPW motif necessary to bind the transcriptional co-repressor *Groucho* in the C-terminus. Only DEC1 and DEC2 do not possess WRPR motif [30].

Moreover, human DEC1 has 412 amino acid residues and a proline-rich domain in the C-terminus, whereas human DEC2 has 482 amino acid residues with alanine and glycine-rich regions in the C-terminus. DEC1 and DEC2 share high (97%) and moderate (57%) similarities of the bHLH region and the Orange domain, respectively (figure 4) [29].

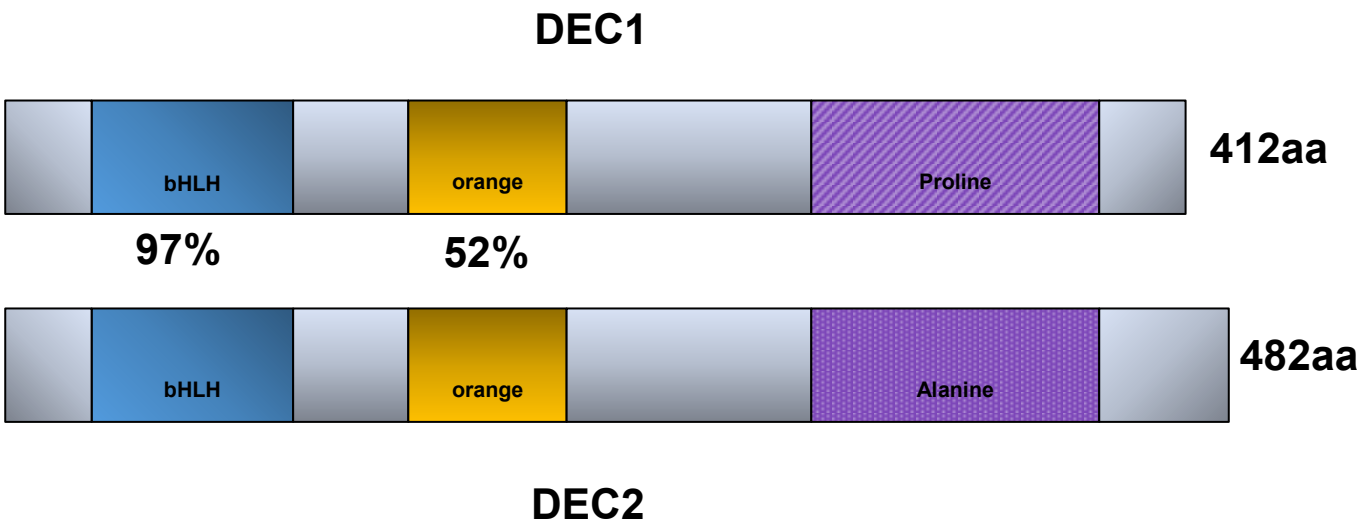

Figure 4. DEC1 and DEC2 structure.

DEC1 and DEC2 are expressed in a variety of normal developing and adult tissues. Their transcription starts in response to different environmental stimuli, such as hypoxia, cytokines, drugs. For instance, Hypoxia inducible factor 1–alfa (HIF1α) binds the promoter of both DEC1 and DEC2 and activates their transcription [31]. Thus, their role changes in relation to different cellular context and it is mostly linked to crucial biological processes including development, cell differentiation, cell growth, and oncogenesis [32].

Differently from other bHLH factors, DEC1 and DEC2 usually suppress the expression of their target genes, often related to cell differentiation and to the regulation of the molecular clock. They may also mediate the crosstalk between circadian rhythm and physiological and pathological processes [33].

DEC1 and DEC2 in cancer.

Many studies underlined the tissue and tumor-specificity of DEC1 and DEC2 localization in epithelial tumors [34]. High levels of *DEC1* transcript have been found in different types of cancer (pancreatic, lung cancer, etc.) suggesting a role for DEC1 as oncogenic molecule [35]. Moreover, in tumor cells, DEC1 is mainly localized in the nuclei and cytoplasm and close to the necrotic area, while it is absent in normal tissue [36]. DEC1 overexpression is also associated with tumor grade and malignancy in oral and esophageal squamous cell carcinomas [37, 38, 39], positively correlate with marker of aggressiveness, such as Ki-67 and hypoxia inducible factor1-alpha (HIF1α) in invasive breast ductal carcinomas [40, 41]. On the contrary, DEC2 expression is variable and tightly depends on the tissue analyzed. Few reports described the involvement of DEC1 and DEC2 in mesenchymal tumors: in osteosarcoma DEC2 expression correlates with tumor invasiveness and HIF1α expression [42].

The current body of evidences suggested that exposure to various stresses, such as transforming growth factor-β (TGF-β), cytokines, anti-tumor drugs and hypoxia regulate DEC1 and DEC2 expression and their effects in different cancer-related processes (i.e. cell cycle regulation, EMT, differentiation and apoptosis) [29]. Many studies also indicated that DEC1 and DEC2 might play

opposite function in cancer. For example, DEC1 has been shown to have pro-apoptotic effects while DEC2 has anti-apoptotic effects in human breast cancer cells [43]. Further, DEC1 enhances while DEC2 inhibits EMT (epidermal to mesenchymal transition) in pancreatic cancer [44]. Moreover, other evidences indicated that DEC1 might negatively regulate the expression of DEC2 in different tumors, such as lung, colon and kidney cancers [45].

Currently, nothing is known about the role of DEC1 and DEC2 in thyroid cancer. We recently reported that forced expression of the transcriptional regulator Id1 in PTC cells promotes aggressiveness by regulating the expression of many genes [46]. DEC1 and DEC2 were profoundly up regulated in this model offering a hint that these factors may be involved in the Id1-regulation of thyroid cancer aggressiveness.

NOTCH1 and cancer

NOTCH1 belongs to a family of four receptors (NOTCH 1, 2, 3, 4) and consists of three domains: extracellular (ECD), transmembrane (TMB), and intracellular (NICD). In the canonical NOTCH signaling pathway, the intracellular NOTCH1 domain, NICD, after the binding of the receptor to its ligands (Delta1 or Jagged1), expose a site of cleavage that allows first to ADAM17, then to γ-secretase to release in the cytoplasm NICD, the activated form of NOTCH1. NCID do not possess a DNA-binding domain, thus after translocation into the nucleus, it forms a transcriptional complex with the transcription factor RBP- Jκ/CSL. The binding of NICD/RBP-Jκ to consensus region of NOTCH1 downstream target genes allows transcription, whereas in absence of NICD, RBP- Jκ works as transcriptional repressor (figure 5) [47]. On the contrary, a non-canonical NOTCH signaling pathway has also been described. In this case, the activation of NOTCH1 signaling is RBP- Jκ independent and generally leads to the activation or inactivation of the Wnt/β-catenin or the PI3K/Akt signaling. Moreover, NICD may activate a non-canonical pathway also without the previous binding of NOTCH1 with their ligands [48]. Thus, it is clear the multiplicity potential of NOTCH1 both in

physiological and pathological processes [49].

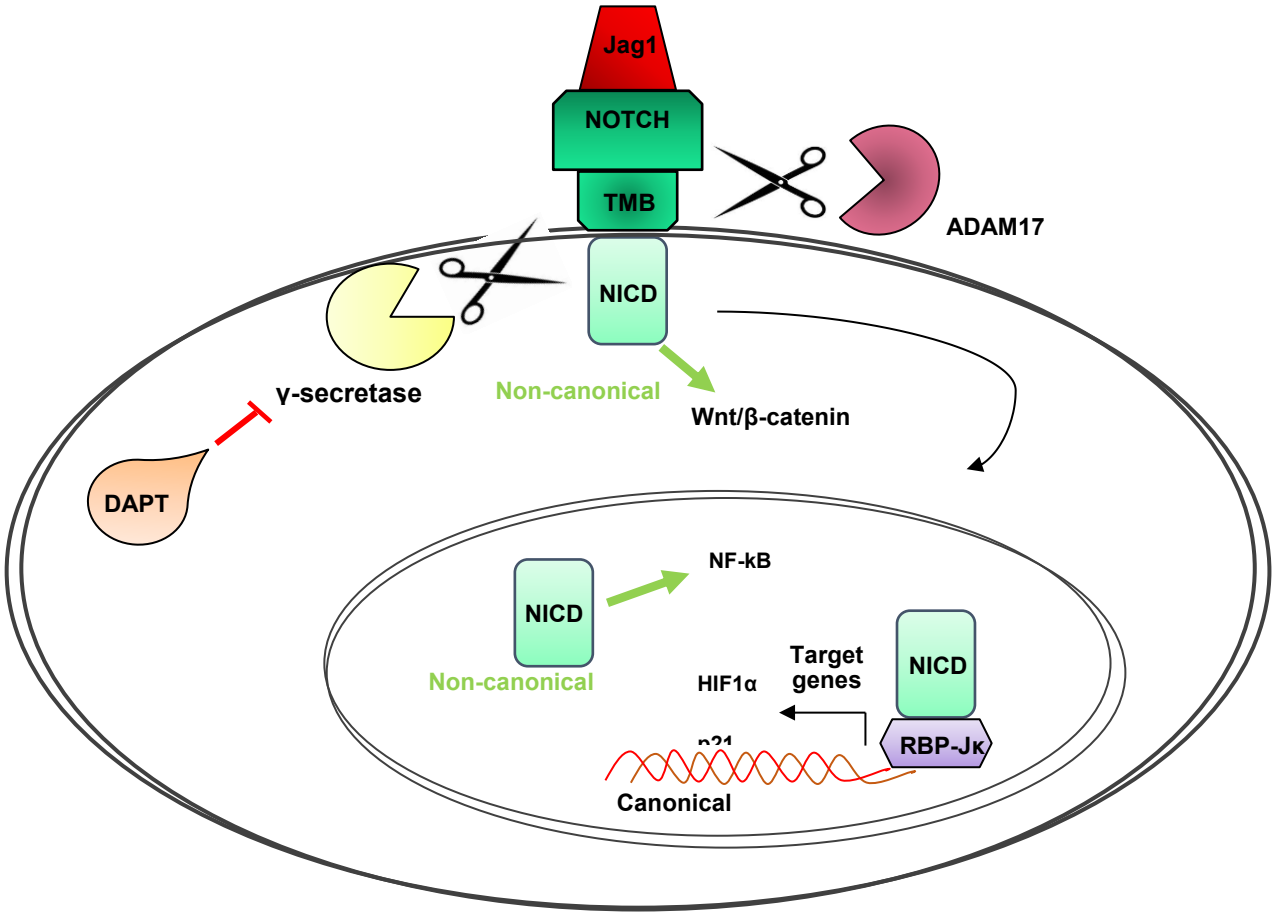

Figure 5. NOTCH canonical and non-canonical pathways. DAPT, the chemical inhibitor of γ-secretase inhibites NICD release and consequently downregulates the canonical and the non-canonical pathway.

Many evidences also suggested a key role for NOTCH1 in carcinogenesis and tumor progression [50]. Depending on tissue, cellular context and tumor stage, aberrant gain or loss of NOTCH1 signaling has been directly linked to the tumor suppressor or oncogene function [51, 52]. For instance, in T-cell acute lymphoblastic leukemia (T-ALL) NOTCH signaling activated HIF1α to trigger cell proliferation, invasion and chemo-resistance [53]. Moreover, NOTCH1 played a crucial role in the EMT process up regulating mesenchymal markers in kidney [54]. In esophageal adenocarcinomas NOTCH signaling drives stemness [55]. NOTCH1 expression correlated with poor prognosis and tumor progression in-patient with breast and cervical cancer [56, 57]. Nevertheless, it has been reported that in solid tumors there are few activating mutation in the NOTCH pathway, whereas a

high incidence of NOTCH mutations (over 50% of cases) have been described in T-ALL [58, 59].

Beyond its reported pro-oncogenic function, NOTCH1 activation has also been linked to tumor suppressive events. In mice skin, as well as in hepatocellular carcinomas, NOTCH1 loss of function caused the insurgence and accelerates tumor development [60, 61]. In neuroblastoma cells the activation of NOTCH signaling blocked cell growth and in small cell lung cancer high expression of NOTCH1 is associated with favorable prognosis [62, 63, 64].

Interestingly, a controversial role for NOTCH1 in thyroid cancer has also been proposed. On one side the activation of NOTCH signaling mediates growth suppression by cell cycle arrest in well-differentiated thyroid carcinomas (WDTC) cells, thus its activation has been suggested as potential therapeutic strategy to block follicular and papillary thyroid carcinomas growth [65, 66]. On the other side, NOTCH1 has been described highly expressed in WDTC with *BRAF*, *RET/PTC* mutation or active MAPK signaling [67, 68]. In this context, activated NOTCH1 signaling promotes tumor growth. Noticeable, Hyeon Jin Kim et al., postulated that NOTCH signaling influences the malignant potential of thyroid cancer and observed a NOTCH1 dependent significant reduction of the EMT and cancer stem cells markers in anaplastic tumors [69].

Despite the lack of a general consensus about the role of NOTCH signaling in WDTC, increasing data implied the role of NOTCH1 signaling pathway activation in thyroid cancers aggressiveness. Of note, the expression of NOTCH1 receptor seems to be related to tumor invasiveness in PTC and it has been proposed as molecular marker associated to poor prognosis [70, 71].

NOTCH1 and DECs: a potential interaction?

The HES and HEY transcription factors, as DEC1 and DEC2 belong to the class E of bHLH transcription factors. They have been recognized primary NOTCH1 target genes [72]. They act as NOTCH1 effectors negatively regulating the transcription of NOTCH1 downstream targets in many contexts, from the development of various physiological systems by the maintenance of stem cells to

the sustenance of tumorigenesis regulating cell proliferation and differentiation [73, 74, 75]. Moreover, evidences suggested that these families might mediate the crosstalk between NOTCH1 and BMP/TGF-β, WNT/β-catenin or JAK-STAT signaling [76, 77, 78].

Notable, it has been also observed a mechanism for a negative feedback on NOTCH signaling that requires a physical interaction of RBP-Jκ with transcription factor belonging to the bHLH family, which act as co-repressors [79].

Currently no evidence of a functional crosstalk between DECs and NOTCH1 have been reported. Since NOTCH1 and DEC1 share some target genes, such as P21 and c-MYC, both involved in the regulation of cell growth, raised the hypothesis that NOTCH pathway might cooperate with DEC1.

AIM OF THE PROJECT

In the recent years a role for DEC1 and DEC2 in cancer began to emerge. In tumor cells these transcription factors seems to play multiple functions affecting apoptosis, proliferation and angiogenesis by orchestrating response to chemokines and hypoxia. However, a complete picture of the role of these factors in cancer (and in particular in thyroid cancer) is missing as well as the knowledge of the molecular mechanisms through which DEC factors influences cancer cells is still limited.

Recently, we found DEC1 and DEC2 significantly up-regulated in a genetically engineered cellular model of PTC, which presented features of high aggressiveness [46]. Thus, we hypothesize that these factors may be part of the molecular program that sustains progression of PTC.

The goals of this project are:

1. Characterize the biological function of DEC1 and DEC2 in thyroid cancer.

2. Understanding the potential interplay between DEC1 and DEC2 in these processes.

3. Dissect the molecular mechanisms by which DEC factors participate to thyroid cancer progression.

4. Explore the potential interplay of the DEC factors with the NOTCH1 pathway in thyroid cancer.

Two different PTC-derived cell lines will be employed in this study: TPC1 harboring the RET/PTC translocation and the BCPAP harboring mutations in BRAF-V600E and p53.

MATERIALS AND METHODS

Reagents

The Silencer® Select Pre-designed siRNA targeting DEC1 or DEC2 and the Silencer® Select negative control siRNA were purchased from Ambion, by Thermo Fisher Scientific. Lipofectamine RNAiMAX, Lipofectamine 2000 were purchased from Invitrogen by Thermo Fisher Scientific. Optimem, Puromycine, DMEM GlutaMAX medium and FBS (fetal bovin serum) were purchased from Gibco by Life technologies. MitomycinC from *Streptomyces caespitosus* was purchased from Sigma Aldrich as powder and solubilized in PBS 1X. Primers were synthesized by Eurofins Genomics GoTaq polymerase was purchased from Promega, Phusion Polymerase from Invitrogen and Sso Fast EvaGreen Super Mix and iScript cDNA Synthesis Kit from Biorad. Plasmid vector pSG213 was kindly gifted from Prof. R. Tupler (University of Modena and Reggio Emilia), whereas N-terminal p3XFLAG-CMV was obtained from Sigma Aldrich. Kits for DNA extraction and purification were purchased from Machery-Nagel. Restriction enzyme and buffer from Invitrogen, whereas Ligase enzyme and its buffer from Promega. CIP enzyme for dephosphorilation was obtained by New England BioLabs®. Doxycyclin was purchased from Sigma Aldrich as ready to use solution, whereas DAPT (N-[N-(3,5-Difluorophenacetyl)-L-alanyl]-S-phenylglycine t-butyl ester) as powder and was solubilized in DMSO.

Cell lines and cell culture medium

TPC1 and BCPAP human cell lines were obtained from Dr. Massimo Santoro, University of Naples (Naples, Italy). This cell lines derived from PTC samples and were cultured at 37 °C in 5 % CO_2 in DMEM medium supplemented with 10% heat-inactivated fetal bovine serum (or TET-free FBS for culturing clones). Subcloning Efficency DH5α Competent Cells and One shot Stbl3 were used for cloning and were purchased from Invitrogen.

Cloning strategy

Since our inducible plasmid pSG213 do not possess a tag, we first cloned DEC1 or DEC2 in a pCMV

vector with a 3xFlag. Then we moved DEC1/DEC2 and the 3xFlag in the pSG213. Briefly, DEC1 and DEC2 was amplified by PCR from the cDNA of PC3 (prostate cancer) in which DEC1 and DEC2 were higher expressed, using the restriction sites 5'HindIII – 3'EcoRV (for DEC1) or 5'BglII-3'EcoRV.

DEC1 Primers:

FOR_GTCAAGCTTGGGGAGCGGATCCCCAG

REV_GGCGATATCTTAGTCTTTGGTTTCTAAG

DEC2 Primers:

FOR_GTCAGATCTGGGGGACGAAGGAATTCCTCATTTG

REV_GGCGATATCTCAGGGAGCTTCCTTTCCTGGCT

The ATG was replaced with Glycine (blue) and in red the restriction sites.

DEC1 PCR condition:

Initial Denaturation: 98° x 1'

Denaturation: 98° x 10"

Annealing: 55° x 30"

Elongation: 72° 1'

Final elongation: 72° 5'

Tot: 25 cycles

The mix of reaction was prepared according manufacturing protocol for the Phusion Polymerase.

DEC2 PCR condition:

Initial Denaturation: 95° x 2’

Denaturation: 95° x 30”

Annealing: 54° x 30”

Elongation: 72° 1’40”

Final Elongation: 72° 5’

Tot: 30 cycles

The mix of reaction was prepared according manufacturing protocol for the GoTaq polimerase. Since the CDS of DEC2 is a GC-rich region we also added 3% of DMSO and 0.5 µl of PFU to the mix.

DEC1 and DEC2 were run on a 1.5% extra pure agarose gel. Lanes were extracted and purified according the manufacturing protocol and the DEC1 cDNA was digested with HindIII –EcoRV for 3h at 37°C in Buffer R, whereas DEC2 cDNA was digested with BglII-EcoRV in 2XTango Buffer. After digestion, cDNAs were purified and ligated with the previously dephosphorylated N-terminal-p3xFlag-CMV, at room temperature 1 hour. Transformation was performed in DH5α cells. Briefly, 5µl of DEC1-pCMV or DEC2-pCMV was added to 50µl of bacteria 30’ on ice, then shocked 45” at 42° and 2’ on ice again. 1ml of LB (Luria Broth) was added and after 1 hour at 37° on shaking, bacteria were seeded on a petri dish and incubated overnight.

The day after, colony were picked, controlled by diagnostic digestion followed by gel electrophoresis and inoculated for Miniprep.

Plasmid DNA was extracted and purified according the manufacturing protocol of the Kit. DNA was then sequenced by an external support company, and the not mutated sequences were used to the following procedures.

To move Flagged DEC1 and DEC2 in the pSG213 we used the following primers: for DEC1 a 5’NotI-3’EcoRV, whereas for DEC2 5’EcoRV-3’EcoRV.

DEC1 Primers:

FOR_CGGTCGCGGCCGCATGGACTACAAAGACCATGACGGT

REV_GGCGATATCTTAGTCTTTGGTTTCTAAGTT

DEC2 Primers:

FOR_GCCGATATCATGGACTACAAAGACCATGACGGT

REV_GGCGATATCTCAGGGAGCTTCCTTTCCTGGCT (The same of the first cloning)

In red the restriction sites, in blue the transcription starting site, in green the sequence match the 3xFlag.

We performed the same PCR condition, gel extraction and purification described above. Then we digested DEC1 and DEC2 with the corresponding restriction enzymes 3 hours at 37°C. After pSG213 dephosphorylation we performed the transformation. This time we used the Stbl3 bacteria with an increased transformation efficiency than DH5α. The day after we pick colonies, and repeated the same protocols. After validation by sequencing we re-inoculated the colonies analyzed overnight in 200ml of LB. The day after we extracted plasmid DNA of DEC1-pSG213 and DEC2-pSG213, according the manufacturing protocol of the kit.

Clones isolation

For stable clone derivation, 4 x 10^5 BCPAP or 3 x 10^5 TPC1 were transfected with 2.5 µg DEC1 or DEC2-pSG213 or with the empty vector using 7,5µl of Lipofectamine 2000 in a 6well multiplate. Twenty-four hours after transfection cells were seeded in a p10 plate and Puromycine was added to the medium at the final concentration of 0.5 µg/ml. After selection, single clones were picked, expanded and the overexpression of DEC1 or DEC2 was assessed by Doxycycline induction. Among all clones we obtained, only BCPAP overexpressed DEC1. Neither BCPAP nor TPC1 overexpressed

DEC2.

Transfection by siRNA

Transient transfection of specific DEC1 or DEC2 siRNA was performed using Lipofectamine RNAiMAX, according to the manufacturer's protocol of the inverted transfection. Briefly, on day 1, 30nM siRNA, of Lipofectamine, Optimem in a 25cm^2 flask. After 20 minutes TPC1 or BCPAP were seeded at a density of 2,5x 10^6 in the plate, without antibiotics. The following day, cells were harvested, counted and seeded for the different assays. Transfection efficiency was verified over time starting 24 hours after seed by qPCR or western blotting.

MTT assay

Cell viability was measured by the MTT test. After 24h of silencing cells were harvested and 2000 cells/well were seeded into 96-multiwell plates in complete medium. Otherwise, for the overexpressing clones, 2000 cells/well were seeded into 96-multiwell plates in complete medium and after adhesion, medium was replaced with fresh medium containing Doxycycline (100 ng/ml) or vehicle (DMSO) and the medium was refreshed every day. For both the experiments, 3 hours before each time point, MTT reagent (3-(4,5-dimethylthiazol-2-yl)-2,5-diphenyltetrazolium bromide; Sigma Aldrich, Milano) was added to the wells and plates were incubated at 37ºC. MTT reagent was prepared solubilizing the powder in PBS 1X plus Ca and Mg at the final concentration of 0.005g/ml. During the incubation time the metabolic enzymes reduced the tetrazolium dye into its insoluble formazan, which precipitate on the bottom has a colored crystals. Then we added 200 µl of DMSO to dissolve formazan into a purple solution. Absorbance at 540 nm was then measured by a FLUOstar spectrophotometer (FLUOstar Omega BMG LABTECH).

Trypan Blue Exclusion Count

Cell proliferation was assessed by the Trypan Blue dye. This dye selectively colors the dead cells blue, whereas life cells with intact cell membranes are not colored. Briefly, 10µl of cell suspension was added to 10µl of Trypan Blue and 10µl of this solution was inserted in a Bürker chamber. The

chamber has 9 large squares, divided by double lines into 16 group squares. The cells were counted in each of the 4 large squares (identified by the triple line) and to calculate cell number the average of the 4 readings (from 4 large squares) was used as follows:

$$\left[\frac{cell}{ml}\right] = \left[\sum \frac{cell\ counted\ in\ \mathbf{4}\ large\ squares}{\mathbf{4}}\right]\ x\ (dilution\ factor)\ x\ 1ml\ x\ 10^4$$

Colony formation assay

This assay is an *in vitro* cell survival assay based on the ability of a single cell to grow into a colony. Briefly, $1x10^3$ TPC1 or BCPAP knocked-down for DEC1 or DEC2 were seeded on a 100 mm plate in complete medium. After 10 days colony were fixed in 4% PFA (paraformaldehyde), washed with water and stained with Crystal Violet 0.2% in H_2O (0.2% CV). The number and the size of colony were manually counted.

Cell cycle assay

Assessment of cell cycle was evaluated with Propidium Iodide (PI) followed by flow cytometry. 3 x 10^5 cells knocked-down for DEC1 or DEC2, or clones after 48h of Doxycycline induction (or DMSO as vehicle), were counted. Then cells were washed twice with cold Phosphate Buffer Solution 1X and stained for 15 minutes in ice with PI solution (50 µg/ml PI in H_2O, 0.1% Triton-X100, 0.1% trisodium citrate dehydrate, 6.25 µg/ml RNase A). Cells were analyzed by flow cytometry using a FACSCanto machine (BD) and analyzed with BD FACSDiva Software 6.0.

Invasion assays

Invasion assay was performed using the BD matrigel- invasion chambers according to the manufacturing protocol. Briefly, 5×10^4 cells, previously silenced for DEC1 or DEC2 or induced 48h with doxycycline, were washed with PBS 1X, and placed in the upper compartment in serum-free medium. Serum (10% in DMEM) was used as chemoattractant and added to the lower compartment of the chambers. Cells were incubated for 22h at 37°C. Then, cells on the upper surface were mechanically removed with a cotton swab and invading cells were fixed with absolute ethanol and

stained with a 0.2% solution of Crystal violet. Cells were counted in a double-blinded manner in five consecutive fields with an inverted microscope (Nikon Eclipse Ni). All experiments were performed three times in duplicate.

Adhesion Assay

We performed a static adhesion assay able to detect how many cells acquire or lose the ability to adhere to a collagen substrate after particular changes. In our cases we evaluated the ability of TPC1 or BCPAP knocked down for DEC1 or DEC2 to adhere on a pre-coated collagen surface. We pre-coated the surface of a 24 wells multi-plate with 0.1 % of Collagen type IV. Then we discarded collagen exceeding and seeded cells in complete medium. After 30 minutes, we washed cells 3 times with PBS1X to eliminate not adherent cells. Then we fixed cells in 4% PFA (paraformaldehyde) and we stained cells with 0.2% CV.

Wound Healing assay

Migration assay was performed by the wound healing or scratch assay. More the cell migrate, faster the closing occurred. On day 1, 1.5 x 104 TPC1 or BCPAP previously silenced for DEC1 or DEC2 or 1.5 x 104 DEC1 overexpressing clones were seeded on a 12 wells multi-plate. When cells achieved 90% of confluence, we stopped proliferation by 2 hours of 20μM Mitomycin C treatment in serum free medium. Mitomycin C is an inhibitor of DNA synthesis and suppress mitosis, thus we excluded that closing occurred due to cells proliferation. After that, we washed cells and blocked Mitomycin C activity by replacing FBS in the medium. Then, we get the scratch, by the tip. Cell images were captured at time zero and after 6, 18 or 24 hours to monitor the closing. The scratch closing was quantified by the ImageJ software, using the "MRI Wound Healing" tool.

Western Blotting

Cells were lysed in 2X Laemmle Buffer (Bio-rad), the total lysate was frozen and boiled to break membranes. The lysate volume was normalized on the number of cells. Equal amounts of proteins for each sample were resolved on 10% sodium dodecyl sulfate–polyacrylamide gel electrophoresis

using the Bio-Rad Mini-Protean apparatus. Gel was blotted onto nytrocellulose membrane using the Trans-Blot Turbo, transfer system, Bio-rad. Following blocking with 5% non-fat milk powder (wt/vol) in Tris-buffered saline (10mM Tris–HCl, pH 7.5, 100mM NaCl, 0.1% Tween-20) for 1h at room temperature, membranes were incubated with primary antibodies directed against the following human antigens: β-actin, anti-FLAG, NOTCH1 (Sigma Aldrich), DEC1 (Bethyl Laboratories) DEC2 (Santa Cruz Biothecnology), total and phospho-AKT (Thr308 and Ser473), p21, HIF1α (all purchased from Cell Signaling Technology, Danvers, MA). The antibodies were diluted in 2% bovine serum albumin–Tris-buffered saline–0.1% Tween according to the manufacturer's instructions. The bound antibodies were visualized by horseradish-peroxidase-conjugated secondary antibodies and an enhanced chemiluminescence detection system, Clarity from Bio-rad.

Quantitative Real-Time PCR

Total mRNA was collected using Maxwell® RSC simplyRNA Cells (Promega) and retro-transcribed using iScript cDNA Synthesis Kit. Quantitative PCR was carried out using the Sso Fast EvaGreen Super Mix in the CFX96 Real Time PCR Detection System (Bio-Rad).

PCR protocol:

Initial Denaturation: 98° x 2'

Denaturation: 98° x 2"

Annealing: 59° x 5"

Elongation: 72° 1"

Final Elongation: 95° 5'

Tot: 39 cycles

Relative expression of target genes was calculated using standard curve method and normalized to GUSB mRNA content.

Primers:

Name	Forward	Reverse
Dec1	CCTTGAAGCATGTGA	CATGTCTGGAAACCT
Dec2	TAACCGAGCAACAGC	GCATGTTTGAAATCC
NOTCH1	AAGTGTGAAGCGGCCAAT	CATGTCCCGGCGTTCTTG
p21	CATGGGTTCTGACGGACATC	TGCCGAAGTCAGTTCCTTGT
c-Myc	ACTCTGAGGAGGAACAAGAA	TGGAGACGTGGCACCTCTT
Delta1	CAGGCCATCTGCTTCACCA	AAGACGATACCCACAGTGCCC
Jaggad1	CGGGAACATACTGCCATGAAAATA	ATGCACTTGTAGGAGTTGACACCA
Hey1	CTGCAGATGACCGTG	GGCATTCCCGAAATC
Gusb	TTGAGCAAGACTGATACCACCTG	TCTGGTCTGCCGTGAACAGT

RNA-Seq analysis

RNA quality was assessed by Bianalyzer using Agilent RNA 6000 nano kit and quantify by Nanodrop. RNAseq libraries were prepared starting from 1 microgram of RNA. Next generation sequencing was performed using NextSeq 500 platform (Illumina) and a minimum of 20 Million of sequencing reads for each sample replicate was expected.

Bioinformatic analysis was conducted applying Cufflink RNA-Seq workflow. Differential gene expression was calculated as fold-change (siDEC1/siCtrl). Genes with a q-value < 0.05 were considered significantly deregulated. Q-value was obtained adjusting p-value by an optimised FDR approach (FDR cutoff=0.05).

Immunohistochemistry

Samples were derived from a cohort of thyroid cancer patients belonging to different histotypes and collected at our Institution in the Pathological Anatomy archive. Thanks to Dr. Simonetta La Piana we obtained 35 thyroid cancer sample and Dr. Ione Tamagnini performed for us the staining for DEC1 at the final Antibody dilution of 1:300.

Statistical analysis

Data are expressed as means ± SD. The statistical significance between multiple data sets was determined by one-way ANOVA, whereas T-test was used for comparing two group of values, using Graph-Pad Prism software. FACS data were analyzed by the FACSDiva6 software. ImageJ software was used for western blotting quantification.

RESULTS

DEC1 and DEC2 are expressed aggressive models of PTC

In a previous work we found DEC1 and DEC2 significantly upregulated in a genetically modified model of thyroid cancer that acquired high feature of aggressiveness (BCPAP_Id1Cl2). First, we confirmed these data by analyzing DEC1 and DEC2 levels by qRT-PCR and western blot in BCPAP_Id1Cl2 and parental control clones (BCPAP_Ctrl). As shown in Figure 1, both DEC1 and DEC2 mRNA (1A) and protein (1B) levels were significantly higher in BCPAP_Id1Cl2 as compared to control. To strengthen the hypothesis that DEC1 is associated with aggressiveness in thyroid cancer we also compared its expression in TPC1 and BCPAP. We observed that DEC2 more than DEC1 is more expressed in TPC1 than in BCPAP (1C), in line with our previous work and the hypothesis that these factors are more expressed in the aggressive phenotype of PTC.

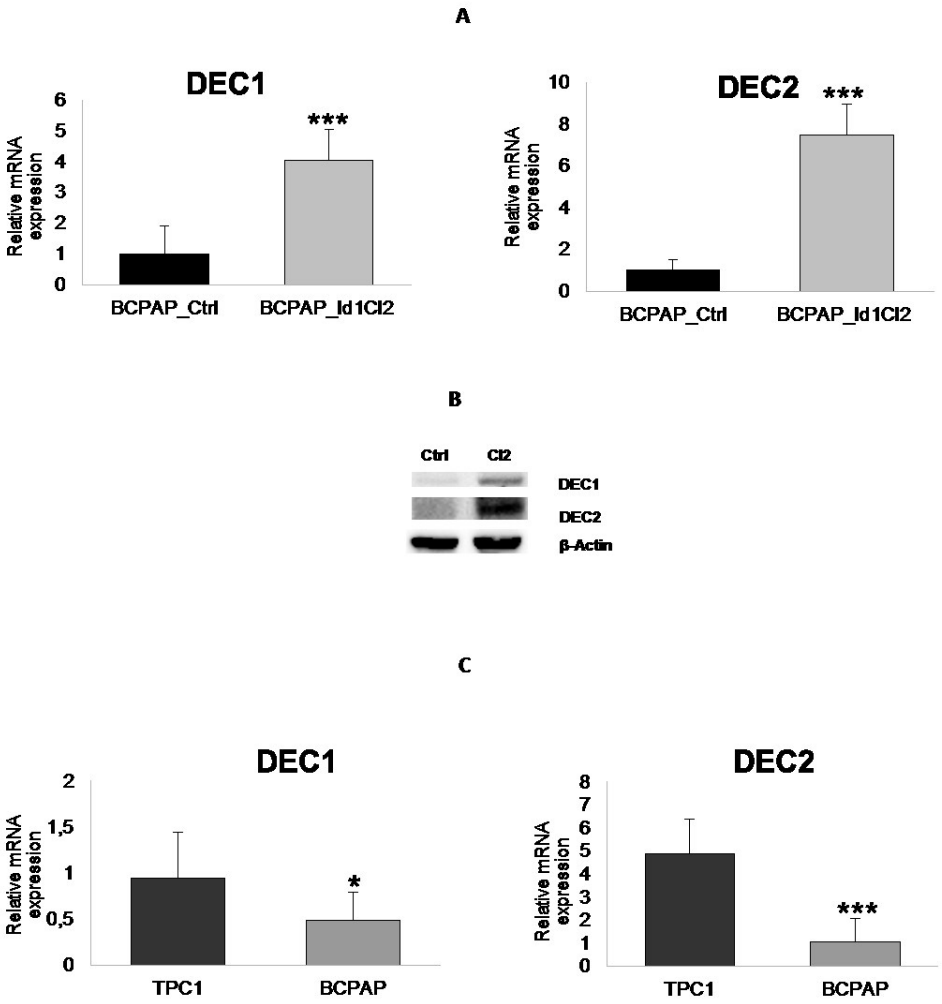

Figure 1. Expression of DEC1 and DEC2 in different papillary thyroid cell lines. (A) DEC1 and DEC2 mRNA levels were assessed in BCPAP overexpressing Id1clone (BCPAP_Id1Cl2) and compared to its control clone (BCPAP_Ctrl) by qRT-PCR. (B) DEC1 and DEC2 protein levels were measured by Western Blotting. (C) DEC1 and DEC2 mRNA levels were evaluated in TPC1 and BCPAP by qRT-PCR. Statistical analysis: t-test (*<0.05, **<0.01, **<0.001).

Silencing of DEC1 but not DEC2 impairs cell proliferation in thyroid cancer cells

In order to evaluate the role of DEC1 and DEC2 we performed loss of function experiments by silencing DEC1 and DEC2 with two specific siRNAs for each protein. Figure 2 shows silencing efficiency in TPC1 and BCPAP cells upon transfection of DEC1-siRNAs or DEC2-siRNAs as compared with scramble transfected cells (siCtrl). A strong reduction over 80% in the mRNA levels was observed for both DEC1 and DEC2 in TPC1 and BCPAP that remained stable up to 96h from transfection (2A and C). Western blot analysis confirmed the silencing effect also at the protein level in both cell lines (2B and D).

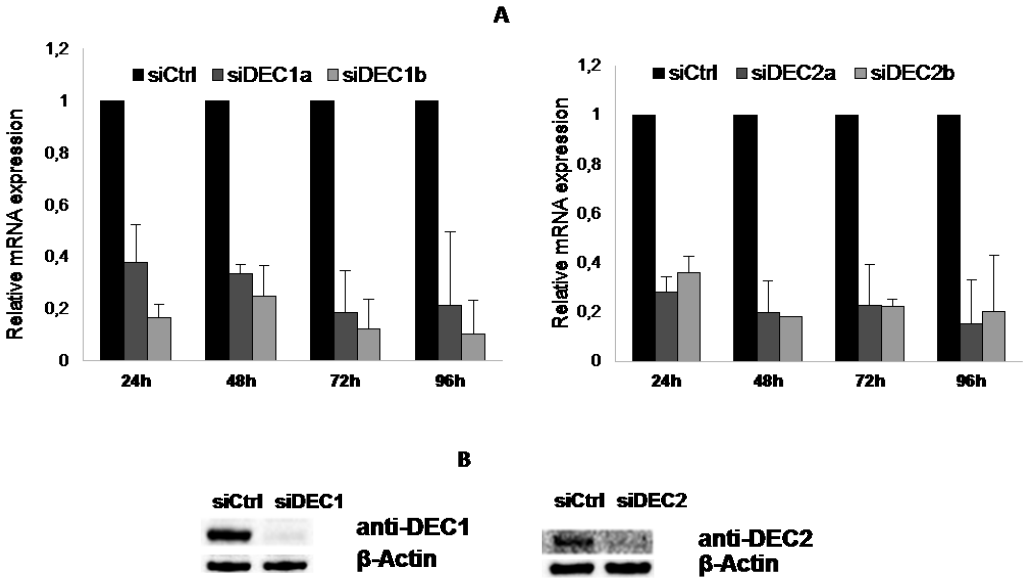

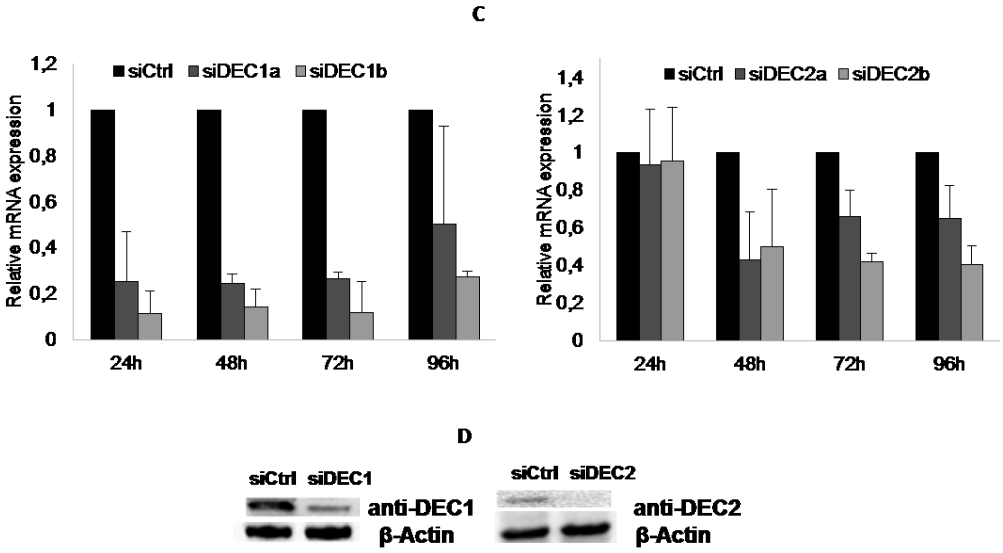

Figure 2. Downregulation of DEC1 and DEC2 by specific siRNA. TPC1 were transfected with 30nM of each siRNA and DEC1 or DEC2 downregulation was evaluated over time by qRT-PCR (A) or after 72h by Western Blotting (B). The same experiments were performed on BCPAP and DEC1 or DEC2 knock-down was assessed by qRT-PCR (C) and by Western Blotting (D).

First, we analyzed the effect of the DEC1 or DEC2 silencing on cell growth. In TPC1 (Fig. 3) DEC1 silencing resulted in a significant reduction of cell proliferation (figure 3A) and cell viability (Figure 3B). By contrast, silencing of DEC2 had not evident effects on either cell proliferation (figure 3A) or viability (Figure 3B). As well, silencing of DEC1 but not DEC2 impaired cell proliferation and viability of BCPAP cells (Figure 4A and 4B). Next, we analyzed the effect of DEC1 and DEC2 silencing on the colony forming capacity of TPC1 (Figure 3C) and BCPAP cells (Figure 4C). Both, number and size of the colonies were significantly reduced upon siDEC1 transfection in TPC1. A similar effect was also observed in BCPAP cells were a significantly smaller number of colonies were observed in siDEC1 transfected cells as compared with siCtrl cells. Unfortunately, the small dimension of colonies formed by BCPAP limited the possibility of quantifying reduction in size. In accordance with the limited effect observed on cell proliferation and viability DEC2 silencing did not affect significantly colony formation either in TPC1 or BCPAP cells. To further confirm the DEC1 effect on cell proliferation and to better understand its role in this process we analyze how DEC1 silencing affected cell cycle progression in TPC1 and BCPAP.

Noticeably, in both lines siDEC1 cells showed a 30% significant reduction of the S phase and a consequent accumulation of cells in G1 as compared to siCtrl cells. This observation, in line with the reduced proliferation and colony forming capacity of siDEC1 cells indicate that silencing of DEC1 impairs the transition between G1 and S delaying cell cycle progression. By contrast, DEC2 silencing did not have any effect on cell cycle in both TPC1 and BCPAP cells.

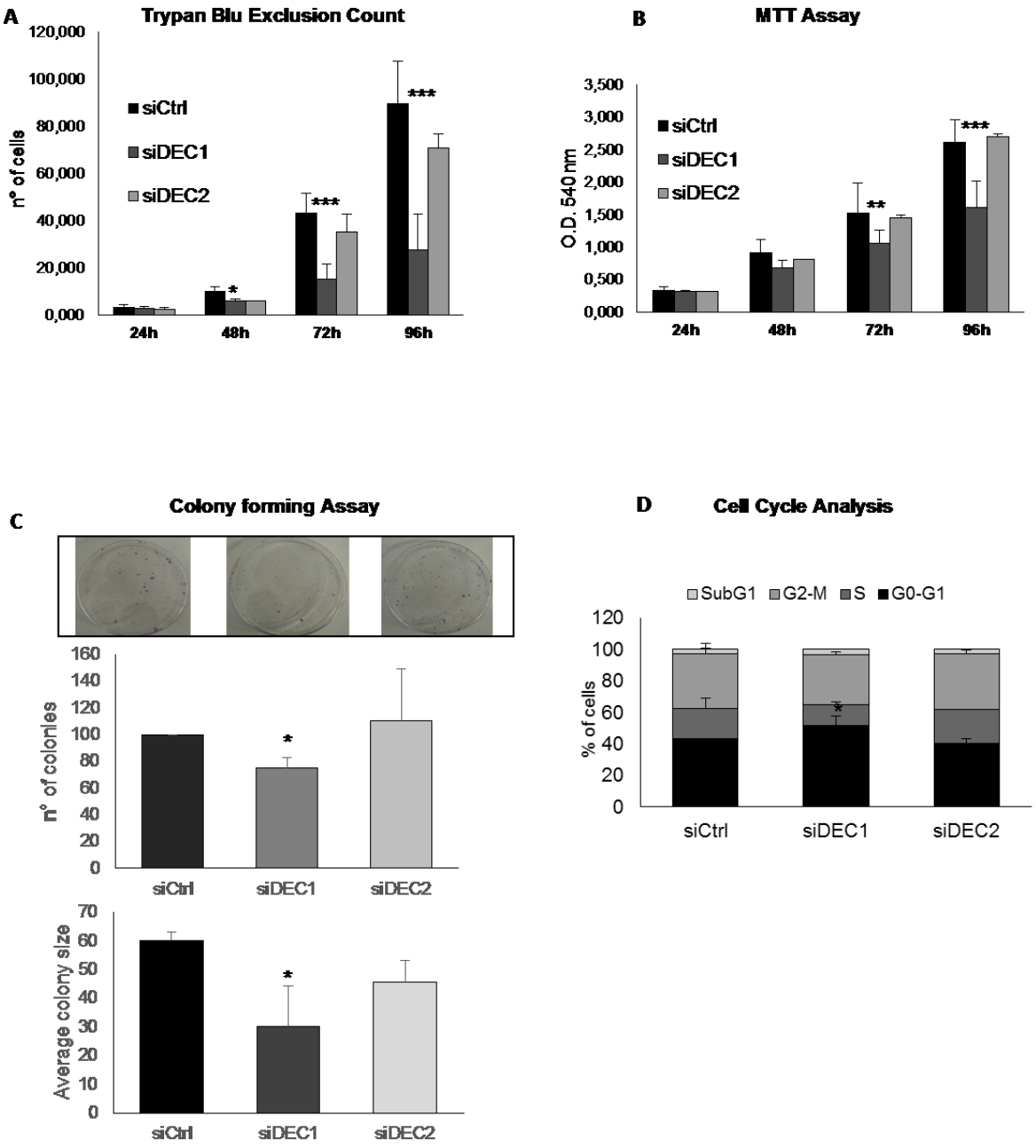

Figure 3. Effect of DEC1 or DEC2 silencing on TPC1 growth. TPC1 were transfected with 30nM siDEC1 or siDEC2 up to 96 hours and proliferation (A) and viability (B) were assessed by Trypan Blue Exclusion Count or MTT assay, respectively. Colony formation (C) was evaluated after 10 days form transfection and the number and the size of colonies was calculated ImageJ Cell Counter Tool and expressed as percentage of control. Cell cycle (D) was evaluated after 72h from transfection by PI staining and the distribution of cells in the cell cycle phases was expressed as percentage of total cells.

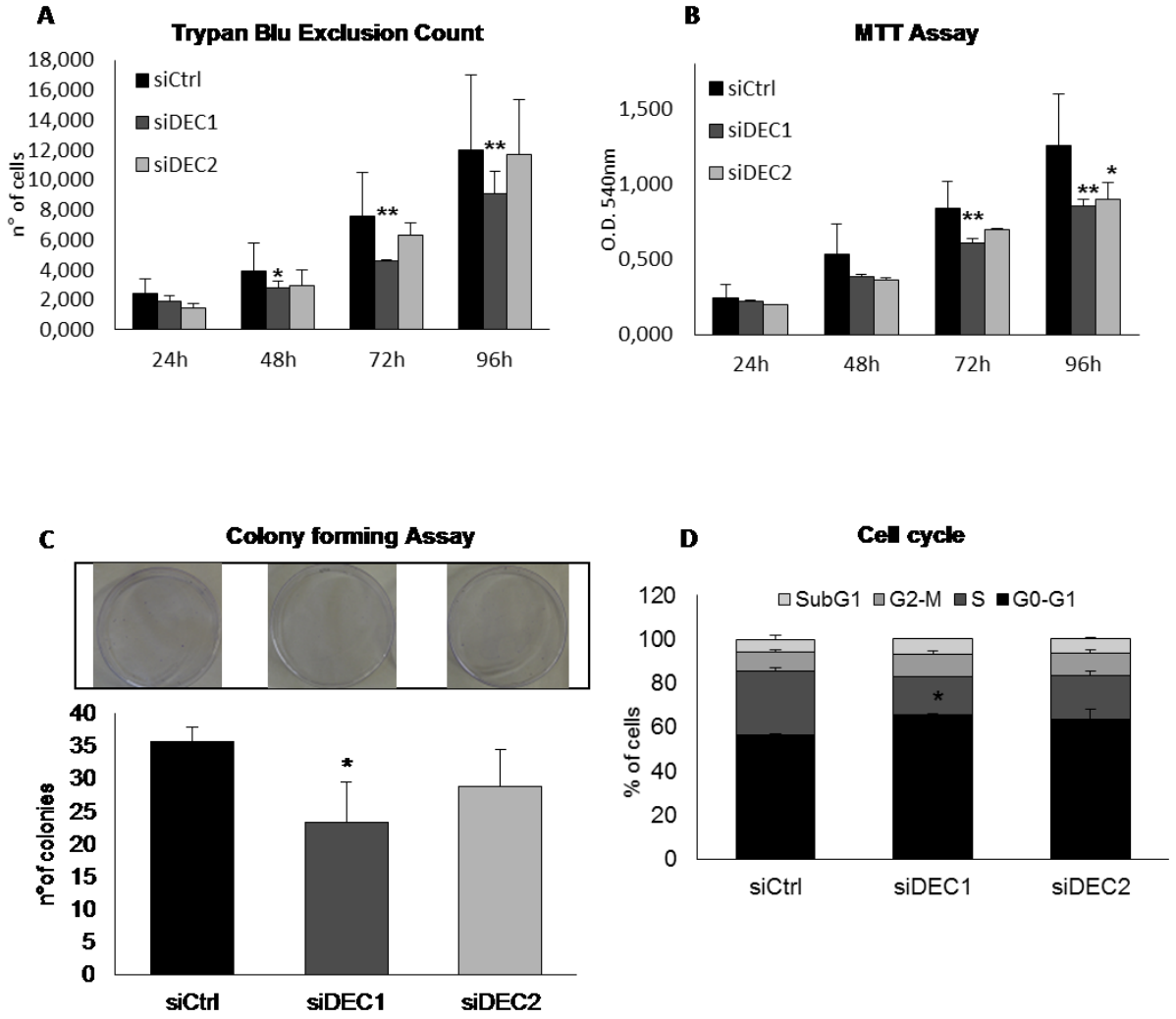

Figure 4. Effect of DEC1 or DEC2 silencing on BCPAP growth. BCPAP were transfected with 30nM siDEC1 or siDEC2 and proliferation (A) and viability (B) were assessed by Trypan Blue Exclusion Count from 24 to 96 hours. Colony formation (C) was evaluated after 10 days form transfection and the number and the size of colonies was calculated ImageJ Cell Counter Tool and expressed as percentage of control. Cell cycle (D) was evaluated after 72h from transfection by PI staining and the distribution of cells in the cell cycle phases was expressed as percentage of total cells.

DEC1 and DEC2 both affect cell migration and invasion in thyroid cancer cells

Then, we evaluated the effects of DEC1 and DEC2 knock-down on the ability of the cells to invade and migrate. As shown in figure 5, silencing of both DEC1 and DEC2, resulted in a reduced ability of TPC1 to invade (5A). In agreement with this observation, siDEC1 and DEC2 TPC1 cells showed increased adhesion capacities as compared with siCtrl cells (5B). Noticeably, silencing of DEC1 and DEC2 seems to equally affect invasion while DEC1 had a stronger effect on cell migration (5C).

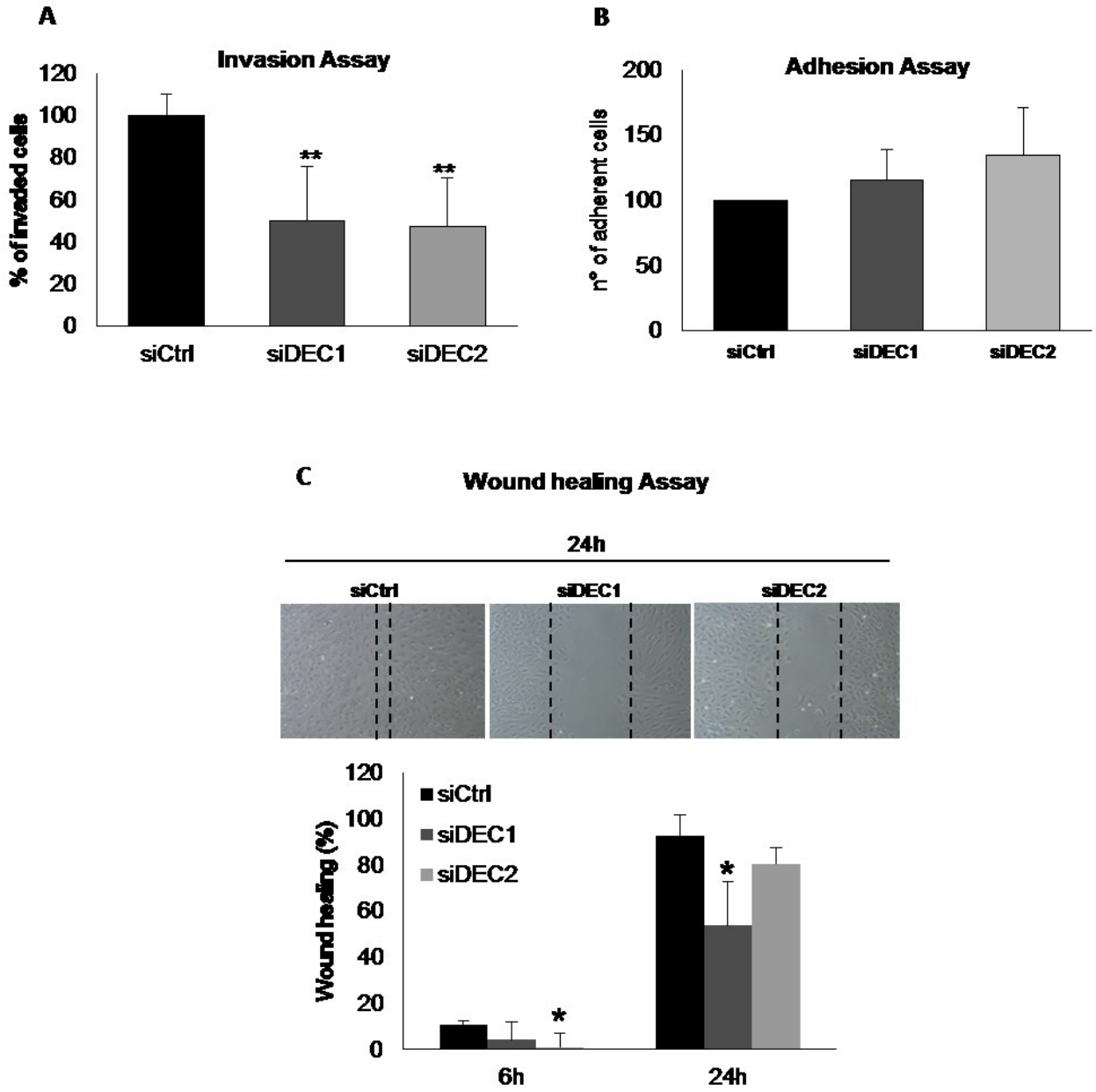

Figure5. Effect of DEC1 or DEC2 silencing on TPC1 invasiveness and motility. TPC1 were transfected with 30nM siDEC1 or siDEC2. For the invasion assay (A) cells were placed in serum-free medium in the upper side of a matrigel coated chambers and were allowed to invade up to 22h. For the adhesion assay (B) cells were seeded on a collagen coated plate and allowed to adhere for 30 minute. The number of invaded or adherent cells were counted by ImageJ Cell Counter tool and expressed as percentage of control. For the wound healing assay (C) cells were seeded and at 90% of confluence, they were scratched with a tip. Images were captured at 0, 6 and 24h, the scratch closure was measured by the ImageJ MRI Wound Healing tool and expressed as percentage of control at 24h.All the experiments was performed in triplicate. In C representative images of three independent experiments

A similar result was observed in BCPAP. Figure 6 shows the effects of DEC1 and DEC2 knock-down on cell invasion (6A), adhesion (6B) and migration (6C). DEC1 silencing more than DEC2 decreased the ability of BCPAP to invade. In the wound healing assay, we observed that only DEC1 silencing inhibited the gap closing after 6 hours, whereas after 24 hours both DEC1 and DEC2 silencing decreases the speed of migration.

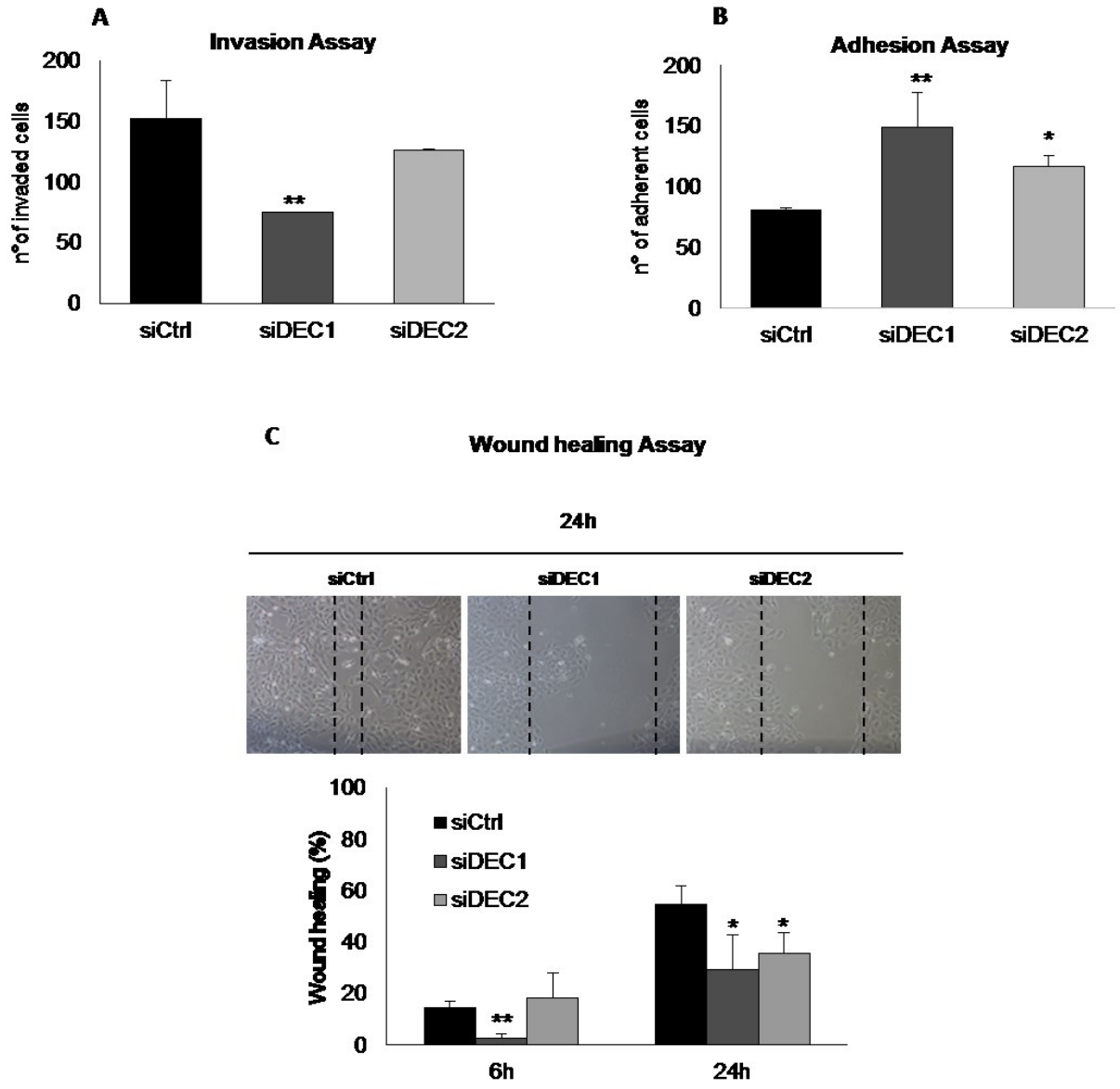

Figure 6. Effect of DEC1 or DEC2 silencing on BCPAP invasiveness and motility. BCPAP were transfected with 30nM siDEC1 or siDEC2. For the invasion assay (A) cells were placed in serum-free medium in the upper side of a matrigel coated chambers and were allowed to invade up to 22h. For the adhesion assay (B) cells were seeded on a collagen coated plate and allowed to adhere for 30 minute. The number of invaded or adherent cells were counted by ImageJ Cell Counter tool and expressed as percentage of control. For the wound healing assay (C) cells were seeded and at 90% of confluence, they were scratched with a tip. Images were captured at 0, 6 and 24h, the scratch closure was measured by the ImageJ MRI Wound Healing tool and expressed as percentage of control at 24h. All the experiments was performed in triplicate. In C representative images of three independent experiments

DEC1 overexpression induced thyroid cancer proliferation and promote invasiveness

To confirm the observation that DEC1 and DEC2 affect (even if with different extent) thyroid cancer biology, we used a gain-of function approach to prove that DEC1 and DEC2 overexpression promotes the acquisition of aggressive feature in thyroid cancer cells. To this purpose, we cloned DEC1 and DEC2 cDNAs in the pSG213 expression vector fused with a Flag epitope at the N-terminal and under control of a doxycycline inducible promoter. These constructs were transfected in TPC1 and BCPAP and DEC1 and DEC2 protein levels assessed upon doxycycline induction. As shown in figure 7 induction resulted in a strong Flag-DEC1 expression in both TPC1 and BCPAP and a Flag-DEC2 overexpression only in BCPAP.

Figure 7. Transient overexpression of DEC1 and DEC2. Cells were transfected with the DEC1-pSG213 or DEC2-pSG213 and the day after proteins overexpression were induced by 100ng/ml Doxycycline. Total proteins were extracted 24h after treatment. The lysate volume was normalized on the number of cells and DEC1 and DEC2 overexpression was evaluated by Western Blotting.

Next, BCPAP and TPC1 transfected with DEC1 or DEC2 inducible vector or with the empty vector were selected with Puromycin to derive stable clones. We were able to obtained stable clones only with DEC1 in BCPAP. Figure 8 shows Flag-DEC1 expression in three separate clones (DEC1-D3, DEC1-E2 and DEC1-E11) upon doxycycline induction.

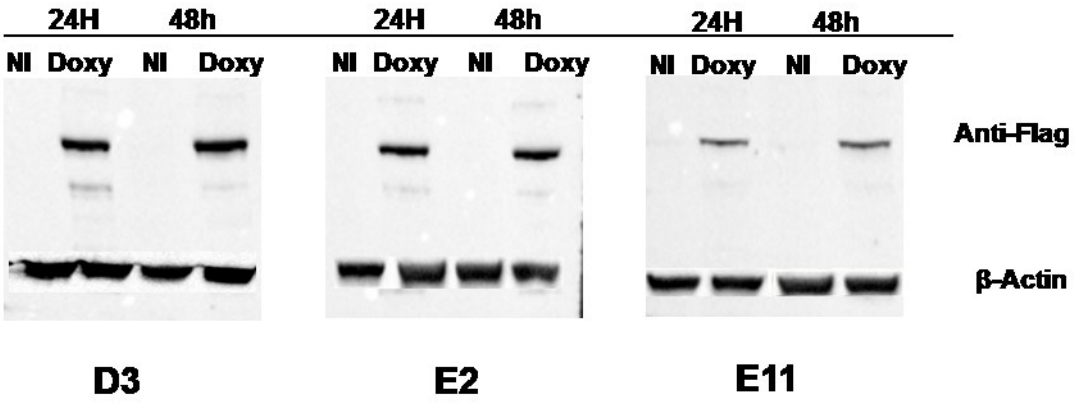

Figure 8. DEC1 overexpression in Doxycycline induced clones. All clones were treated 24h with 100ng/ml Doxycycline and overexpression was evaluated over time by Western Blotting. β-actin was used as normalizer.

Next, we performed functional assays to determine the biological properties of DEC1 overexpressing cells. Cell proliferation analysis showed that all 3 DEC1 overexpressing clones, upon doxycycline induction, proliferate faster than control cells (Ctrl-H3) (figure 9A), but DEC1 overexpression did not affect cell viability as displayed in the MTT assay (9B). Noticeably, in accordance with the data obtained in the silencing experiments, cell cycle analysis showed that DEC1 overexpressing clones displayed a faster S-phase entry and a consequent decrease of the G1-phase (9C).

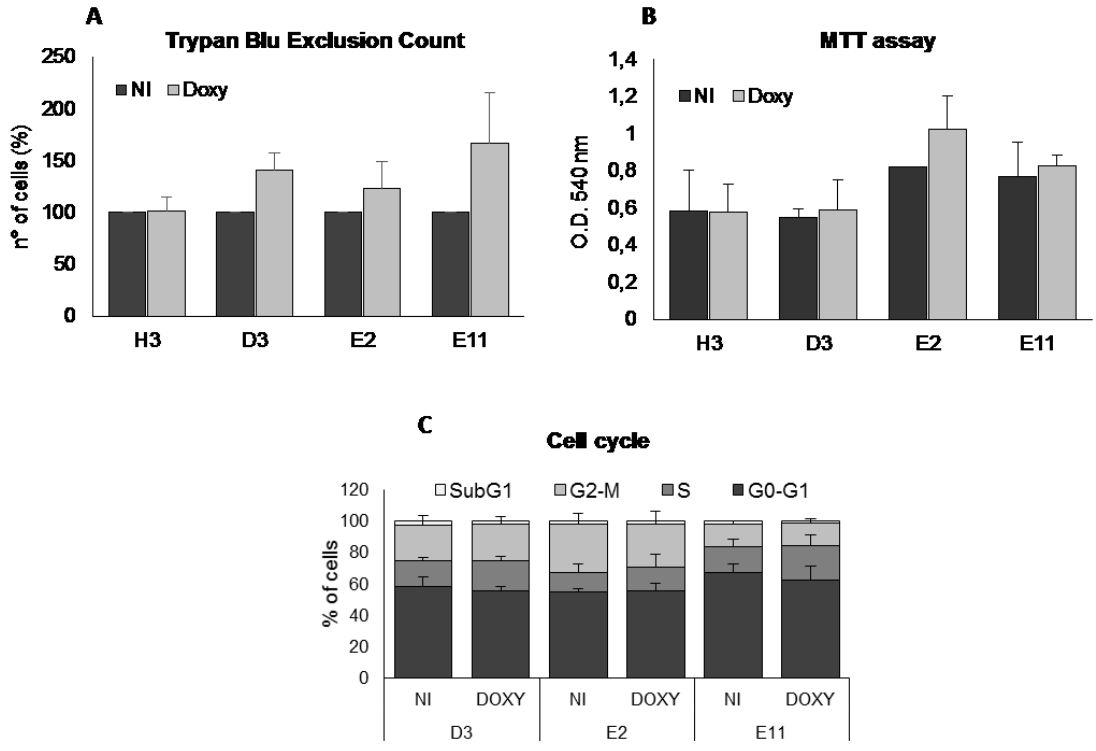

Figure 9. Effect of DEC1 overexpression on BCPAP clones growth. All clones were induced with 100ng/ml Doxycycline or DMSO (NI) for 72h and proliferation (A) and viability (B) were assessed by Trypan Blue Exclusion and MTT assay, respectively. The number of cells was expressed as percentage of control. Cell cycle (C) was evaluated after 72h of Doxycycline induction by PI staining and the distribution of cells in the cell cycle phases was expressed as percentage of total cells.

Next, we assessed the effect of DEC1 overexpression on invasion and migration of thyroid cancer cells. DEC1-E2 and DEC1-E11, showed a strong increase in invasiveness upon doxycycline induction, while the Crtl-H3 clone did not (figure 10A). By contrast, overexpression of DEC1 did not significantly affect cell migration. Only DEC1-E11 clone seems to fill scratch slightly faster than control (10B). Overall, these data demonstrate that DEC1 play a significant role in controlling aggressive features of thyroid cancer. In particular, DEC1 promotes proliferation by increase S-phase entry and cell cycle progression. In contrast, DEC2 seems to have only a marginal role in thyroid cancer.

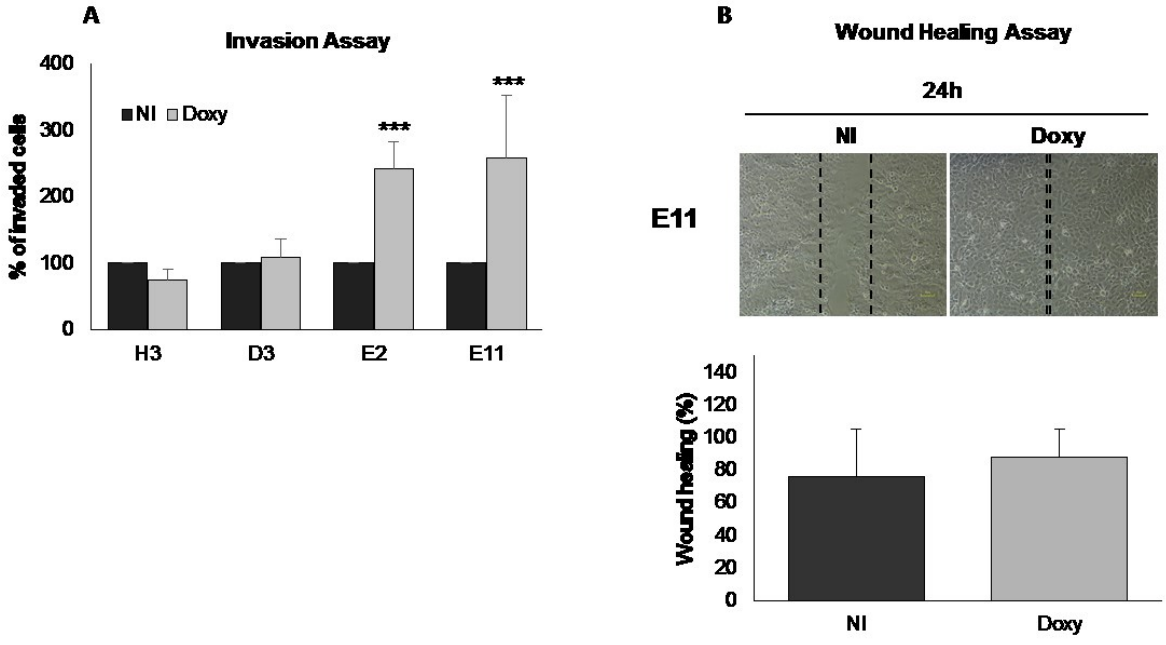

Figure 10. Effect of DEC1 overexpression on BCPAP clones motility. All clones were induced with 100ng/ml Doxycycline or with DMSO (NI) for 72h and invasion (A) was performed by matrigel coated chambers. The number of invasive cells was expressed as percentage of the not-induce control. For the wound healing assay (B), cells were seeded at low density and induced with Doxycycline. After 72h, achieved 90% of confluence, cells were scratched with a tip. Images were captured at 0, 6 and 24h and the scratch closure was measured by the ImageJ MRI Wound Healing tool and expressed as percentage of control at 24h.

DEC1 expression in vivo is specifically induced in thyroid tumor cells and characteristic of both well differentiated and undifferentiated form of thyroid cancer

Our in vitro data indicate a role of DEC1 in promoting thyroid cancer. To confirm these observations, we analyzed the expression of DEC1 in a retrospective cohort of 35 thyroid cancers representative of the 4 major histotypes: Anaplastic Thyroid Cancer (ATC), poorly differentiated thyroid cancer (PDTC), Papillary thyroid cancer (PTC) and Follicular thyroid cancer (FTC) (Table 1).

HISTOTYPES	ATC	PDTC	PTC	FTC
N° of Samples (%)	6 (17,1%)	7 (20%)	13 (37,2%)	9 (25,7%)

Table 1. Distribution of the thyroid cancer histotypes in the analyzed cohort.

The large majority of tested samples displayed a strong expression of DEC1 with only two samples negative for DEC1 expression. Noticeably, DEC1 expression was specific of tumor cells, since normal adjacent thyroid tissue scored negative for DEC1 expression in all samples (figure 11). This observation indicates that expression of DEC1 is aberrantly reactivated during tumorigenesis and mark the difference with normal thyrocytes. In all samples, DEC1 showed a nuclear localization and a homogenous expression. In some cases, we observed an increased concentration of DEC1 positive cells around pre-necrotic area suggesting that nutrient and oxygen deprivation may trigger DEC1 expression. This is in agreement with the reported observations that DEC1 expression is induced under stress condition and in particular under hypoxia. DEC1 expression was consistently overexpressed in all histotypes analyzed without significant difference (11A). Noticeably, DEC1 was strongly expressed also in ATCs which represent the most aggressive and ominous form of thyroid cancer. Overall these observations confirm in vivo the relevance of DEC1 in thyroid development and progression.

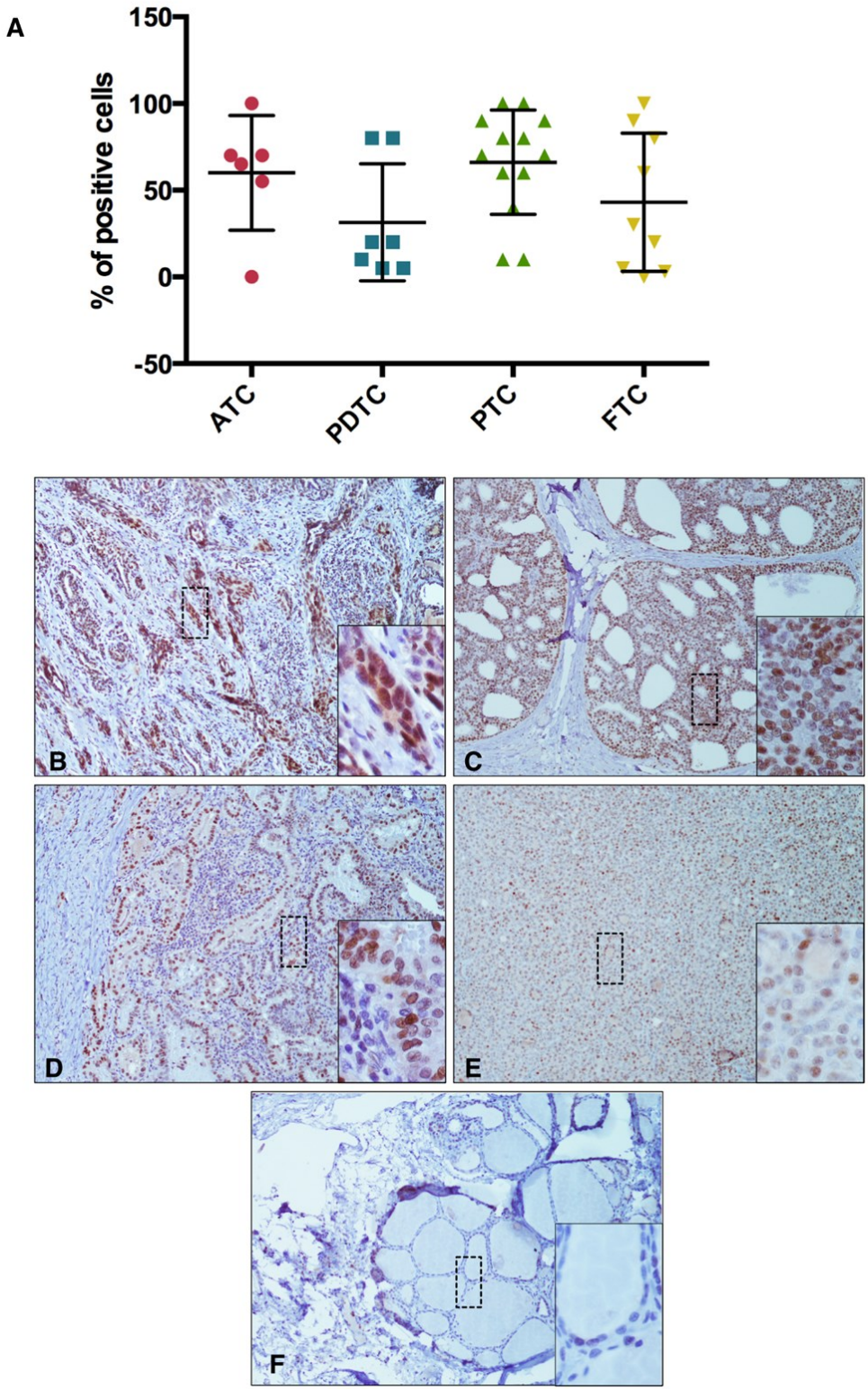

Figure 11. DEC1 expression in the analyzed cohort of thyroid tumors. (A) Distribution of DEC1 expression in the different histotypes included in the cohort. DEC1 resulted highly represented in Anaplastic thyroid carcinomas (B), Follicular thyroid cancer (C), Papillary thyroid carcinomas (D), poorly-differentiated thyroid cancer (E) as compared to the normal tissue (F).

NOTCH pathway cooperates with DEC1 to support thyroid cancer progression

NOTCH signaling is an evolutionarily conserved intercellular pathway involved in many relevant biological processes including cell fate specification, differentiation, proliferation, and survival. Activation of NOTCH has been shown to promote tumorigenesis and increased expression of NOTCH receptors has been observed in a variety of human cancers types. Recent studies indicate a role for NOTCH1 also in thyroid tumors where activation of NOTCH signaling supports aggressiveness.

After the activation of NOTCH1 by cleavage, NICD is released in cytoplasm. NICD reaches the nucleus to up-regulate the expression of NOTCH1 target genes. The activation of target genes transcription occurs due to the binding to RBP-Jκ. The HES and HEY family, belonging to the class E of bHLH transcription factors, are primary NOTCH1 target genes and act as NOTCH effectors by regulating the repression of NOTCH1 downstream targets and by mediating the crosstalk between NOTCH signaling and other cancer related pathway. Notable, members of these family may physically interact with RBP-Jκ to promote a mechanism of negative feedback on NOTCH signaling. Thus, since DEC1 is a member of the same class E of bHLH proteins we hypothesize that NOTCH pathway may cooperate with DEC1 in controlling thyroid cancer. Supporting this hypothesis, some known targets of DEC1 have been reported to be also targeted by NOTCH1.

In order to prove our hypothesis in the context of thyroid cancer, we silenced DEC1 in TPC1 and analyzed the effect on the expression and activation of NOTCH pathway related proteins. We showed that the expression of NOTCH1 was significantly downregulated both at the mRNA and protein levels in DEC1 knocked-down cells (Figure 12A and B). Viceversa, transient overexpression of DEC1 resulted in increased levels of the activated form of NOTCH1, NICD in TPC1 (12C). Furthermore, we observed that the expression of NOTCH1 ligands (Delta1 and Jagged1) was also repressed upon DEC1 silencing (12D).

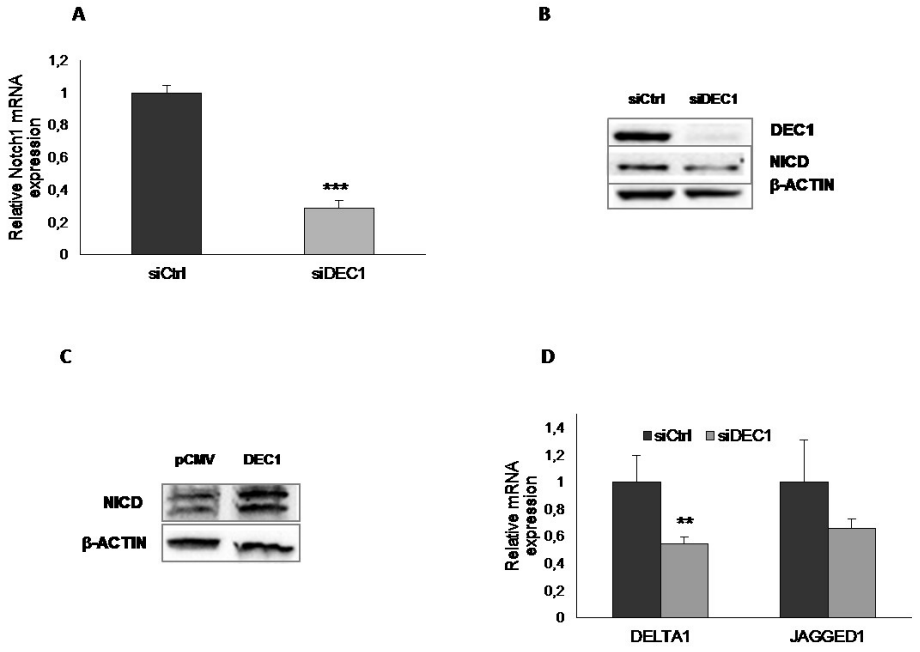

Figure 12. Effect of DEC1 knock-down on NOTCH1 expression. TPC1 were transfected with DEC1 siRNA and NOTCH1 expression was evaluated after 72h by qRT-PCR (A) and by Western Blot analysis (B). Then, DEC1 was transient overexpressed in TPC1 and NOTCH1 expression was assessed by Western Blotting (C). The mRNA expression of NOTCH1 ligand, DELTA1 and JAGGED1 was also measured after DEC1 knock-down by qRT-PCR (D).

To ascertain the role of DEC1 on NOTCH pathway activation we checked the effect of DEC1 silencing on some targets of the canonical and non-canonical pathway of NOTCH1. qRT-PCR and western blot analysis demonstrated that NOTCH target genes c-MYC, p21, Hey1 and HIF1a were inhibited upon DEC1 silencing (figure 13A). Furthermore, reduced DEC1 expression resulted in an evident decrease in the Ser473 phosphorylation of Akt, which is induced upon NOTCH1 activation (13B).

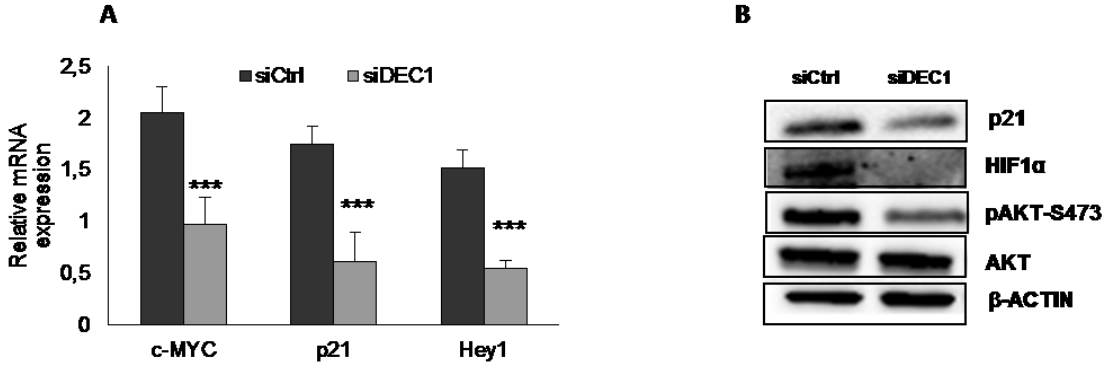

Figure 13. Effect of DEC1 knock down NOTCH1 target genes. TPC1 knocked-down for DEC1 was harvested and mRNA and protein were extracted. The expression of c-Myc, p21 and Hey1 was evaluated by qRT-PCR (A), whereas the expression of p21, HIF1α and AKT was verified by Western Blot analysis (B). The activation of the NOTCH pathway was also evaluated by monitoring the phosphorylation of AKT on the Ser473.

All together these results demonstrated that DEC1 positively controls NOTCH pathway in thyroid cancer cells. Next, we investigated whether activation of the NOTCH pathway is functionally relevant for the DEC1-mediated thyroid cancer aggressiveness. To this purpose we treated TPC1 cells with DAPT a chemical inhibitor of the γ-secretase that cleaves and activates NOTCH1 upon ligand engagement (Introduction, figure 5). First, we confirmed the inhibitory activity of DAPT on NOTCH pathway in our system. As expected, western blot analysis showed that the levels of NICD dropped dramatically upon DAPT treatment. As well, levels of p21 and HIF1α were also strongly repressed by the treatment (14).

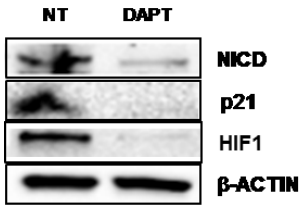

Figure 14. Effect of DAPT treatment on NOTCH signaling. TPC1 were treated 48h with 30μM DAPT and the effects on NOTCH signaling was assessed by Western Blotting. β-actin was used as normalizer of protein concentration.

Next, we explored the effects of DAPT on thyroid cancer behavior. Noticeably, we observed that DAPT treatment inhibited cell proliferation and viability of both TPC1 (figure 15 A and B) and BCPAP (15C and D) in a dose dependent manner, similarly to the effect observed by inhibiting DEC1.

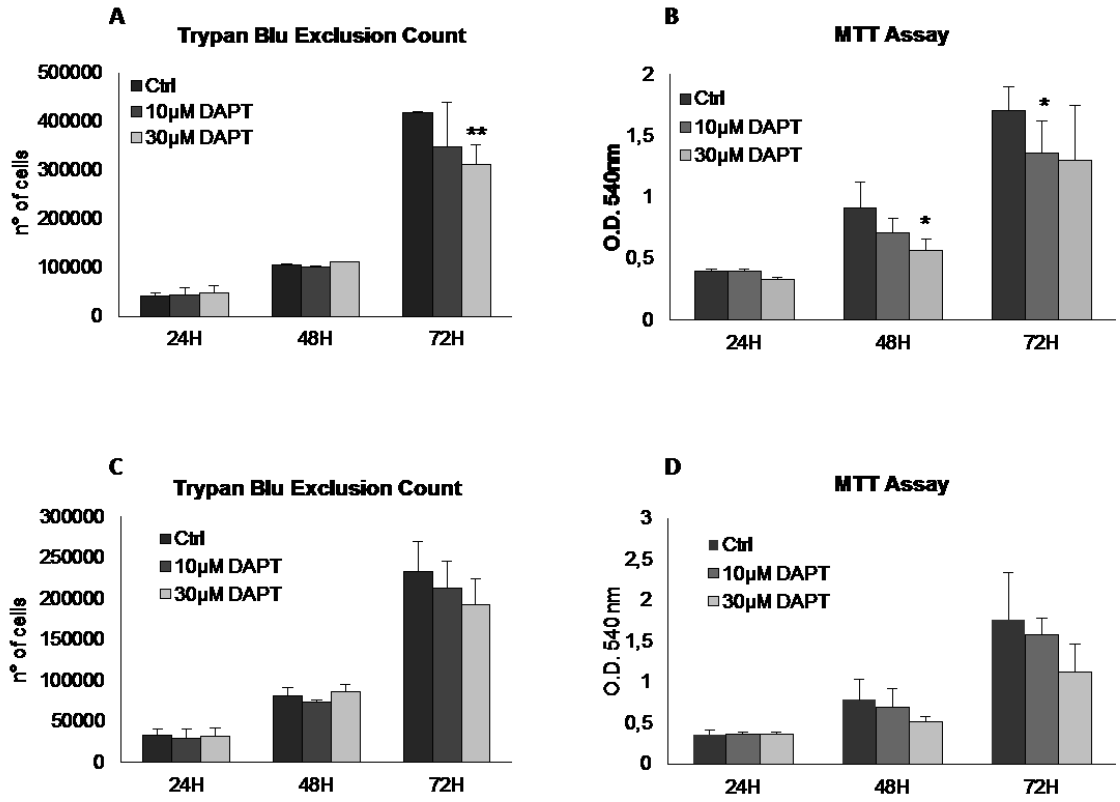

Figure 15. Effect of DAPT on TPC1 and BCPAP growth. Cells were treated with 10 and 30μM DAPT or with vehicle (DMSO) and TPC1 (A) and BCPAP (C) proliferation was assessed by Trypan Blue Exclusion Count up to 72h, whereas TPC1 (B) and BCPAP (C) viability was evaluated by MTT assay.

To demonstrate, that activation of the NOTCH pathway is necessary for the DEC1 aggressiveness promoting function in thyroid cancer we analyzed the effect of NOTCH inhibition in DEC1 overexpressing clones. Thus, we treated the DEC1-E11 and DEC1-D3 clones with DAPT and we evaluated changes in cell proliferation, migration and invasiveness. Noticeably, NOTCH1 inhibition completely abolished the gain in cell proliferation induced by DEC1 overexpression in both clones (figure 16A). As well in the invasion assay all clones lose their capability to enhance invasion through DEC1 overexpression when they are treated with the NOTCH1 inhibitor (16B). Since DEC1 overexpression weakly affects migration, the effect of DAPT treatment is observable only on DEC1-E11 clone, which seems to lose the ability to faster fill the slit and it effect is more similar compared to the not induced control (16C).

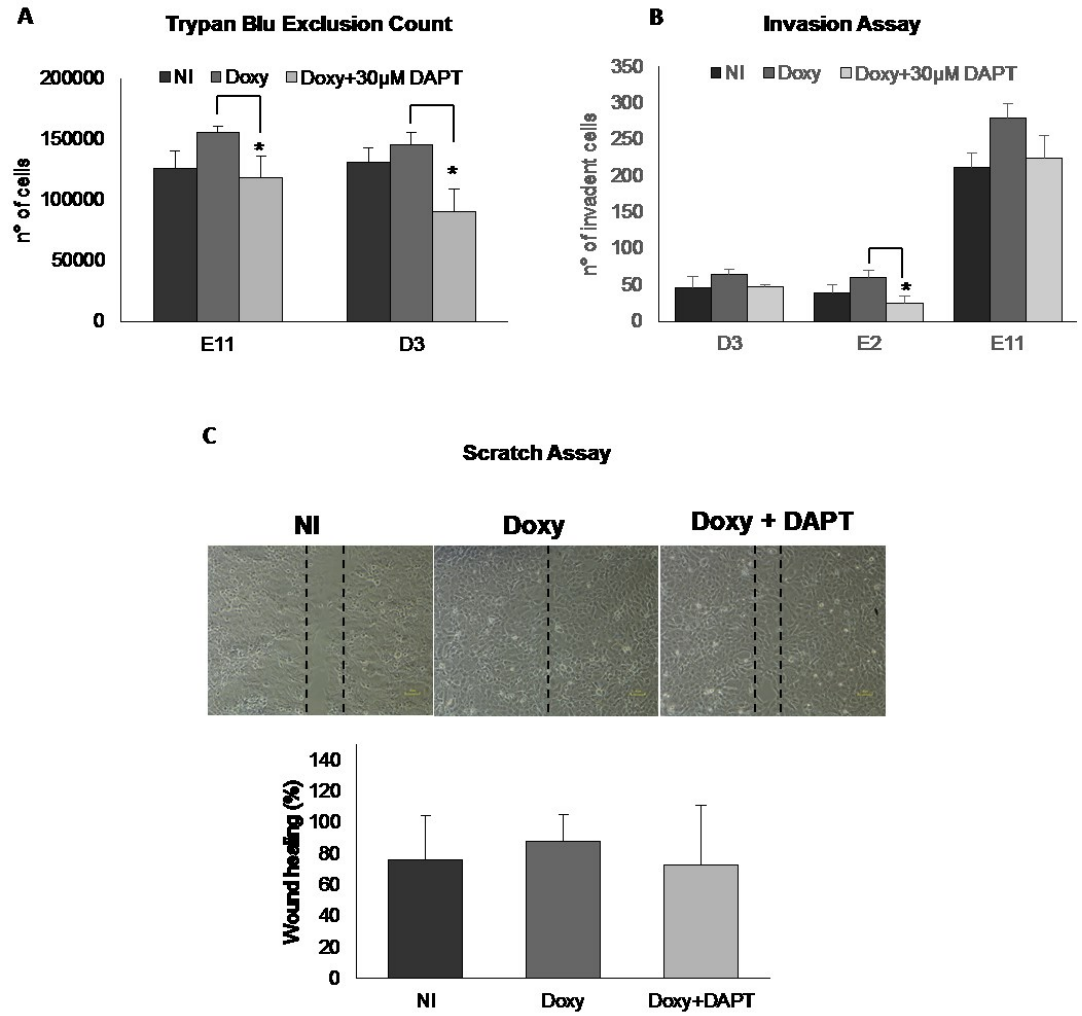

Figure 16. Effects of DAPT treatment on DEC1 overexpressing clones. Clones were treated with vehicle (DMSO), or induced by 100ng/ml Doxycycline or induced and treated with 30µM DAPT. Cell proliferation (A) was evaluated by counting cells after Trypan Blue staining after 72h of treatment. Invasion assay (B) and wound healing assay were performed after 48h of treatment, and cells were allowed to invade or migrate in treated medium for other 22h or 18h, respectively. Pictures are representative of three independent experiments.

All together these observations indicate that: 1) DEC1 promotes the activation of the NOTCH pathway primarily by stimulating the expression of NOTCH1, 2) Activation of the NOTCH pathway is necessary for the tumor promoting function of DEC1 in the thyroid. Noticeably, we also demonstrated that DAPT treatment reduced both the mRNA and the protein levels of DEC1 (figure 17A and B).

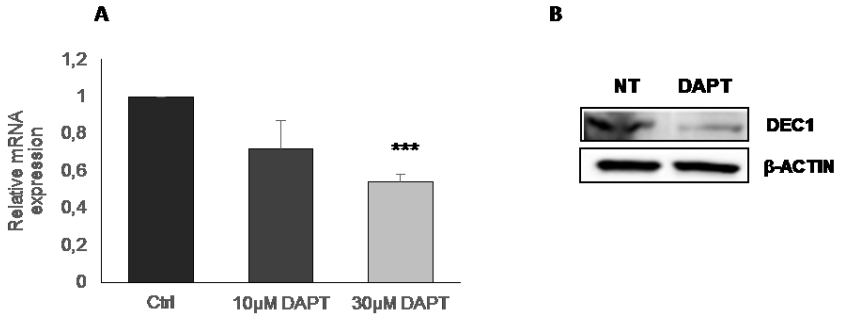

Figure 17. Effect of DAPT treatment on DEC1 expression. TPC1 were treated 48h with 10 and 30μM DAPT and DEC1 expression was evaluated by qRT-PCR and Western Blot analysis.

To the best of our knowledge, this is the first report describing DEC1 as target of NOTCH1. This observation implies the existence of a possible positive feedback between DEC1 and NOTCH that would further fuel thyroid cancer development and progression.

DEC1 coordinates the expression of a gene network functionally involved in cell cycle activation

To get further insights into the molecular mechanisms through which DEC1 sustains thyroid cancer progression, we explored the gene expression profile associated with this transcription factor in TPC1 cells. To this purpose, we performed RNA-Sequencing analysis on TPC1 cells transfected with siRNA against DEC1 of with scramble Ctrl siRNA. After, reads alignment and normalization, we performed a differential analysis between siDEC1 and siCtrl. 320 genes were significantly differentially expressed in siDEC1 cells and compared to controls. A higher number of genes resulted significantly repressed upon DEC1 silencing (n=166) as compared to up-regulated genes (n=154). DEC1 biological functions have been largely associated with its ability of working as transcriptional repression. By contrast these data suggest that DEC1 transcriptional activation play a relevant part in mediating DEC1 effect in thyroid cancer. Next we performed a Gene Ontology enrichment analysis to establish which pathways were majorly affected by DEC1 silencing.

Gene upregulated upon DEC1 silencing, were enriched for pathways related to developmental process regulation, extracellular matrix and collagen regulation and blood vessel formation (figure 18). These

function could mediate the DEC1 function in controlling invasiveness of thyroid cancer cells.

A

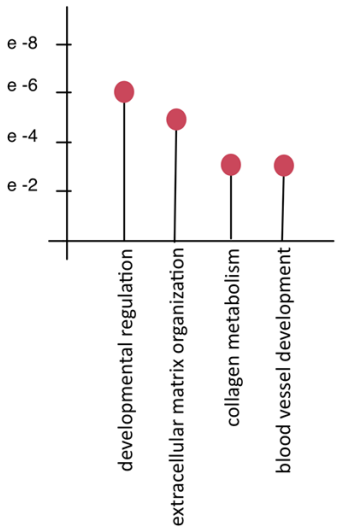

B

Developmental regulation			Extracellular Matrix Organization	Collagen Metabolism	Blood Vessel development
ACVR2B	CRMP1	PAK3	COL12A1	COL12A1	HEG1
ADAM19	CRYAB	PAX2	ITGB8	P3H4	ANTXR1
ADGRG1	ECM1	PTHLH	P3H4	COL5A2	ACVR2B
ANTXR1	EPHB2	PYGO1	COL5A2	FURIN	TGFBR3
APBB2	F2RL1	RAPGEFL1	FURIN	COL5A1	ITGB8
ARF4	FJX1	SLC38A2	COL5A1	COL4A4	EPHB2
ATN1	FURIN	SMPD1	COL9A2	CTSO	CCL2
BHLHE41	GBP3	SPOCK1	COL4A4		UNC5B
BMP1	GLI3	TGFBR3	ADAM19		ECM1
C5AR1	HEG1	TLR4	CTSO		GLI3
CAV1	INHBA	UNC5B	BMP1		COL5A1
CCL2	ITGB8	WNT5A	APBB2		CAV1
CD109	KDM6B	YBX3	COL16A1		ADGRG1
COL12A1	KLF10	ZNF703			
COL4A4	LHX1				
COL5A1	MBOAT7				
COL5A2	MXRA8				
COL9A2	NTN4				

Figure 18. Gene Ontology analysis of up-regulated genes. (A) Top scoring enriched pathways obtained by GO analysis of the up-regulated genes.

By contrast, no significant enriched pathways were detected in the down-regulated genes. Thus, we performed a network analysis to establish whether these genes were linked within a common functional network. As reported in figure 19, this analysis revealed the existence of a module of functionally related genes. These genes were involved in biological processes directly or indirectly

linked to the cell cycle regulation. Two aspect of cell cycle seemed to be particularly affected: the G1/S phase transition and chromosomal segregation. These data are in agreement with the DEC1 effect on cell cycle regulation observed in the functional assays and unveil a previously unknown function of DEC1 in cancer.

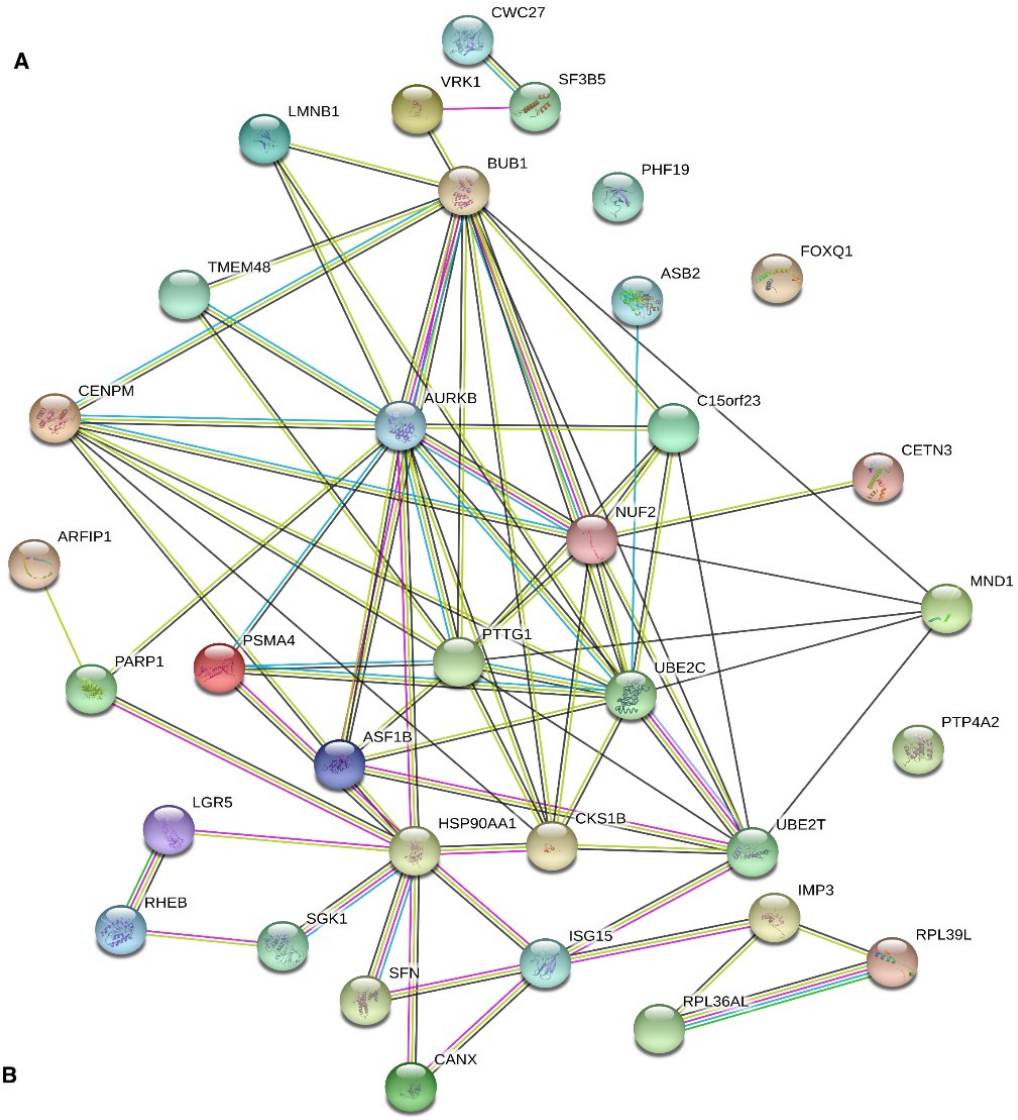

	BIOLOGICAL PROCESS		
pathway ID	pathway description	count in gene set	false discovery rate
GO:0007049	Cell cycle	15	3.49e-06
GO:0000278	Mitotic cell cycle	12	8.61e-06
GO:0022402	Cell cycle process	13	8.61e-06
GO:1903047	Mitotic cell cycle process	11	2.84e-05
GO:0000280	Nuclear division	9	4.17e-05
GO:0007059	Chromosome segregation	6	7.48e-04

Figure 19. Network analysis of down-regulated genes. This analysis was performed by the online free software STRING that reviled functional network within a list of genes (A). The genes involved in this functional network was also classified based on the relation with specific processes (B).

Since we showed the interplay with the NOTCH pathway is relevant to mediate the DEC1 function in thyroid cancer we searched for NOTCH targets among the DEC1 target genes. Noticeably, both NOTCH1 and p21 resulted significantly downregulated in this analysis confirming our data. Beside, 24 genes in the down-regulated list and 26 genes in the up-regulated genes were directly or indirectly linked to NOTCH pathway (table 2). In particular, genes like CDCA7 known to be target of NOTCH pathway functionally cooperate to the pro-oncogenic function of c-MYC. Noticeable, we also identified a series of deregulated genes directly involved in other two relevant cancer-related pathways, the TGFβ/BMP and WNT/β-catenin signaling (table 2), unveiling novel potential DEC1 roles.

	Down-regulated genes	**Up-regulated genes**
Differentially Expressed Genes	166 (51.9%)	154 (48.1%)
NOTCH1-related	24 (14.4%)	26 (16.8%)
BMP/TGFβ-related	1 (0.6%)	10 (6.5%)
WNT-related	3 (1.8%)	7 (4.5%)

Table 2. Distribution of DEC1 deregulated genes based on the relation with specific pathways.

Of note, DEC2 resulted significantly up-regulated upon DEC1 silencing. We confirmed this observation by checking DEC2 mRNA and protein levels in DEC1 silenced TPC1. As shown in figure 20, DEC2 levels were profoundly affected by DEC1 silencing demonstrating that DEC2 is negatively regulated by DEC1, consistently with the report of Yuxin Li et al [45]. Understanding the functional implication of this regulation requires further investigation.

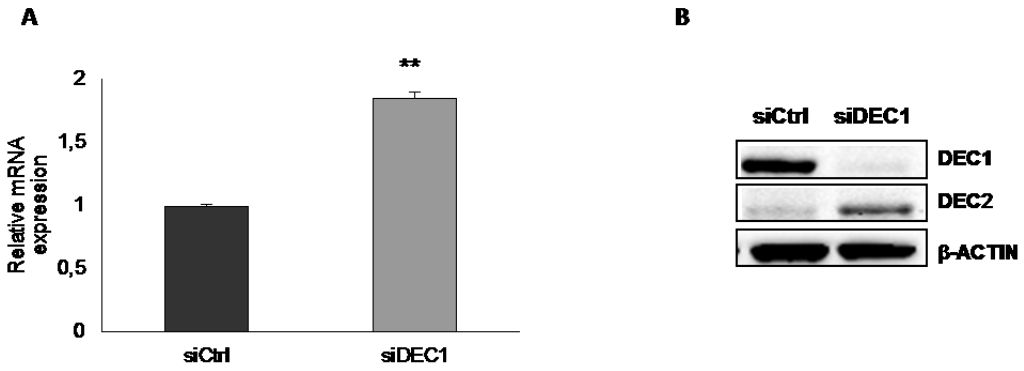

Figure 20. Effect of DEC1 knock down on DEC2. TPC1 were silenced for DEC1 and DEC2 expression was evaluated both by qRT-PCR (A) and Western Blotting (B).

DISCUSSION

PTC are usually indolent lesions with low rate of growth and low metastatic potential. Nonetheless, a small but significant percentage of PTC (5–10%) develop an aggressive phenotype with distant metastases, leading to poor outcome [1]. The identification of prognostic markers able to discriminate PTC that will switch toward a metastatic phenotype would be of great relevance to improve diagnostic tools and the therapeutic approaches. In this context, we recently identify Id1 as a driver of thyroid tumor aggressiveness [46]. Among the Id1 upregulated gene we found highly ranked DEC1 and DEC2. Thus, our starting hypothesis placed DEC1 and DEC2 inside the driving mechanisms of PTC aggressiveness.

It has been reported that DEC1 and DEC2 were deregulated in esophageal squamous cell carcinoma, breast, pancreatic, and human endometrial cancer [39, 41, 80]. However, in many cases DEC1 and DEC2 have been suggested to play opposite roles in several cancer-related processes. Here we explored DEC1 and DEC2 role in papillary thyroid cancer. To this purpose we deregulated DEC1 and DEC2 expression level by loss and gain of function approaches. We choose two different cell lines, TPC1 and BCPAP, as two model of PTC with different grade of aggressiveness. For the first time we demonstrated that DEC1 is involved in PTC aggressiveness. Both TPC1 and BCPAP capability to growth and invade were significantly inhibited upon DEC1 knock-down with a more pronounced effect on TPC1, the more aggressive cell lines, consistent with our hypothesis. Moreover, DEC1 overexpression enhances proliferation and invasiveness of thyroid tumor cells. This observation is in contrast with previous report on breast cancer cells MCF-7, where DEC1 displayed pro-apoptotic effects and its overexpression reduced proliferation and colony formation [43].

It has been reported that DEC2 may play both as tumor suppressor and oncogene [29, 33, 37, 81]. The overexpression of DEC2 inhibited cell proliferation in lung, breast and gastric cancer [43, 83]. Contrariwise, DEC2 is involved in anti-apoptotic processes in human oral cancer and increased invasiveness in osteosarcomas [37, 42]. However, in our system DEC2 seemed to have a marginal

role. We observed that DEC2 had only a low effect on PTC where it controlled cell invasion but not proliferation.

Differently from what has been reported in literature, we did not observe an opposite behavior between DEC1 and DEC2 in relation to PTC biology regulation. Rather, we observed that DEC2 displays a similar but less evident effect on cell motility and invasiveness as compared to DEC1. We may speculate that in PTC these transcription factors converge on the same target genes, orchestrating a similar phenotype. This is in line with what has been reported by Asanoma et al., who described how, in endometrial cancer DEC1 and DEC2 work together with a prominent activity for DEC2 on their target genes [80].

For the first time we evaluated the expression of DEC1 in a cohort of thyroid tumors with different histotypes and we demonstrated that DEC1 expression is specific of tumor cells. This is consistent with the report of Yuxin Li et al., who observed that DEC1 is strongly associated to tumor in a comparative experiment among different paired tumor-normal tissues [45]. Further, we observed a nuclear localization of DEC1 and a strong expression in ATCs which represent the most aggressive form of thyroid cancer. Notable, our finding is consistent with the evidence that DEC1 is highly expressed, in samples of gastric cancer with poor histologic differentiation [83]. By contrast, DEC1 nuclear expression correlates with increased hepatic tumor cells differentiation, even if in normal hepatocytes DEC1 localization is cytoplasmic [36].

The increased expression of NOTCH1 receptors has been associated to aggressiveness in thyroid tumors, even if reports are often in contrast and do not clearly elucidate the role of NOTCH signaling in papillary thyroid cancer. Xiao-Min Yu et al, observed that TPC1 exhibit higher NICD levels as compared to BCPAP, but they also observed that NOTCH1 knock-down in TPC1 cells resulted in increased ability of cell migration [70]. Differently we observed that the NOTCH1 chemical inhibition DAPT caused a decreased in cell proliferation. Moreover, when we blocked NICD formation by DAPT treatment in DEC1 overexpressing clones, we observed a significant inhibition

of cell invasion and a reduction in cell proliferation. Our data fit with the report of Hyeon Jin Kim et al., where they demonstrated the correlation between NOTCH1 activation and aggressive feature in anaplastic thyroid tumors [69]. They also observed that DAPT treatment weakly reduced BCPAP migration and cell proliferation as compared to anaplastic cells, where the effect of NOTCH inhibition was largely higher. Since, Vasko et al. demonstrated that the invasive front of PTC showed increased expression of EMT-related genes compared to the central lesion of PTC [84], they postulated that NOTCH signaling influenced the malignant potential of thyroid cancers. In accordance to their conclusion we also observed that DEC1 knock-down decreased the transcription of NOTCH1 receptor and the levels of NICD formation, while transient overexpression of DEC1 caused increased NICD. Hongliang Fu et al., also observed a close relation between the expression of NOTCH1 receptor and some aggressive features such as the larger tumor size (>2 cm), distant metastasis and capsule invasion [71]. In agreement with Hyung Seok Park et al., these authors concluded that PTC patients with positive expression of NOTCH1 receptor tend to have higher tumor invasiveness and NOTCH1 expression may be related to poor prognostic markers in patients with PTC [85]. Furthermore, Chang Won Jung et al., showed that the activation of NOTCH1-Hey1 pathway was associated with severe clinical factors, such as lymph node metastasis, extra-thyroidal extension and recurrence [86]. HEY1 is the effector of NOTCH1 and a marker of NOTCH pathway activation. In our model, the knock-down of DEC1 ended in a significantly reduction of both NOTCH1 and HEY1 expression. Intriguingly, HEY1, together with DEC1 and DEC2, belong to the class E of bHLH transcription factors. Within this family, several bHLH genes has been recognized as NOTCH1 target genes [72]. For the first time we demonstrated that NOTCH1 is a target of DEC1. Moreover, we also observed an inhibition of DEC1 expression both on the mRNA and the protein level when NOTCH pathway was inhibited by by DAPT treatment. These results suggest the existence of a potential feed-back mechanism between DEC1 and NOTCH1.

HIF-1α is one of the major NOTCH1 target in cancer [87]. Here, we showed that HIF-1α expression is significantly reduced by DEC1 knock-down. HIF-1α is the main regulator of tumor angiogenesis

and its activation sustains tumor progression by promoting tumor cell migration and proliferation in many solid tumors. Its overexpression has been correlated with high risk of metastasis and high mortality in many human cancers [88]. Under hypoxic stress, HIF-1α binds to hypoxia response element in the DEC1 and DEC2 promoter [89, 90]. Recent studies suggested that DEC2 promotes HIF-1α degradation in breast and endometrial cancers, whereas in osteosarcoma DEC2 activated HIF-1α [91, 92]. Hu et al. also observed that in osteosarcoma DEC2 and HIF-1α formed a vicious circle, promoting one the expression of the other [42]. Consistent with this observation we speculated that the potential DEC1-NOTCH1 loop may control HIF-1α or that this loop may occurs due to the HIF-1α mediated regulation, but further experimental evidences need to be collected. Other deregulated factors related to the NOTCH pathway confirmed the interplay between NOTCH1 and DEC1. We for the first time unveiled that DEC1 and NOTCH1 participate to the pro-oncogene function of c-MYC by the direct regulation of CDCA7, a cell division associated protein contributing in c-MYC mediated tumorigenesis [93].

To further explain the molecular mechanism through which DEC1 sustains aggressiveness of papillary thyroid carcinomas, we explored the gene expression profile associated with this transcription factor. Among the significantly differentially expressed genes we observed that the 51.9% of genes were down-regulated, suggesting the fundamental role of DEC1 as transcriptional activator in papillary thyroid cancer. Although DEC1 is generally considered a transcriptional repressor, our observation is consistent with previous studies where DEC1 works as transcriptional activator of p73 (a member of p53 family) or Survivin in other context [94, 95]. Moreover, among the DEC1 activating genes we observed a higher percentage of cell cycle related genes mostly involved in the G1/S phase transition and chromosomal segregation and this is in accordance with our functional data showing that silencing of DEC1 reduces cell cycle progression. The Vaccina Related Kinase1 (VRK1) was among the genes significantly downregulated in siDEC1 cells. VRK1 is required for the exit of G0 and entry in G1 phase and its knock-down has been proven to induce a reduction of cell proliferation [96]. Previous studies suggest the role of DEC1 in apoptosis and in the

S phase of cell cycle [43, 97]. In breast cancer, DEC1 regulates cyclin E and delays the progression of cell cycle S phase [98]. Our data for the first time underline a potential role for DEC1 in the G2M phase. Consistent with the reduced malignant phenotype of TPC cells after DEC1 knock-down, we found AURKB, the Aurora kinases, in our list of downregulated genes. Overexpression of AURKB, has been reported in a variety of cancers and several evidences suggested that inhibition of Aurora kinases could potentiate the effect of chemotherapies [99]. In Anaplastic thyroid tumors, AURKA and B are overexpressed [100]. Moreover, drugs against AURKs have been successfully tested in pre-clinical model of ATCs and are currently in trials for these patients [101-103]. Since deregulation of genes essential for genome stability and chromosomes segregation are a source for cancer cell selection and accumulation of mutations, we unveiled a previously unknown function of DEC1, in this context.

Noticeable, analysis of the RNA-Seq data also indicate that, beside NOTHC pathway, DEC1 may interfere with the TGFβ/BMP and WNT/β-catenin signaling pathways. Both these pathways, are key signaling cascade during embryonic development and cell fate determination. Their role has also been widely demonstrated in cancer with prominent roles in cell differentiation and survival [104, 105]. Interestingly TGFβ/BMP and WNT/β-catenin signaling may cooperate both in synergy and antagonism with NOTCH signaling [106-109]. Moreover, a recent study unveiled that a bHLH transcription factor, also a direct target of NOTCH signaling, may mediate the crosstalk between TGFβ/BMP and NOTCH signaling [110].

Noticeable, we demonstrated that DEC1 activates the NOTCH signaling but, within our lists of up- and down-regulated genes, we counted more or less the same number of proteins directly or indirectly linked to NOTCH. When we screened all these proteins for their potential or proved involvement in cancer related processes, we found that DEC1 activated about 3.8% and repressed about 1.9% of the deregulated genes belonging to NOTCH1 pathway. On the contrary, DEC1 repressed the majority of the genes involved in the TGFβ/BMP and WNT/β-catenin signaling.

Of note, among the up-regulated genes, DEC2 resulted significantly repressed by DEC1 and we confirmed this result. Thus, we demonstrate that DEC2 is negatively regulated by DEC1, consistently with the report of Yuxin Li et al., which underlined the DEC1 ability to directly bind the E-Box and to repress the DEC2 promoter [45]. Overall, our data described DEC1 as a transcriptional repressor of DEC2, but also as transcription activator of NOTCH1, its effector HEY1 and their common target genes c-Myc and CDCA7.

In conclusion we demonstrate that DEC1 is highly expressed in thyroid tumors and it is involved in the processes driving PTC aggressiveness. Moreover we described the existence of a novel axis between DEC1 and NOTCH1, further clarifying the role of NOTCH1 signaling in PTC. Finally, we identify a novel DEC1function, as activator of a novel network of target genes involved in mitosis and chromosomes segregation.

REFERENCES

1. Randle RW, Bushman NM, Orne J, Balentine CJ, Wendt E, Saucke M et al. Papillary Thyroid Cancer: The Good and Bad of the "Good Cancer". Thyroid 2017; 27: 902-907.
2. Pietrowska M, Diehl HC, Mrukwa G, Kalinowska-Herok M, Gawin M, Chekan M et al. Molecular profiles of thyroid cancer subtypes: Classification based on features of tissue revealed by mass spectrometry imaging. Biochim Biophys Acta 2017; 1865: 837-845.
3. Ragazzi M, Ciarrocchi A, Sancisi V, Gandolfi G, Bisagni A, Piana S. Update on anaplastic thyroid carcinoma: morphological, molecular, and genetic features of the most aggressive thyroid cancer. Int J Endocrinol 2014; 2014: 790834.
4. Xing M. Molecular pathogenesis and mechanisms of thyroid cancer. Nat Rev Cancer 2013; 13: 184-199.
5. Lewiński A, Adamczewski Z. Papillary thyroid carcinoma: a cancer with an extremely diverse genetic background and prognosis. Pol Arch Intern Med 2017; 127: 388-389.
6. Xu B, Ghossein R. Evolution of the histologic classification of thyroid neoplasms and its impact on clinical management. Eur J Surg Oncol 2017.
7. Nikiforov YE. Thyroid carcinoma: molecular pathways and therapeutic targets. Mod Pathol 2008; 21 Suppl 2: S37-43.
8. Ciarrocchi A, Cavuto S, Piana S. BRAF V600E mutation and papillary thyroid cancer. JAMA 2013; 310: 534.
9. Kim SJ, Lee KE, Myong JP, Park JH, Jeon YK, Min HS et al. BRAF V600E mutation is associated with tumor aggressiveness in papillary thyroid cancer. World J Surg 2012; 36: 310-317.
10. Sancisi V, Nicoli D, Ragazzi M, Piana S, Ciarrocchi A. BRAFV600E mutation does not mean distant metastasis in thyroid papillary carcinomas. J Clin Endocrinol Metab 2012; 97: E1745-1749.

11. de Biase D, Cesari V, Visani M, Casadei GP, Cremonini N, Gandolfi G et al. High-sensitivity BRAF mutation analysis: BRAF V600E is acquired early during tumor development but is heterogeneously distributed in a subset of papillary thyroid carcinomas. J Clin Endocrinol Metab 2014; 99: E1530-1538.
12. Gandolfi G, Sancisi V, Torricelli F, Ragazzi M, Frasoldati A, Piana S et al. Allele percentage of the BRAF V600E mutation in papillary thyroid carcinomas and corresponding lymph node metastases: no evidence for a role in tumor progression. J Clin Endocrinol Metab 2013; 98: E934-942.
13. Gandolfi G, Sancisi V, Piana S, Ciarrocchi A. Time to re-consider the meaning of BRAF V600E mutation in papillary thyroid carcinoma. Int J Cancer 2015; 137: 1001-1011.
14. Ciampi R, Knauf JA, Kerler R, Gandhi M, Zhu Z, Nikiforova MN et al. Oncogenic AKAP9-BRAF fusion is a novel mechanism of MAPK pathway activation in thyroid cancer. J Clin Invest 2005; 115: 94-101.
15. Romei C, Elisei R. RET/PTC Translocations and Clinico-Pathological Features in Human Papillary Thyroid Carcinoma. Front Endocrinol (Lausanne) 2012; 3: 54.
16. Tallini G, Asa SL. RET oncogene activation in papillary thyroid carcinoma. Adv Anat Pathol 2001; 8: 345-354.
17. O'Keeffe DA, Hill AD, Sheahan K, Ryan F, Barton D et al. Ret-proto-oncogene analysis in medullary thyroid carcinoma. Ir J Med Sci. 1998; 167:226-30.
18. Howell GM, Hodak SP, Yip L. RAS mutations in thyroid cancer. Oncologist 2013; 18: 926-932.
19. Castro P, Rebocho AP, Soares RJ, Magalhães J, Roque L, Trovisco V et al. PAX8-PPARgamma rearrangement is frequently detected in the follicular variant of papillary thyroid carcinoma. J Clin Endocrinol Metab 2006; 91: 213-220.

20. Gandolfi G, de Biase D, Sancisi V, Ragazzi M, Acquaviva G, Pession A et al. Deep sequencing of KIT, MET, PIK3CA, and PTEN hotspots in papillary thyroid carcinomas with distant metastases. Endocr Relat Cancer 2014; 21: L23-26.
21. Gandolfi G, Ragazzi M, Frasoldati A, Piana S, Ciarrocchi A, Sancisi V. TERT promoter mutations are associated with distant metastases in papillary thyroid carcinoma. Eur J Endocrinol 2015; 172: 403-413.
22. Cancer Genome Atlas Research Network. Integrated genomic characterization of papillary thyroid carcinoma. Cell. 2014; 159:676-90.
23. Skinner MK, Rawls A, Wilson-Rawls J, Roalson EH. Basic Helix-Loop-Helix Transcription Factor Gene Family Phylogenetics and Nomenclature. Differentiation 2010; 80: 1–8.
24. Joan S. An overview of the basic helix-loop-helix proteins. Genome Biol. 2004; 5: 226.
25. Massari EM, Murre C. Helix-Loop-Helix Proteins: Regulators of Transcription in Eucaryotic Organisms. Mol. Cell. Biol. 2000; 20:429-440.
26. Forrest S, McNamara C. Id Family of Transcription Factors and Vascular Lesion Formation. Arterios.Thromb. and Vasc. Biol. 2004; 24:2014-2020.
27. Atchley WR, Fitch WM. A natural classification of the basic helix-loop-helix class of transcription factors. Proc Natl Acad Sci U S A 1997; 94: 5172-5176.
28. Hudson KA, Hudson ME. A classification of basic helix-loop-helix transcription factors of soybean. Int J Genomics 2015; 2015: 603182.
29. Yamada K, Miyamoto K. Basic helix-loop-helix transcription factors, BHLHB2 and BHLHB3; their gene expressions are regulated by multiple extracellular stimuli. Front Biosci 2005; 10: 3151-3171.
30. Teramoto M, Nakamasu K, Noshiro M, Matsuda Y, Gotoh O, Shen M et al. Gene structure and chromosomal location of a human bHLH transcriptional factor DEC1 x Stra13 x SHARP-2/BHLHB2. J Biochem 2001; 129: 391-396.

31. Miyazaki K, Kawamoto T, Tanimoto K, Nishiyama M, Honda H, Kato Y. Identification of functional hypoxia response elements in the promoter region of the DEC1 and DEC2 genes. J Biol Chem 2002; 277: 47014-47021.
32. Kato Y, Kawamoto T, Fujimoto K, Noshiro M. DEC1/STRA13/SHARP2 and DEC2/SHARP1 coordinate physiological processes, including circadian rhythms in response to environmental stimuli. Curr Top Dev Biol 2014; 110: 339-372.
33. Sato F, Bhawal UK, Yoshimura T, Muragaki Y. DEC1 and DEC2 Crosstalk between Circadian Rhythm and Tumor Progression. J Cancer 2016; 7: 153-159.
34. Turley H, Wykoff CC, Troup S, Watson PH, Gatter KC, Harris AL. The hypoxia-regulated transcription factor DEC1 (Stra13, SHARP-2) and its expression in human tissues and tumours. J Pathol 2004; 203: 808-813.
35. Wang W, Reiser-Erkan C, Michalski CW, Raggi MC, Quan L, Yupei Z et al. Hypoxia inducible BHLHB2 is a novel and independent prognostic marker in pancreatic ductal adenocarcinoma. Biochem Biophys Res Commun 2010; 401: 422-428.
36. Shi XH, Zheng Y, Sun Q, Cui J, Liu QH, Qü F et al. DEC1 nuclear expression: a marker of differentiation grade in hepatocellular carcinoma. World J Gastroenterol 2011; 17: 2037-2043.
37. Wu Y, Sato F, Bhawal UK, Kawamoto T, Fujimoto K, Noshiro M, Seino H et al. BHLH transcription factor DEC2 regulates pro-apoptotic factor Bim in human oral cancer HSC-3 cells. Biomed Res. 2012; 33:75-82.
38. Seino H, Wu Y, Morohashi S, Kawamoto T, Fujimoto K, Kato Y et al. Basic helix-loop-helix transcription factor DEC1 regulates the cisplatin-induced apoptotic pathway of human esophageal cancer cells. Biomed Res 2015; 36: 89-96.
39. Xu Q, Ma P, Hu C, Chen L, Xue L, Wang Z et al. Overexpression of the DEC1 protein induces senescence in vitro and is related to better survival in esophageal squamous cell carcinoma. PLoS One 2012; 7: e41862.

40. Currie MJ, Hanrahan V, Gunningham SP, Morrin HR, Frampton C, Han C et al. Expression of vascular endothelial growth factor D is associated with hypoxia inducible factor (HIF-1alpha) and the HIF-1alpha target gene DEC1, but not lymph node metastasis in primary human breast carcinomas. J Clin Pathol 2004; 57: 829-834.
41. Chakrabarti J, Turley H, Campo L, Han C, Harris AL, Gatter KC et al. The transcription factor DEC1 (stra13, SHARP2) is associated with the hypoxic response and high tumour grade in human breast cancers. Br J Cancer 2004; 91: 954-958.
42. Tu H, Nengbin H, Yunsong Y, Chengqian Y, Nianli S, Qingcheng Y. DEC2 expression is positively correlated with HIF-1 activation and the invasiveness of human osteosarcomas. J Exp Clin Cancer Res. 2015; 34: 22.
43. Wu Y, Sato F, Bhawal UK, Kawamoto T, Fujimoto K, Noshiro M et al. Basic helix-loop-helix transcription factors DEC1 and DEC2 regulate the paclitaxel-induced apoptotic pathway of MCF-7 human breast cancer cells. Int J Mol Med 2011; 27: 491-495.
44. Wu Y, Sato F, Yamada T, Bhawal UK, Kawamoto T, Fujimoto K et al. The BHLH transcription factor DEC1 plays an important role in the epithelial-mesenchymal transition of pancreatic cancer. Int J Oncol 2012; 41: 1337-1346.
45. Li Y, Xie M, Song X, Gragen S, Sachdeva K, Wan Y et al. DEC1 negatively regulates the expression of DEC2 through binding to the E-box in the proximal promoter. J Biol Chem 2003; 278: 16899-16907.
46. Ciarrocchi A, Piana S, Valcavi R, Gardini G, Casali B. Inhibitor of DNA binding-1 induces mesenchymal features and promotes invasiveness in thyroid tumour cells. Eur J Cancer 2011; 47: 934-945.
47. Borggrefe T, Oswald F. The NOTCH signaling pathway: transcriptional regulation at NOTCH target genes. Cell Mol Life Sci 2009; 66: 1631-1646.
48. Ayaz F, Osborne BA. Non-canonical NOTCH signaling in cancer and immunity. Front Oncol 2014; 4: 345.

49. Aster JC, Pear WS, Blacklow SC. The Varied Roles of NOTCH in Cancer. Annu Rev Pathol 2017; 12: 245-275.

50. Brzozowa-Zasada M, Piecuch A, Dittfeld A, Mielańczyk Ł, Michalski M, Wyrobiec G et al. NOTCH signalling pathway as an oncogenic factor involved in cancer development. Contemp Oncol (Pozn) 2016; 20: 267-272.

51. Brahmi M, Bally O, Eberst L, Cassier P. [Therapeutic targeting of NOTCH signaling in cancer]. Bull Cancer 2017.

52. Li L, Tang P, Li S, Qin X, Yang H, Wu C et al. NOTCH signaling pathway networks in cancer metastasis: a new target for cancer therapy. Med Oncol 2017; 34: 180.

53. Belmonte M, Hoofd C, Weng AP, Giambra V. Targeting leukemia stem cells: which pathways drive self-renewal activity in T-cell acute lymphoblastic leukemia? Curr Oncol 2016; 23: 34-41.

54. Zhao Y, Qiao X, Wang L, Tan TK, Zhao H, Zhang Y et al. Matrix metalloproteinase 9 induces endothelial-mesenchymal transition via NOTCH activation in human kidney glomerular endothelial cells. BMC Cell Biol 2016; 17: 21.

55. Wang Z, Da Silva TG, Jin K, Han X, Ranganathan P, Zhu X et al. NOTCH signaling drives stemness and tumorigenicity of esophageal adenocarcinoma. Cancer Res 2014; 74: 6364-6374.

56. Maliekal TT, Bajaj J, Giri V, Subramanyam D, Krishna S. The role of NOTCH signaling in human cervical cancer: implications for solid tumors. Oncogene 2008; 27: 5110-5114.

57. Rong C, Feng Y, Ye Z. NOTCH is a critical regulator in cervical cancer by regulating Numb splicing. Oncol Lett 2017; 13: 2465-2470

58. Ferrando AA. The role of NOTCH1 signaling in T-ALL. Hematology Am Soc Hematol Educ Program 2009: 353-361.

59. Previs RA, Coleman RL, Harris AL, Sood AK. Molecular pathways: translational and therapeutic implications of the NOTCH signaling pathway in cancer. Clin Cancer Res 2015; 21: 955-961.

60. Nicolas M, Wolfer A, Raj K, Kummer JA, Mill P, van Noort M et al. NOTCH1 functions as a tumor suppressor in mouse skin. Nat Genet 2003; 33: 416-421.

61. Qi R, An H, Yu Y, Zhang M, Liu S, Xu H et al. NOTCH1 signaling inhibits growth of human hepatocellular carcinoma through induction of cell cycle arrest and apoptosis. Cancer Res 2003; 63: 8323-8329.

62. Zage PE, Nolo R, Fang W, Stewart J, Garcia-Manero G, Zweidler-McKay PA. NOTCH pathway activation induces neuroblastoma tumor cell growth arrest. Pediatr Blood Cancer 2012; 58: 682-689.

63. Xiong J, Zhang X, Chen X, Wei Y, Lu DG, Han YW et al. Prognostic roles of mRNA expression of NOTCH receptors in non-small cell lung cancer. Oncotarget 2017; 8: 13157-13165.

64. Activated NOTCH-Induced Intratumoral Heterogeneity Drives Lung Cancer. Cancer Discov 2017; 7: OF16.

65. Xiao X, Ning L, Chen H. NOTCH1 mediates growth suppression of papillary and follicular thyroid cancer cells by histone deacetylase inhibitors. Mol Cancer Ther 2009; 8: 350-356.

66. Ferretti E, Tosi E, Po A, Scipioni A, Morisi R, Espinola MS et al. NOTCH signaling is involved in expression of thyrocyte differentiation markers and is down-regulated in thyroid tumors. J Clin Endocrinol Metab 2008; 93: 4080-4087.

67. Yamashita AS, Geraldo MV, Fuziwara CS, Kulcsar MA, Friguglietti CU, da Costa RB et al. NOTCH pathway is activated by MAPK signaling and influences papillary thyroid cancer proliferation. Transl Oncol 2013; 6: 197-205.

68. Zhang M, Qin Y, Zuo B, Gong W, Zhang S, Gong Y et al. Overexpression of NOTCH-regulated Ankyrin Repeat Protein is associated with papillary thyroid carcinoma progression. PLoS One 2017; 12: e0167782.

69. Kim HJ, Kim MJ, Kim A, Jung CW, Park S, Koh JS et al. The Role of NOTCH1 Signaling in Anaplastic Thyroid Carcinoma. Cancer Res Treat 2017; 49: 509-517.

70. Yu XM, Jaskula-Sztul R, Georgen MR, Aburjania Z, Somnay YR, Leverson G et al. NOTCH1 Signaling Regulates the Aggressiveness of Differentiated Thyroid Cancer and Inhibits SERPINE1 Expression. Clin Cancer Res 2016; 22: 3582-3592.

71. Fu H, Ma C, Guan W, Cheng W, Feng F, Wang H. Expression of NOTCH 1 receptor associated with tumor aggressiveness in papillary thyroid carcinoma. Onco Targets Ther 2016; 9: 1519-1523.

72. Katoh M. Integrative genomic analyses on HES/HEY family: NOTCH-independent HES1, HES3 transcription in undifferentiated ES cells, and NOTCH-dependent HES1, HES5, HEY1, HEY2, HEYL transcription in fetal tissues, adult tissues, or cancer. Int J Oncol 2007; 31: 461-466.

73. Fischer A, Schumacher N, Maier M, Sendtner M, Gessler M. The NOTCH target genes Hey1 and Hey2 are required for embryonic vascular development. Genes Dev 2004; 18: 901-911.

74. Leal MC, Surace EI, Holgado MP, Ferrari CC, Tarelli R, Pitossi F et al. NOTCH signaling proteins HES-1 and Hey-1 bind to insulin degrading enzyme (IDE) proximal promoter and repress its transcription and activity: implications for cellular Aβ metabolism. Biochim Biophys Acta 2012; 1823: 227-235.

75. Iso T, Kedes L, Hamamori Y. HES and HERP families: multiple effectors of the NOTCH signaling pathway. J Cell Physiol 2003; 194: 237-255.

76. Kamakura S, Oishi K, Yoshimatsu T, Nakafuku M, Masuyama N, Gotoh Y. Hes binding to STAT3 mediates crosstalk between NOTCH and JAK-STAT signalling. Nat Cell Biol 2004; 6: 547-554.

77. Fischer A, Gessler M. Delta-NOTCH--and then? Protein interactions and proposed modes of repression by Hes and Hey bHLH factors. Nucleic Acids Res 2007; 35: 4583-4596.

78. Kay SK, Harrington HA, Shepherd S, Brennan K, Dale T, Osborne JM et al. The role of the Hes1 crosstalk hub in NOTCH-Wnt interactions of the intestinal crypt. PLoS Comput Biol 2017; 13: e1005400.

79. King IN, Kathiriya IS, Murakami M, Nakagawa M, Gardner KA, Srivastava D et al. Hrt and Hes negatively regulate NOTCH signaling through interactions with RBP-Jkappa. Biochem Biophys Res Commun 2006; 345: 446-452.

80. Asanoma K, Liu G, Yamane T, Miyanari Y, Takao T, Yagi H et al. Regulation of the Mechanism of TWIST1 Transcription by BHLHE40 and BHLHE41 in Cancer Cells. Mol Cell Biol 2015; 35: 4096-4109.

81. Li P, Jia YF, Ma XL, Zheng Y, Kong Y, ZhangY, et al. DEC2 suppresses tumor proliferation and metastasis by regulating ERK/NF-κB pathway in gastric cancer. Am J Cancer Res 2016; 6:1741-1757.

82. Falvella FS, Colombo F, Spinola M, Campiglio M, Pastorino U and DraganiTA. BHLHB3: a candidate tumor suppressor in lung cancer. Oncogene 2008; 27: 3761–3764.

83. Zheng Y, Jia Y, Wang Y, Wang M, Li B, Shi X et al. The hypoxia-regulated transcription factor DEC1 (Stra13, SHARP-2) and its expression in gastric cancer. OMICS 2009; 13: 301-306.

84. Vasko V, Espinosa AV, Scouten W, He H, Auer H, Liyanarachchi S, et al. Gene expression and functional evidence of epithelial-to-mesenchymal transition in papillary thyroid carcinoma invasion. Proc Natl Acad Sci U S A. 2007; 104:2803–8.

85. Park HS1, Jung CK, Lee SH, Chae BJ, Lim DJ, Park WC et al. NOTCH1 receptor as a marker of lymph node metastases in papillary thyroid cancer. Cancer Sci. 2012; 103(2):305-9.

86. Jung CW, Kong JS, Seol H, Park S, Koh JS, Lee SS et al. Expression of activated NOTCH1 and Hey1 in papillary thyroid carcinoma. Histopathology 2017; 70: 301-308.

87. Yuan X, Wu H, Xu H, Xiong H, Chu Q, Yu S et al. NOTCH signaling: an emerging therapeutic target for cancer treatment. Cancer Lett. 2015; 369:20-7.

88. Georgina N. Masoud and Wei Li. HIF-1α pathway: role, regulation and intervention for cancer therapy. Acta Pharm Sin B. 2015; 5: 378–389.

89. Ma W, Shi X, Lu S, Wu L, Wang Y. Hypoxia-induced overexpression of DEC1 is regulated by HIF-1α in hepatocellular carcinoma. Oncol Rep 2013; 30: 2957-2962.

90. Choi SM, Cho HJ, Cho H, Kim KH, Kim JB, Park H. Stra13/DEC1 and DEC2 inhibit sterol regulatory element binding protein-1c in a hypoxia-inducible factor-dependent mechanism. Nucleic Acids Res 2008; 36: 6372-6385.

91. Montagner M1, Enzo E, Forcato M, Zanconato F, Parenti A, Rampazzo E. et al. SHARP1 suppresses breast cancer metastasis by promoting degradation of hypoxia-inducible factors. Nature. 2012; 487:380-4.

92. Wu Y1, Sato F, Bhawal UK, Kawamoto T, Fujimoto K, Noshiro M et al. BHLH transcription factor DEC2 regulates pro-apoptotic factor Bim in human oral cancer HSC-3 cells. Biomed Res. 2012; 33:75-82.

93. Gill RM1, Gabor TV, Couzens AL, Scheid MP. The MYC-associated protein CDCA7 is phosphorylated by AKT to regulate MYC-dependent apoptosis and transformation. Mol Cell Biol. 2013; 33:498-513.

94. Qian Y, Zhang J, Jung YS, Chen X. DEC1 coordinates with HDAC8 to differentially regulate TAp73 and ΔNp73 expression. PLoS One 2014; 9: e84015.

95. Li Y, Xie M, Yang J, Yang D, Deng R, Wan Y et al. The expression of antiapoptotic protein survivin is transcriptionally upregulated by DEC1 primarily through multiple sp1 binding sites in the proximal promoter. Oncogene 2006; 25: 3296-3306.

96. Huang W, Cui X, Chen Y, Shao M, Shao X, Shen Y et al. High VRK1 expression contributes to cell proliferation and survival in hepatocellular carcinoma. Pathol Res Pract. 2016; 212:171-8.

97. Liu Y, Wang L, Lin XY, Wang J, Yu JH, Miao Y et al. The transcription factor DEC1 (BHLHE40/STRA13/SHARP-2) is negatively associated with TNM stage in non-small-cell lung cancer and inhibits the proliferation through cyclin D1 in A549 and BE1 cells. Tumour Biol 2013; 34: 1641-1650.

98. Bi H, Li S, Qu X, Wang M, Bai X, Xu Z et al. DEC1 regulates breast cancer cell proliferation by stabilizing cyclin E protein and delays the progression of cell cycle S phase. Cell Death Dis 2015; 6: e1891.

99. Tang A, Gao K, Chu L, Zhang R, Yang J, Zheng J. Aurora kinases: novel therapy targets in cancers. Oncotarget 2017; 8: 23937-23954.

100. Baldini E, Sorrenti S, D'Armiento E, Guaitoli E, Morrone S, D'Andrea V et al. Effects of the Aurora kinases pan-inhibitor SNS-314 mesylate on anaplastic thyroid cancer derived cell lines. Clin Ter 2012; 163: e307-313.

101. Baldini E, Sorrenti S, D'Armiento E, Prinzi N, Guaitoli E, Favoriti P et al. Aurora kinases: new molecular targets in thyroid cancer therapy. Clin Ter 2012; 163: e457-462.

102. Baldini E, Tuccilli C, Prinzi N, Sorrenti S, Antonelli A, Fallahi P et al. Selective inhibitors of aurora kinases inhibit proliferation, reduce cell viability and impair cell cycle progression in papillary thyroid carcinoma cells. J Biol Regul Homeost Agents 2015; 29: 793-803.

103. Baldini E, Arlot-Bonnemains Y, Sorrenti S, Mian C, Pelizzo MR, De Antoni E et al. Aurora kinases are expressed in medullary thyroid carcinoma (MTC) and their inhibition

suppresses in vitro growth and tumorigenicity of the MTC derived cell line TT. BMC Cancer 2011; 11: 411.

104. de Caestecker MP, Piek E, Roberts AB. Role of transforming growth factor-beta signaling in cancer. J Natl Cancer Inst. 2000; 92:1388-402.

105. MacDonald BT, Tamai K, He X. Wnt/beta-catenin signaling: components, mechanisms, and diseases. Dev Cell. 2009;17:9-26.

106. Li B1, Jia Z, Wang T, Wang W, Zhang C, Chen P et al. Interaction of Wnt/β-catenin and NOTCH signaling in the early stage of cardiac differentiation of P19CL6 cells. J Cell Biochem. 2012; 113:629-39.

107. Wang R, Sun Q, Wang P, Liu M, Xiong S, Luo J et al. NOTCH and Wnt/β-catenin signaling pathway play important roles in activating liver cancer stem cells. Oncotarget. 2016; 7:5754-68.

108. Klüppel M, Wrana JL. Turning it up a NOTCH: cross-talk between TGF beta and NOTCH signaling. Bioessays. 2005; 27:115-8.

109. Wang R, Sun Q, Wang P, Liu M, Xiong S, Luo J et al. NOTCH and Wnt/β-catenin signaling pathway play important roles in activating liver cancer stem cells. Oncotarget 2016; 7: 5754-5768.

110. Han L, Diehl A, Nguyen NK, Korangath P, Teo W, Cho S et al. The NOTCH pathway inhibits TGFβ signaling in breast cancer through HEYL-mediated crosstalk. Cancer Res 2014; 74: 6509-6518.